Reaction and Transport in Industrial-Scale Packed Bed Steam Reforming of Glycerol

A Major Qualifying Project Report

Submitted to the Faculty of the

WORCESTER POLYTECHNIC INSTITUTE

In partial fulfillment of the major requirements for the

Degree of Bachelor of Science in

Chemical Engineering

By

Bryan MacDonald and Amanda Olm

March 2014

1. Abstract

The ubiquity of biodiesel production, which generates 10% glycerol as a by-product, has led to an abundance of glycerol waste and a reduction of value. Steam reforming presents an alternative to optimize the use of glycerol by converting it to hydrogen. The present study simulated the process in COMSOL Multiphysics using a bimetallic Ni–Co/Al2O3 catalyst in a packed bed reactor. The model was developed to simultaneously analyze the kinetics and thermodynamics of the system on an industrial scale, allowing for recommendations regarding process and reactor design. After comparing the process to methane steam reforming, it was found that glycerol steam reforming in a packed bed reactor is a feasible solution for the transformation of waste into a clean sustainable commodity.

Table of Contents:

Table of Figures:

2. Introduction

In the production of biodiesel the yield includes approximately 10% by volume glycerol as a by-product. The resulting crude glycerol has little value and is difficult to dispose of. Refining glycerol is an option for generating feed appropriate to be used in other industries; however, the volume of glycerol generated from the production of biodiesel greatly surpasses the demand for refined glycerol. The remaining crude glycerol produced has become a potential environment pollutant, consequently resulting in a devaluation of biodiesel [1]. With the prominent rapid increase in biodiesel production over the past decade and a concern for its sustainability, there has been a need for alternative applications of glycerol, either in crude or refined forms [2]. One alternative is the chemical conversion of glycerol into value-added products, such as hydrogen. Hydrogen is widely used in the energy industry, and its demand is expected to increase in the future as a clean sustainable energy commodity. Steam reforming of one mole of glycerol yields seven moles of hydrogen, as shown in Equation 1, making this a good and seemingly feasible alternative.

$$C_3H_8O_3 + 3H_2O \leftrightarrow 3CO_2 + 7H_2 \quad (1)$$

Previous studies have explored the catalytic steam reforming of glycerol using different catalysts and operating conditions. Different kinetics models and heat transfer analysis have been proposed as well. However, the feasibility of steam reforming in a fixed bed reactor or reactor segment on an industrial scale has not been investigated to date. The present study aimed at simultaneously analyzing the kinetics and thermodynamics of the system on an industrial scale, allowing for recommendations regarding process and reactor design. Potential diffusion limitations and the effects of temperature gradients in the reactor were also studied.

Glycerol steam reforming is an endothermic process optimally conducted at high temperatures and relatively low pressures, as compared to other processes, such as methane steam reforming. The operating conditions used in this study were on the order of 823K and 202.65kPa, based on suggestions in the literature, and heat was added directly to the reactor in order to allow the endothermic reaction producing hydrogen to proceed effectively. A feed containing a high steam-to-glycerol ratio favors the production of hydrogen, and the general consensus for the optimal ratio is 9:1. The feed enters a packed bed reactor, consisting of several hundred tubes, containing bimetallic Ni-Co/Al_2O_3 catalyst pellets that allow for the reaction to take place. The process is believed to be diffusion-limited, due to the difficulty of glycerol in diffusing into the macroporous catalyst particles and the high reaction rate. The reactor segment used to simulate the process was initially established as 1m long with a 0.15m diameter and packed with spherical catalyst pellets of 0.0254m diameter, values on the same scale as existing steam reformers.

The process was simulated in COMSOL Multiphysics in a packed bed reactor segment. The heterogeneous catalytic process model provided axial profiles of radially averaged concentrations and temperatures in the tubular reactor and analyzed the transfer of mass, energy and momentum in the system. The system kinetics was modeled using a Langmuir-Hinshelwood model with dual-site associative adsorption of both glycerol and steam with bimolecular surface reaction [3]. Such a model is dependent on the partial pressures of both glycerol and steam, as well as temperature.

Steam reforming of glycerol was compared with methane steam reforming, a process now widely used industrially for hydrogen production. Given the right conditions, it was found that glycerol steam

reforming in a packed bed reactor is a feasible solution for the transformation of by-product waste into a clean sustainable commodity.

3. Background

3.1 Biodiesel Production

3.1.1 Outlook on Biodiesel Production

Fossil fuels are an unsustainable energy source, yet one the world depends on. There has been strong support to expand the biodiesel market to promote increased use of a renewable, clean-burning diesel replacement. Biodiesel is made from agricultural oils, recycled cooking oil, and animal fats, and it is the first Advanced Biofuel designated by the EPA to reach 1 billion gallons of annual production. Biodiesel production in the United States has increased from 500,000 gallons in 1999 to 500 million in 2007, eventually surpassing 1.8 billion gallons in 2013 [4]. The production of biodiesel from 1999 to 2012 is shown in Figure 3-1.

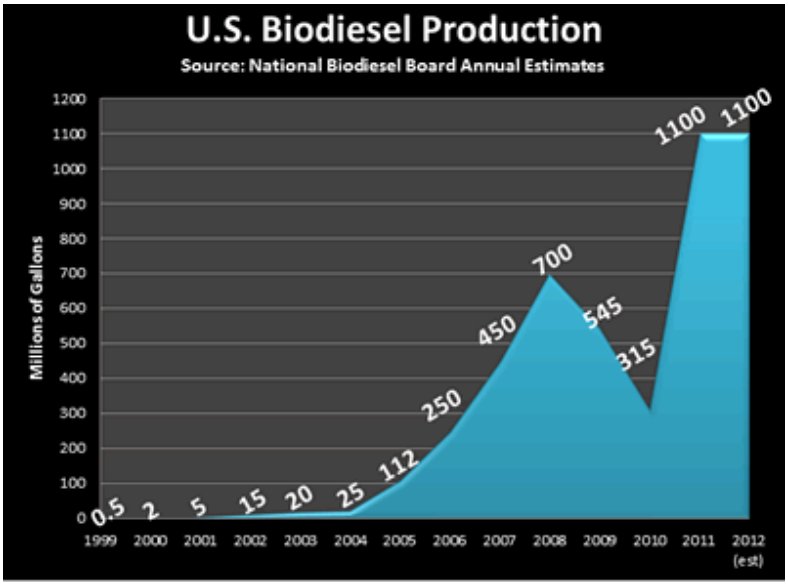

Figure 3-1. Production of Biodiesel in the US [1]

The production of biodiesel now not only exceeds the requirements under the Renewable Fuel Standard (RFS), but it reduces harmful emissions and helps support approximately 50,000 jobs in the United States. The biodiesel industry encompasses production plants in nearly every state, as shown in Figure 3-2 [4]. The production of biodiesel in the United States strengthens the nation's energy portfolio and reduces reliance on foreign fossil fuels. A tax incentive of $1 per gallon was placed on biodiesel in 2005, which has helped stimulate the industry's growth over the past decade [5]. Thanks to the incentive, in recent years biodiesel has reached a lower price than petroleum diesel.

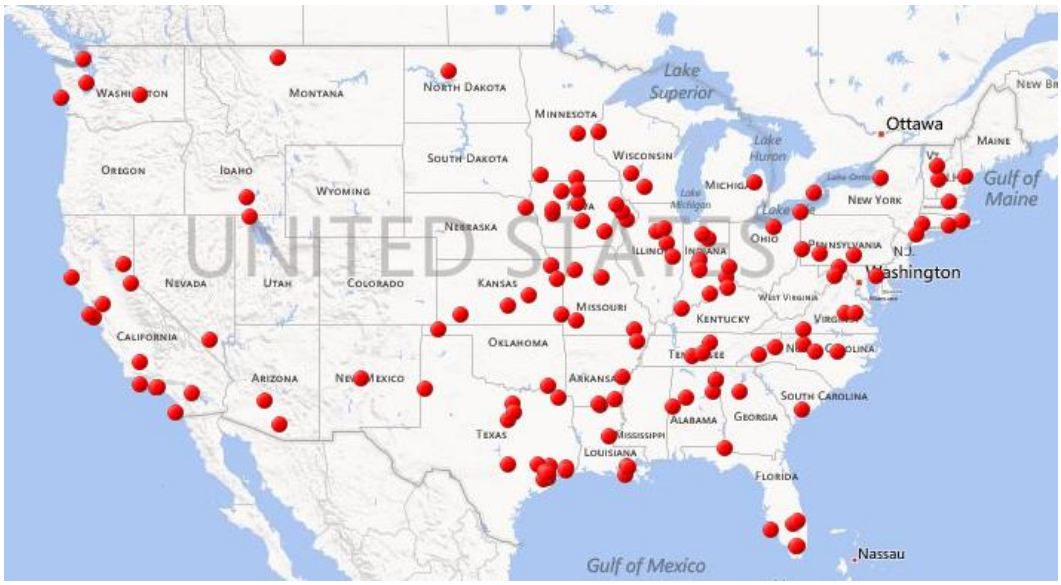

Figure 3-2. Biodiesel Plants in the US [1]

The main by-product of biodiesel production is crude glycerol, making up about 10% of the production yield. It results from the biodiesel process's transesterification reaction, illustrated in Figure 3-3 [7]. The reaction involves triglycerides, such as fats, oils, or lipids, and methyl alcohol in the presence of a catalyst, yielding glycerol and methyl ester (biodiesel).

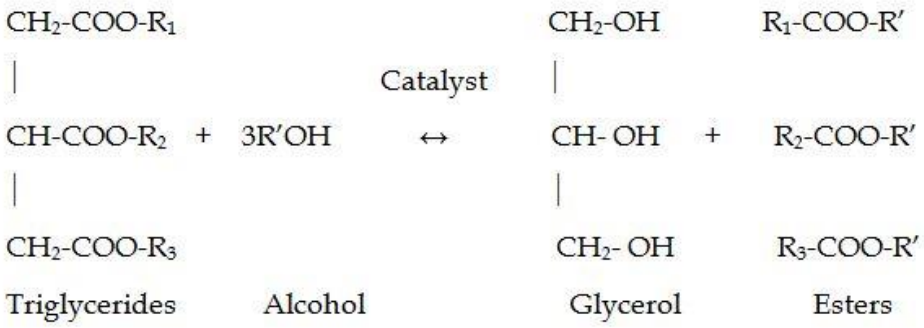

Figure 3-3. Transesterification Reaction [7]

Crude glycerol derived from biodiesel production contains impurities, and therefore holds low value. The specific composition of crude glycerol depends on the feedstock used in production, as well as other sources of contamination introduced along the process. Further refining of crude glycerol enables its use as feedstock in applications in the food, drug, cosmetics, and tobacco industries. However, the refining process is expensive and involves several purifying steps before the refined glycerol meets the necessary specifications for use in the aforementioned applications.

The production of biodiesel is expected to steadily grow, and with it, so is the production of crude glycerol. Currently, the majority of glycerol production comes from biodiesel plants, and the amount produced yearly far surpasses the demand for glycerol. Consequently, glycerol has become a possible environment

pollutant and has resulted a devaluation of both glycerol and biodiesel [8]. Refining glycerol is becoming increasingly economically infeasible due to the lowered prices following the expansion of the biodiesel market. Crude glycerol is also difficult to dispose of, given the organic impurities that result from the transesterification reaction, and is therefore a waste that generates large operating costs. It is imperative that alternative applications of the low-grade glycerol be found and explored on an industrial level in order to handle the vast amount of glycerol produced annually.

3.1.2 Options for Use of Glycerol By-Product

Glycerol is a trihydric alcohol present in the form of glycerides in all animal and vegetable fats and oils. It is a colorless, odorless, dense liquid that decomposes at 563 K [9]. Glycerol is hygroscopic, meaning it absorbs water from the air. This property makes it an effective moistener when refined. However, due to the impurities present in crude glycerol, it cannot be directly used as feedstock in the production of food, drugs, or cosmetics. The conversion of glycerol into products fit for use in different industries has been explored as the production of biodiesel has continued to expand. Glycerol uses for added-value products include the production of 1,3-propanediol, 1,2-propanediol, dihydroxyacetones, hydrogen, polyglycerols, succinic acid, and polyesters [10]. Other alternatives for the use of crude glycerol include using it in combination with other materials as a source of energy. Some applications include direct glycerol combustion, mixing and combusting with agricultural solid wastes, blending with other fuels, and etherification, among others [6]. However, direct combustion can be a dangerous process due to glycerol's high viscosity, high auto-ignition temperature, and low heating value.

3.1.3 Hydrogen as Desired Product

Hydrogen is considered a very promising, clean, and sustainable source of energy [11]. Hydrogen itself does not occur naturally, yet it is abundantly present in hydrocarbons. Prominent uses of hydrogen are seen in the chemical and petrochemical industries. Most of its production is dependent on fossil fuels, notably from natural gas [12]. It is expected that the use of hydrogen as a fuel will increase as the technology in the field develops. Utilizing glycerol in the production of hydrogen has been identified as an attractive alternative, due its potential for sustainable energy generation. Several processes for extracting hydrogen from glycerol have been explored. They include continuous microbial fermentation [13], catalytic reforming at moderate temperatures and pressures [14], aqueous-phase reforming (APR) [15], pyrolysis and steam gasification [16], and steam reforming in the gas phase with Group 8-10 metal catalysts [17]. Steam reforming is a process that is widely used industrially, particularly for transforming methane into hydrogen. It has proven to be effective, and there is great interest in developing a similar industrial-scale process for glycerol.

3.2 Glycerol Steam Reforming

3.2.1 Steam Reforming in a Packed Bed Reactor

Steam reforming is a highly endothermic process used to convert hydrocarbons into a mixture of hydrogen and carbon dioxide. In steam reforming, the breaking of C-C, C-H, and O-H bonds occurs on the surface of a solid catalyst. This process is a heterogeneous catalytic reaction involving the following steps [18]:

1. Diffusion of the reactants from the bulk fluid to the external surface of the catalyst pellet
2. Diffusion of the reactants through catalyst pores
3. Adsorption of the reactants onto the catalyst surface inside pores
4. Reaction on the catalyst surface
5. Desorption of the products from catalyst surface
6. Diffusion of the products from inside catalyst pores to catalyst surface
7. Diffusion of the products from surface of the catalyst pellet to the bulk fluid

The surface reaction is found to be the rate-limiting step in this reaction mechanism for glycerol steam reforming.

A conventional steam reformer consists of hundreds of tubes packed with porous, solid catalyst pellets through which a mixture of fuel and steam flows. The reactor used is of tube and shell type. The shell side contains a burner that provides the heat necessary for the reaction to proceed effectively. The overall reaction for the steam reforming of glycerol is shown in Equation (3-1).

$$C_3H_8O_3 + 3H_2O \leftrightarrow 3CO_2 + 7H_2 \tag{3-1}$$

This reaction can also be viewed as the sum of the glycerol decomposition reaction and the water-gas shift reaction, as shown in Equations (3-2) and (3-3). Other side reactions also take place, and different reaction mechanisms have been proposed. Side reactions may include methanation, methane steam reforming, methane decomposition, and hydrogenolysis of glycerol, among others [19].

Glycerol decomposition: $$C_3H_8O_3 \leftrightarrow 3CO + 4H_2 \tag{3-2}$$

Water-gas shift: $$3CO + 3H_2O \leftrightarrow 3CO_2 + 3H_2 \tag{3-3}$$

Alumina catalyst support has been predominantly used in studies done on the catalytic steam reforming of glycerol. Findings relating to the process have mainly focused on conversion, selectivity, and yield of products. Few researchers have explored both the kinetics and thermodynamics of the process, and all have been done on a small laboratory scale. Process design has been investigated for optimizing the reaction and reducing the impact of limiting factors.

3.2.2 Mass Transfer

For a heterogeneous catalytic reaction, such as the reforming of glycerol in the gas phase with a solid catalyst, conversion is largely limited by mass transfer. There are two distinct types of mass transfer occurring in the system, referred to as external and internal. First, the reactants must diffuse from the bulk fluid onto the surface of the catalyst pellet; this process is called external mass transfer. The no-slip

condition creates a laminar flow boundary layer around each catalyst particle, through which the only means of mass transport is diffusion, and the only means of heat transport is conduction. Since the chemical reaction on the catalyst pellet consumes both heat and the reactant species, there exists a gradient in reactant concentrations as well as temperature across the boundary layer, with lower concentrations and temperature at the pellet surface than in the bulk fluid. The diffusion limitation created by the boundary layer is referred to as external mass transfer resistance, and the rate of mass transfer across the boundary layer is given by Equation (3-4).

$$N_A = k_A(C_{A0} - C_{AS}) \tag{3-4}$$

Here A is the reactant—glycerol or steam—while N_A is the molar flux of A to the catalyst surface, k_A is the species transfer coefficient, C_{A0} is the concentration of A in the bulk fluid, and C_{AS} is the concentration of A on the surface of the catalyst pellet. The transfer coefficient, k_A, is dependent on the boundary layer thickness, δ, and the diffusion coefficient of species A in species B, D_{AB}, given by Equation (3-5).

$$k_A = \frac{D_{AB}}{\delta} \tag{3-5}$$

This diffusion coefficient can be found from a correlation based on the Sherwood number for a packed bed reactor, shown in Equation (3-6) [20].

$$Sh = 2 + 1.1Re^{0.6}Sc^{1/3} \tag{3-6}$$

Re is the Reynolds number and Sc is the Schmidt Number, given by Equations (3-7) and (3-8), respectively.

$$Re = \frac{\rho DV}{\mu} \tag{3-7}$$

$$Sc = \frac{\mu}{\rho D_{AB}} \tag{3-8}$$

The size, and therefore the influence, of the boundary layer is inversely proportional to the fluid's linear velocity. Figure 3-4 shows the effect of the fluid velocity on the boundary layer around a solid sphere [9]. As the velocity increases, the laminar flow boundary layer decreases, the species transfer coefficient increases, and consequently the reaction rate also increases, improving the conversion of the process.

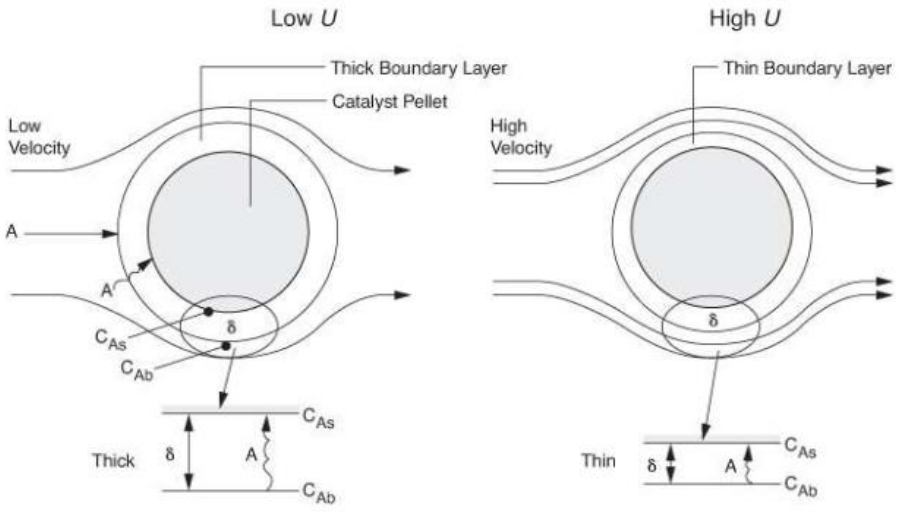

Figure 3-4. Effect of Fluid Velocity on Laminar Flow Boundary Layer around a Solid Sphere [9]

Fuller, Schettler and Giddings [21] developed an empirical correlation to predict binary gas diffusivities using a nonlinear least-squares analysis, as seen in Equation (3-9).

$$D_{AB} = \frac{10^{-3}T^{1.75}\left(\frac{1}{M_A}+\frac{1}{M_B}\right)^{1/2}}{P\left[(\sum V_A)^{1/3}+(\sum V_B)^{1/3}\right]^2} \tag{3-9}$$

Later, Taylor and Smith [22] provided an approximate solution to the Stefan-Maxwell diffusion equations to convert these binary diffusivities to multicomponent ones:

$$D_{im} = \frac{1-y_i\sum_j \frac{N_j}{N_i}}{\sum_j \frac{y_j - y_i(N_j/N_i)}{D_{ij}}} \tag{3-10}$$

The multicomponent diffusivity accounts for all of the resistance to external diffusion in the system, corresponding to the external mass transfer limitation. If the external mass transfer resistance is small or even negligible, the concentration gradient across the boundary layer is small and doesn't hinder the reaction rate.

The process uses a porous catalyst, so only a fraction of the catalytic surface area is on the pellet's geometric surface. The internal mass transfer limitation encompasses the diffusion of the reactants into the catalyst's pores. Inside the pores, molecular diffusion is complemented by the effect of the reactants colliding with the pore walls, known as Knudsen diffusion, D_K. The diffusion coefficient factor is dependent on a tortuosity factor, τ, which accounts for the pores' nonlinear paths and varying cross-sectional areas, as well as a porosity factor, φ, which accounts for the volume of empty space in the catalyst pellet [9].

The effects of molecular diffusion and Knudsen diffusion can be combined into a single effective diffusivity. Since diffusion coefficients represent resistances to mass transfer, the effective diffusivity is related to the sum of the inverses of molecular and Knudsen diffusivities, as shown in Equation (3-11).

$$\frac{1}{D_{eff}} = \frac{1}{D_{AB}} + \frac{1}{D_K} \tag{3-11}$$

In 1977, Jackson [23] showed that Knudsen diffusion is proportional to pore diameter and independent of pressure, while molecular diffusion is independent of pore diameter and inversely related to pressure. The Knudsen diffusion depends on several qualities of the pores, including tortuosity, porosity and diameter. In a recent CFD modeling of glycerol steam reforming, Kent [24] showed that due to the large internal diffusion resistance of this process, external mass transfer resistance is negligible, even in the laminar flow region. However, given that his was an isothermal study, the effect of the boundary layer on heat transfer was not investigated.

The effective diffusivity for each component present in the main reaction of the process was calculated, as shown in Table 3-1. Molecular diffusivity calculations were performed based on the Fuller-Schettler-Giddings Correlation for binary diffusivities and then corrected for the multicomponent system with the correlation from Smith and Taylor [21][22]. For the multicomponent correction, the ratio of the molar fluxes was assumed to be equal to the stoichiometric ratios of the individual components.

Table 3-1. Component Diffusivities Based on Stoichiometric Ratios

Component	Ratio of Molar Fluxes			Effective Diffusivity (m^2/s)
Glycerol	NH_2/Ngly = -7	Nh2o/Ngly = 3	Nco2/Ngly = -3	9.23E-08
H_2O	Ngly/NH_2O = 1/3	Nco2/Nh2o = -1	NH_2/Nh2o = -7/3	2.10E-07
CO_2	Ngly/Nco2 = -1/3	Nh2o/Nco2 = -1	NH_2/Nco2 = 7/3	1.33E-07
H_2	Ngly/NH_2 = -1/7	Nh2o/NH_2 = -3/7	Nco2/NH_2 = 3/7	6.22E-07

Diffusion is affected by the reactant molecule size, and given that glycerol is a large molecule, it is expected that the steam reforming of glycerol is significantly limited by diffusion, predominantly Knudsen diffusion. Glycerol is also much bigger than water, the other reactant in the steam reforming process, making the diffusivity of glycerol the limiting factor in system. Another assumed hindrance to diffusion in the system is the stoichiometry of the main chemical reaction. One mole of glycerol and three moles of water produce three moles of carbon dioxide and seven moles of hydrogen, a net increase of six moles. The generation of additional moles of gas interferes with the inward flux of new reactants. This could significantly slow down the reaction by preventing the internal diffusion of glycerol. The operating temperature and pressure have an effect on both molecular and Knudsen diffusion. Increasing temperature results in higher effective diffusivity, therefore improving the process reaction. Meanwhile, decreasing pressure improves diffusion. However, since glycerol steam reforming is predominantly limited by Knudsen diffusion, which is unaffected by pressure, the operating pressure won't have a pronounced effect on diffusion in the system.

In heterogeneous catalytic reactions with predominant internal diffusion limitations, most of the reaction occurs on or near the geometric surface of the catalyst pellets. This creates a concentration gradient

within the pellet. The effectiveness factor, η, measures the extent to which the reactants diffuse into the catalyst before reacting, as shown in Equation (3-12) [18].

$$\eta = \frac{\text{actual overall rate of reaction}}{\text{rate of reaction at surface}} \tag{3-12}$$

This value is based on the relationship between mass transfer limitations and reaction rate, and can be used as a scalar quantity that adjusts the reaction rate to account for intra-particle mass transfer resistance.

3.2.3 Pressure Drop

The reaction rate and component concentrations in the system are dependent on the partial pressure of each component. The Ergun equation provides a correlation for the pressure drop in a packed bed reactor, as shown in Equation (3-13) [25].

$$\frac{dP}{dz} = -\frac{G}{\rho d_p}\left(\frac{1-\varphi}{\varphi^3}\right)\left[150\frac{(1-\varphi)\mu}{d_p} + 1.75G\right] \tag{3-13}$$

P represents pressure (Pa), z represents the length of the packed bed (m), φ represents the bed voidage ($\frac{volume\ of\ reactor - volume\ of\ catalyst\ particles}{volume\ of\ reactor}$), G represents the mass flux (kg/m^{2}s), d_p represents the catalyst pellet diameter (m), μ represents the fluid viscosity (kg/m s), and ρ is the fluid density (kg/m^3). Small catalyst pellet diameters and large fluid mass flux would result in a higher pressure drop, adversely affecting the reaction rate and the operating cost of the pump working on the reactor feed. While a net difference in pressure is necessary for the bulk fluid to flow through the reactor, it is economically desirable to keep the pressure drop to a minimum.

3.2.4 Process Operating Conditions

Chen et al. [26] performed glycerol steam reforming in a pilot fixed bed reactor with a packed length of 800mm and commercial nickel/nickel oxide-based cylindrical catalyst pellets with 1/8" diameter, with process set up as illustrated in Figure 3-5. This is the only study to date to experimentally examine the process on a scale this large. A thermodynamic analysis was performed based on the minimization of Gibbs free energy (non-stoichiometric method). Both the theoretical model and the pilot reactor were used to measure the effects of temperature, pressure, steam-to-glycerol feed ratio and reactant to inert species feed ratio on product composition, glycerol and steam conversion, hydrogen selectivity and hydrogen purity.

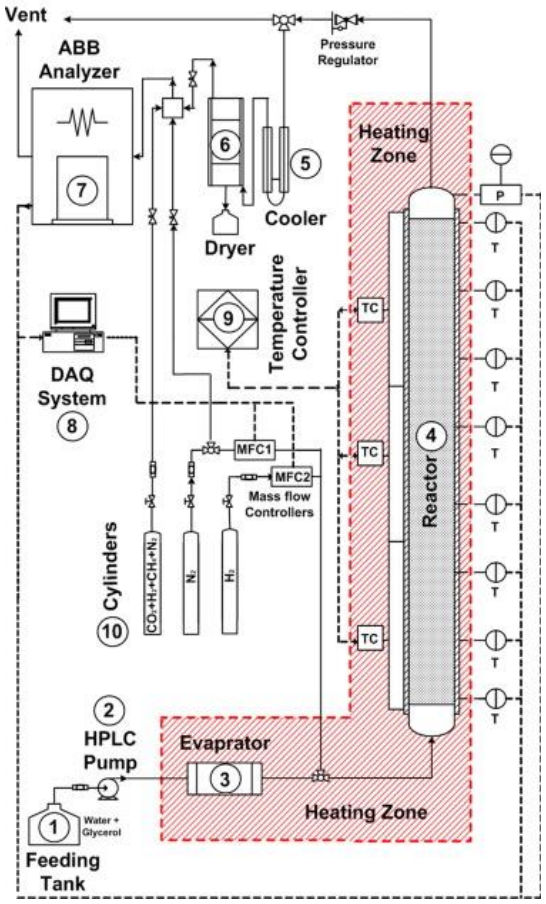

Figure 3-5. Schematic Diagram of Process Setup [26]

The study found that high temperature favors hydrogen production and selectivity with maximum hydrogen production occurring around 853K [26]. Meanwhile, Adhikari et al. [27] performed lab-scale experiments involving the catalytic steam reforming of glycerol. From the experimental data obtained, it is apparent that glycerol conversion is inversely proportional to glycerol partial pressure and directly proportional to steam partial pressure. As seen in Figure 3-6, at differing steam partial pressures the range of appropriate glycerol partial pressures is broad, although similar glycerol conversions are obtained. Carbon deposition was found to be strongly dependent on glycerol's partial pressure, while not significantly affected by steam's partial pressure, suggesting that carbon did not react with steam under chosen process conditions.

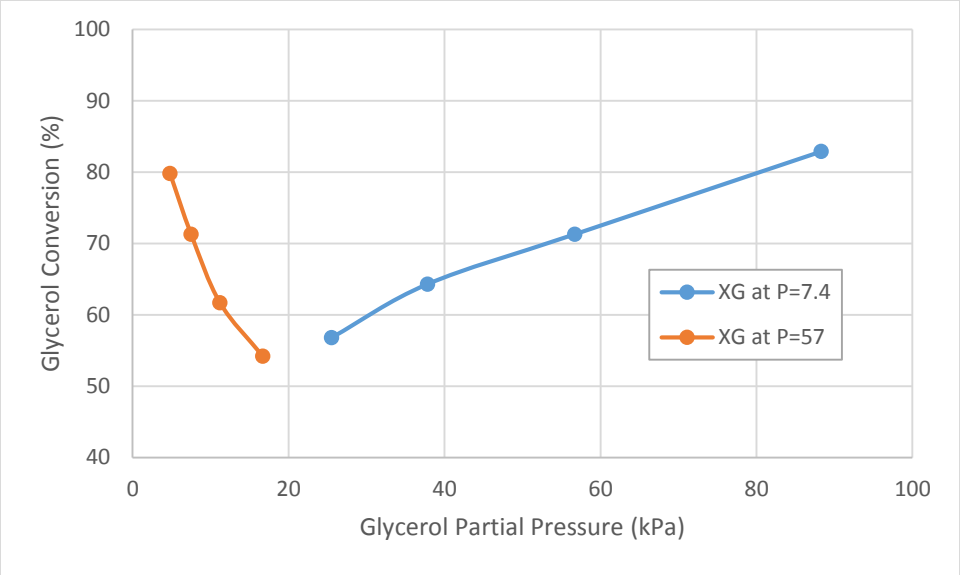

Figure 3-6. Glycerol Conversion vs. Glycerol Partial Pressure at Steam Partial Pressures of 7.4 and 57 psi. From [27]

Figure 3-7 shows the same trends for hydrogen yield with varying glycerol partial pressures at different steam partial pressures. However, in this case higher maximum hydrogen yields are obtained at a lower steam pressure with glycerol partial pressures at the low end of the range obtainable.

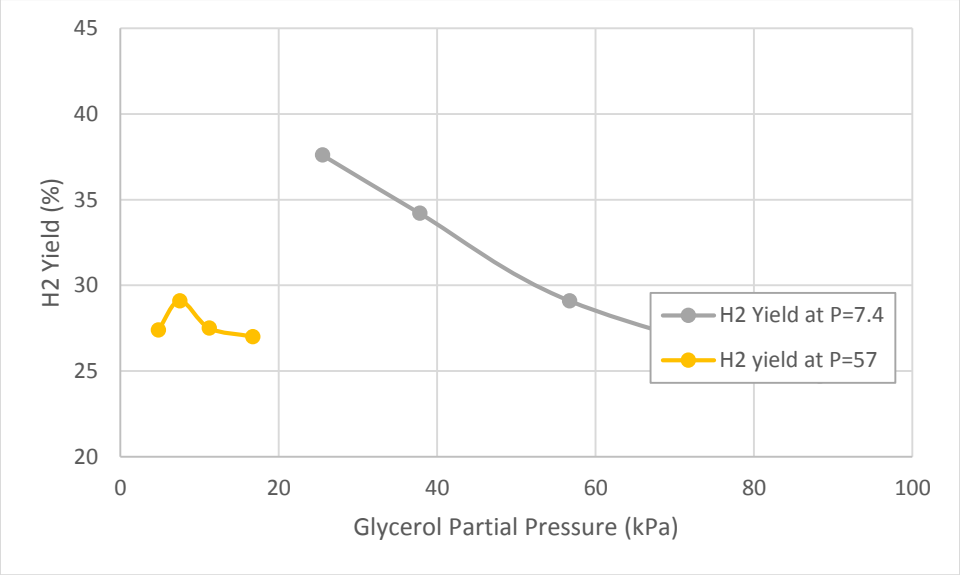

Figure 3-7. Hydrogen Yield vs. Glycerol Partial Pressure at Steam Partial Pressures of 7.4 and 57 psi. From [27]

Similarly, Chiodo et al. [28] determined that operating temperatures above 923K are not favorable for hydrogen production, due to possible catalyst deactivation and glycerol decomposition, which is reported to occur at 1023K. It was also found that lower pressures favor glycerol conversion and hydrogen production. However, since operation below atmospheric pressure is difficult and costly, an operating pressure of 1 bar was suggested as the optimum. Recommendations for process feed composition include

high steam-to-glycerol ratios, which were found to increase glycerol conversion, hydrogen production, and hydrogen selectivity. However, steam conversion was found to decrease with increasing steam-to-glycerol ratios. At a ratio of 9:1, glycerol conversion reaches about 100%. That is the recommended ratio to balance accomplishing high hydrogen production and avoiding excess steam in the effluent. In addition, a low reactant-to-inert feed ratio was found to favor hydrogen production, as predicted by LeChatelier's Principle – the inert gases lower the partial pressure of the reactants and products, shifting the equilibrium toward a greater number of moles. In the case of glycerol reforming, the forward reaction has a large increase in the number of moles.

3.2.5 Heat Transfer

The endothermic reaction within the reactor tubes consumes the heat supplied to the tube from the shell side of the reactor, so there is a temperature gradient along the radius of each tube. The highest temperatures are found at the tube wall and the lowest at the centerline. Thus, assuming the reactor may be isothermal at the desired operating temperature provides a simplified insight into the system, yet a potentially inaccurate one. A temperature gradient is also found across the laminar flow boundary layer around the catalyst pellets. The boundary layer contributes to heat flow resistance from the bulk fluid to the surface of the catalyst, and the conductivity of the catalyst is related to heat flow resistance from the surface of the catalyst into its center. The heat transfer by conduction can be calculated, as seen in Equation (3-14).

$$\dot{Q} = -kA\frac{dT}{dx} \tag{3-14}$$

where $\dot{Q}$ is the rate of heat transfer (W), k is the thermal conductivity [W/(m·K)], A is the area perpendicular to the *x* direction (m^2), and T is temperature (K).

Thermodynamic analysis has been carried out for glycerol steam reforming by the minimization of Gibbs energy. Namely, a study conducted by Adhikari et al. [27] showed that high temperatures, low pressures, and high steam to glycerol feed ratios favored hydrogen production. The operating conditions suggested were an operating temperature of 900K and a molar steam-to-glycerol ratio of 9:1 in order to minimize methane production and inhibit carbon deposition. A study conducted by Wang et al. [29] with a non-stoichiometric approach found that the conversion of glycerol surpassed 95% and the conversion of steam reached approximately 23% at temperatures greater than 773K. Thermodynamic equilibrium was reached at approximately 923K. The production and selectivity of hydrogen was favored with increasing temperatures, while the rate of coke formation decreased.

Using the stoichiometric method, Dieuzeide et al. [30] investigated the behavior of the different reactions involved in the system, and found that glycerol conversion is complete at thermodynamic equilibrium. The two additional contributing reactions were found to be the water-gas shift and methanation reactions. In agreement with Fishtik et al. [31], they found that the methanation reaction is predominant at low temperatures. However, at high temperatures the water-gas shift reaction is the predominant reaction, while the product distribution is not affected by pressure. The study concluded that the aforementioned operating conditions are best for promoting hydrogen production and reducing the formation of coke and methane, while increasing pressures produce the opposite effect. It was also found

that at high temperatures and low steam-to-glycerol feed ratios carbon monoxide production is favored, a phenomenon that should be taken into consideration.

3.2.6 Catalysts

Different studies on glycerol steam reforming have explored the use of different catalysts. Table 3-2 compares the findings of optimal temperature range, reaction rate order with respect to glycerol and steam, and activation energy for each catalyst studied [32]. The temperature ranges favorable for the glycerol steam reforming process are somewhat comparable for different catalysts, however the corresponding activation energy varies greatly. The smallest activation energy reported has been with the use of Ru/Al_2O_3, while the highest has been with the use of Ni/CeO_2. This, however, does not provide conclusive evidence as to which catalyst is the best option for glycerol steam reforming.

Table 3-2. Power-Law Modeling of Glycerol Steam Reforming from Different Studies [32]

Catalyst	T (°C)	Order w.r.t. Glycerol	Order w.r.t. Steam	E_a (kJ/mol)
Ru/Al2O3	350 - 500	1	-	21.2
Pt/C	350 - 400	1	-	60-90
Co/Al2O3	450 - 550	0.1	0.4	67.2
Ni/Al2O3	450 - 550	0.48	0.34	60
Co-Ni/Al2O3	500 - 550	0.25	0.36	63.3
Ni/CeO2	600 - 650	0.233	-	103.4
Ni-ZrO2/CeO2	700	0.3	-	43.4

An important consideration in choosing a catalyst is coke formation. Carbon deposition results in catalyst deactivation by loss of surface area and pore volume.

Additionally, Chen et al. [26] found experimentally that the methanation reaction does take place to a significant extent, producing methane, and therefore any catalyst used for glycerol reforming should also promote the primary reaction of methane steam reforming. Failure to use such a catalyst would not only reduce net hydrogen production, but would also leave large quantities of methane in the reactor effluent, adding difficulty to the post-reaction separation.

3.3 Methane Steam Reforming

Methane steam reforming is a process widely used in industry. Due to the endothermic nature of the primary methane steam reforming reactions, a typical industrial steam reformer has a shell and tube design with long, thin tubes and a burner on the shell side that supplies the process fluid with generous amounts of heat during the reaction [33]. Typical operating conditions from a detailed Johnson Matthey model of a methanol plant reformer [33] are summarized in Table 3-3 in comparison with the suggested operating conditions for glycerol steam reforming.

Table 3-3. Standard Operating Conditions for GSR and MSR

	Feed Temperature (K)	Feed Pressure (bar)	Feed ratio (moles steam:moles glycerol or methane)
Methane Steam Reforming	824.15	21.59	3:1 – 4:1
Glycerol Steam Reforming	823 – 923	1	9:1

For methane steam reforming, molecular diffusion is the limiting type of diffusion, though the Knudsen diffusion coefficient is comparable to the molecular coefficient. When the glycerol process is subjected to a set of operating conditions typical of the methane process, 824 K and 21 bar, both the multicomponent molecular and the Knudsen diffusion coefficients of the key reactant—glycerol—are even smaller. However, optimal glycerol reforming operation is about $1/20^{th}$ of the standard methane reforming operating pressure, which improves molecular diffusion but has no effect on Knudsen. Therefore, in glycerol steam reforming Knudsen diffusion takes over as the limiting factor. Since molecular diffusion also exhibits a stronger dependence on temperature than Knudsen diffusion, the effective diffusivities in a methane steam reforming system will be more temperature dependent than those in a system involving glycerol. Therefore, the relationship between temperature and effectiveness factor will be more pronounced in glycerol reforming due to the even larger impact of temperature on reaction than on diffusion. Thus, this relationship may warrant more consideration than it is given in current methane reforming processes.

Many studies have also looked at the role of heat transfer in the methane steam reforming process. The reaction is highly endothermic, so a continuous supply of heat to the reactor is necessary to maintain reaction rate. The steam reforming of glycerol is less endothermic than the one for methane, but it still consumes a significant amount of heat. Table 3-4 draws a comparison in two potentially important differences—effective diffusivity and reaction enthalpy—between glycerol and methane steam reforming.

Table 3-4. Steam Reforming Characteristics: Glycerol vs. Methane

	Effective Diffusivity of Glycerol/Methane (m^2/s)	Enthalpy of Main Reforming Reaction (kJ/mol)
Methane Steam Reforming	1.30×10^{-6}	+206.1
Glycerol Steam Reforming	9.229×10^{-8}	+128.0

3.4 Reaction Kinetics

Kinetics analysis of glycerol steam reforming in a packed bed reactor with industrial-size catalyst pellets has not been extensively performed in previous studies. The available kinetics interpretations of the

process have generally aimed at modeling the intrinsic reaction rate by using crushed catalyst material to eliminate diffusion limitations. Studies have examined varying operating temperatures and feed steam-to-glycerol molar ratios for specific proposed reaction mechanisms. A kinetic analysis, conducted by Adhikari et al. [34], of glycerol steam reforming using a Ni/CeO_2 catalyst under isothermal conditions used a power law model, as given by Equation (3-15).

$$r_a = k_0 exp\left(\frac{-E}{RT}\right) {C_A}^n \quad (3\text{-}15)$$

Here, E represents the activation energy, T represents the reaction temperature, k_0 represents the reaction constant, R represents the universal gas constant, and n represents the reaction order with respect to glycerol. Water concentration is not taken into account in this model, since it was used in excess. The study's process and reactor conditions used are summarized in Table 3-5.

Table 3-5. Operation Setup Conditions in Study by Adhikari et al. [34]

Operating Conditions	
Catalyst particle size (U.S. sieve)	60-80
Volumetric flow rate (mL/min)	0.25-0.35
Diameter-to-catalyst particle size ratio (d/D_p)	49.1
Catalyst bed–to-catalyst particle size ratio (L/D_p)	142
Operating temperature (K)	873 and 923

A pseudo-homogeneous chemical phase, constant density, constant velocity, constant wall temperature, negligible pressure drop, and ideal gas behavior were assumed. The activation energy and reaction order were found using a nonlinear regression analysis of the power law and were estimated to be 103.4 kJ/mol and 0.233, respectively. Figure 3-8 illustrates the rate of the glycerol steam reforming reaction using the glycerol concentrations from the study at varying temperatures. The figure shows that the reaction rate varies between 5.0×10^{-5} and 1.0×10^{-4} kmol/kg s, when run at 900K. As temperature increases the reaction rate range increases over the same range of glycerol concentration in the feed. An increase in the operating temperature of 200K results in an increase in reaction rate of approximately 4.0×10^{-4} kmol/kg s at a glycerol concentration of 6.0×10^{-9} kmol/s. While this change improves the process outcome, it may not be economically feasible to significantly increase the temperature ad infinitum for a relative increase in the reaction rate.

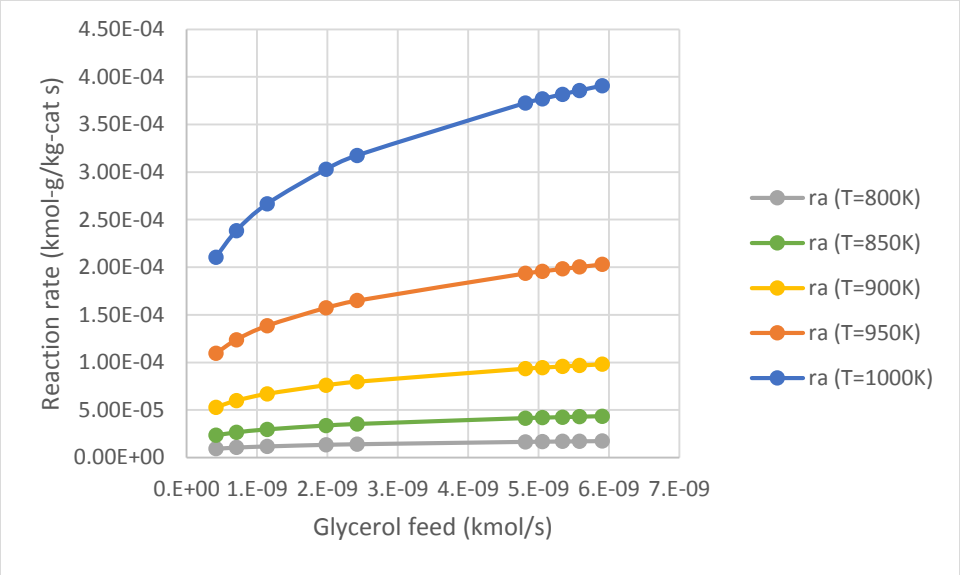

Figure 3-8. Reaction Rate vs. Glycerol Concentration at Different Operating Temperatures. From [34].

Cheng et al. [3] conducted a study investigating glycerol steam reforming in a fixed bed reactor containing bimetallic Ni-Co/Al_2O_3 catalyst. The kinetic study used a high surface area, bimetallic 5% Ni – 10% Co/Al_2O_3 catalyst, a feed with varying steam-to-glycerol ratios in the range of 1.1 to 4, and operating temperatures between 723K and 823K. First, a power law model was used to express the reaction rate, as shown by Equation (3-17).

$$-r_{GSR} = kP_{glycerol}^{\beta}P_{steam}^{\gamma} \tag{3-17}$$

Here r_{GSR} represents the glycerol reforming rate, k represents the rate constant, $P_{glycerol}$ and P_{steam} represent the partial pressures of glycerol and steam, and β and γ represents the order of reaction with respect to each reactant. The activation energy obtained was approximately 60.0 kJ/mol and reaction orders with respect to glycerol and steam were 0.48 and 0.34, respectively. Catalyst performance was evaluated in terms of conversion into gaseous products and yield, as shown in Equations (3-18) and (3-19).

Glycerol conversion: $$X_G = \frac{F_{CO_2}+F_{CO}+F_{CH_4}}{3\,F_{glycerol}} x100 \tag{3-18}$$

H_2 yield: $$Y_{H_2} = \frac{2F_{H_2}}{(8F_{glycerol})+(2F_{water})} x100 \tag{3-19}$$

A Langmuir-Hinshelwood model with dual-site associative adsorption of both glycerol and steam with bimolecular surface reaction was found to provide the most appropriate system representation after a thermodynamic evaluation. The model is dependent on the partial pressures of both glycerol and steam, as well as the system's temperature, as shown in Equation (3-20).

$$R = \frac{k_{rxn}P_G P_W}{(1+K_G P_G)(1+K_W P_W)} \tag{3-20}$$

The model parameters developed at 823K were k_{rxn}=5.570x10^{-7} mol/m^2 s $kPa^{-(\beta+\gamma)}$, K_G=0.2830 kPa^{-1}, K_W=0.0369 kPa^{-1}. Reaction rates were measured over a range of temperatures allowing the development of temperature-dependent parameters.

A recent Major Qualifying Project by John Kent [24] simulated the steam reforming of glycerol in an industrial size fixed bed reactor segment using Computational Fluid Dynamics (CFD) to analyze the process's transport limitations and feasibility. The simulation operated isothermally at a temperature of 823K around atmospheric pressure for a process using a Ni/Al_2O_3 catalyst. The study found that the process undergoes strong internal diffusion resistance, whereas external diffusion limitations are negligible, and low conversion results. Differently shaped catalyst pellets were also considered, and a high surface area shape was recommended in response to finding that the reaction mainly occurs on the outer part of the catalyst. The study used an isothermal kinetic model developed by Cheng et al. [35]. The process was found to have a much lower effectiveness factor than the already low ones observed in methane steam reforming, which was seen as a potential obstacle in operating industrial-scale glycerol steam reforming.

3.5 Heterogeneous Reactions

3.5.1 Modeling Heterogeneous Reaction Systems

Catalysts are ubiquitous in the chemical industry. Effective modeling of catalytic reaction systems is therefore crucial to the rational development of many chemical processes. Heterogeneous catalysis, in which the catalyst is in a different phase—usually solid—from the reactants—generally liquid or gas—involves a complex system that can be difficult to model. The presence of multiple phases introduces two interrelated environments with contrasting properties. Often the solid phase environment is dominated by the presence of chemical reactions, while the surrounding, non-reacting liquid or gas phase is governed largely by its fluid dynamics. Consequently, the behavior of the net system is a function the intricate relationship between the transport phenomena of mass, energy and momentum in the differing phases, usually over complex geometries.

3.5.2 CFD and Pseudo-Homogeneous Models

The field of computational fluid dynamics (CFD) is central to chemical reaction engineering, as the modeling of fluid-phase systems is essential to the study and design of continuous chemical processes. CFD has proven to be very accurate in predicting complex flow fields, extending its applicability to many heterogeneous reaction systems [36]. Typically a pseudo-homogeneous approach is taken, where the catalyst is not explicitly modeled but is accounted for with effectiveness factors that represent its impact on the fluid phase. Experience has shown that this approach is effective when intra-particle mass and heat transfer limitations are small [37]. Previous investigation into glycerol steam reforming in a fixed bed, however, has demonstrated that severe intra-particle diffusion limitations are one of its defining characteristics [24]. Furthermore, the computational demands of a three-dimensional CFD simulation necessitate the use of a very small reactor segment, usually containing one to several catalyst particles [38]. This fails to capture the full profile of chemical and physical behavior along a plant-scale reactor.

3.5.3 Effective Continuum Approach

Effective representation of the catalytic reforming of glycerol with steam demands a modeling strategy that incorporates separate conservation equations describing the catalyst environment. This means that numerous conservation equations from different domains must then be simultaneously solved and coupled. Given the highly non-linear nature of the equations, particularly those representing the catalytic reaction kinetics and the fluid flow in the complex geometry of a packed bed reactor, the numerical solution of this system is very computationally expensive [39].

One method that maintains the integrity of the diffusion-limited catalyst involves keeping the macro- and micro-geometries of the reactor and catalyst separate. Then, the reactor geometry is treated as an effective continuum, where the governing equations in the catalyst domain provide a unique solution at each point along the reactor's length. This two level approach reduces computational demand by simplifying the intricate geometry of a randomly packed reactor bed. The rigorous calculation of a three-dimensional CFD model is eliminated, and in the case of a packed bed reactor the pressure drop may be adequately represented by the Ergun equation [25].

3.6 Finite Element Analysis

3.6.1 The Finite Element Method

The Finite Element Method (FEM) is an engineering tool in which the distribution of a variable in a physical system is approximated by breaking the domain into many small sub-domains, or elements, and finding a simplified solution for each individual element.

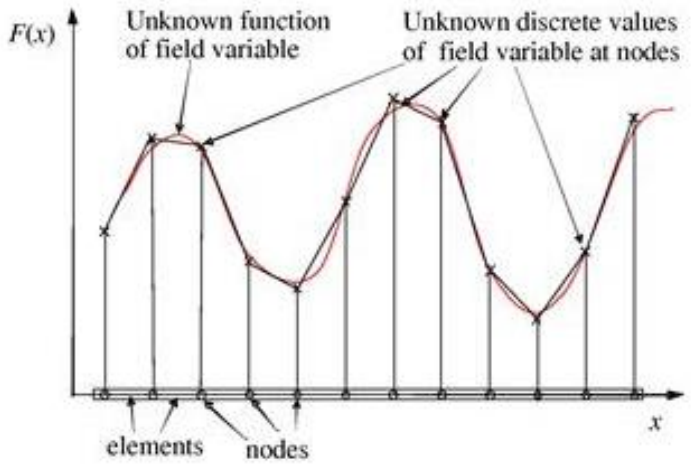

Figure 3-9. Piecewise Linear Function to Approximate Complex Curve [40]

Just as a complex function can be accurately approximated by a piecewise linear function with small enough elements, the physical phenomena in a multidimensional domain may be estimated by a piecewise solution of simple equations over small multidimensional elements with simple geometries.

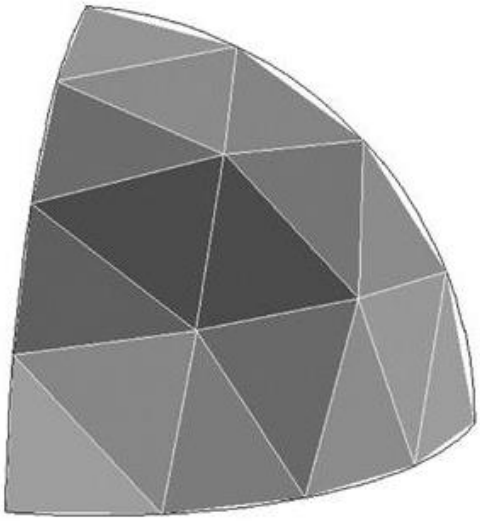

Figure 3-10. Representation of Spherical Domain Discretized into Elements of Simple Geometry [40]

The solution of each element is tied to its surrounding elements, providing the continuous behavior of the variable of focus over the entire domain. With this technique, complex solutions to partial differential equations that are difficult or impossible to describe analytically may be approximated by a system of linear algebraic equations that can be solved by numerical methods.

3.6.2 Multiphysics Simulation

COMSOL Multiphysics® is a solver and simulation software based on the Finite Element Method. The ability of FEM analysis to represent a differential equation as a piecewise algebraic function also makes it ideal for solving systems of differential equations. The governing equations of real, physical events frequently take the form of second-order partial differential equations based on conservation principles. Physical phenomena rarely occur in isolation, and usually a real-life system is a driven by a complicated interplay of mass, energy and momentum transport. COMSOL refers to these as “multiphysics” systems and offers a convenient integration of as many physical phenomena as necessary to create an accurate model.

This setup is well suited to the heterogeneous reaction problem with strong intra-particle diffusion limitations, because the contrasting domains may remain discrete, and the highly non-linear catalytic reaction mechanism is solved numerically by the Finite Element Method.

A comparative study on the simulation of a heterogeneous catalytic reaction found that a one-dimensional multiphysics model can accurately represent some aspects of the reactor, like concentration profiles, when compared to a three-dimensional computational fluid dynamics model [41].

3.6.3 Algorithm for Applying Finite Element Method to Packed Bed Reactor

A recent study proposed a means of applying the effective continuum idea to COMSOL Multiphysics to create a multidimensional model of a packed bed reactor. Here the geometry of the reactor and catalyst were meshed individually and joined with a universal variable coupling. A local micro-mesh representing the catalyst existed at each node of the macro-mesh representing the reactor tube. The distinct domains communicated via mass and heat fluxes, and the areas between nodes were inferred by the interpolation inherent in the Finite Element Method, resulting in temperature and concentration fields for both realms [42].

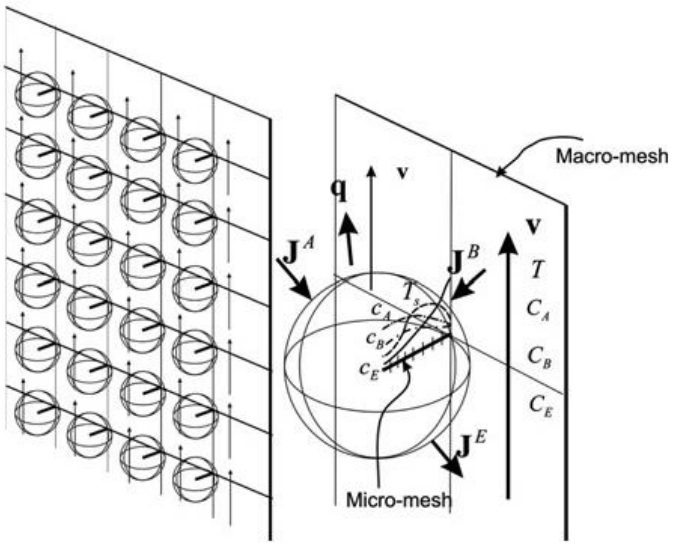

Figure 3-11. Illustration of Geometry Coupling Used to Model a 2D Axisymmetric Packed Bed Reactor [42]

This approach provided the opportunity to account for all of the phenomena which are generally considered important in a heterogeneous reaction system, including:

- An advanced reaction kinetics model
- Density sensitive gas flow
- Intra-particle mass and energy transport
- Mass and heat exchange between catalyst pellet and bulk fluid
- Convection of fluid
- Mass and heat dispersion in the fluid phase
- Heat exchange with the confining walls

while reducing the computation demands of the simulation when compared to a Computational Fluid Dynamics model [42].

4. Methodology

4.1 Overview of Process Simulation and Assumptions

The glycerol steam reforming process was simulated using COMSOL Multiphysics® 4.3b, a software that uses a finite element method (FEM) solver for a multitude of engineering applications. Under the FEM, the model is divided into several elements, and a set of simultaneous algebraic equations is provided to solve the model with a finite number of degrees-of-freedom. COMSOL uses the concept of piecewise polynomial interpolation by connecting elements of a geometry together, allowing even for complex geometries or applications.

The heterogeneous catalytic process was simulated in a one-dimensional (axial direction) packed bed reactor model with spherical catalyst pellets. The model was created to describe axial profiles of radially averaged concentrations and temperatures in a tubular reactor. This was accomplished with a one-dimensional linear reactor model and a two-dimensional catalyst pellet model that represented a unique one-dimensional sphere at each point along the length of the reactor. The two models had discrete domains and were connected by heat and mass fluxes at the surface of the catalyst pellet through variable coupling, as discussed later in this section. The reactor geometry is shown in the left diagram in Figure 1, and the catalyst pellet geometry is shown in the right diagram in Figure 4-1.

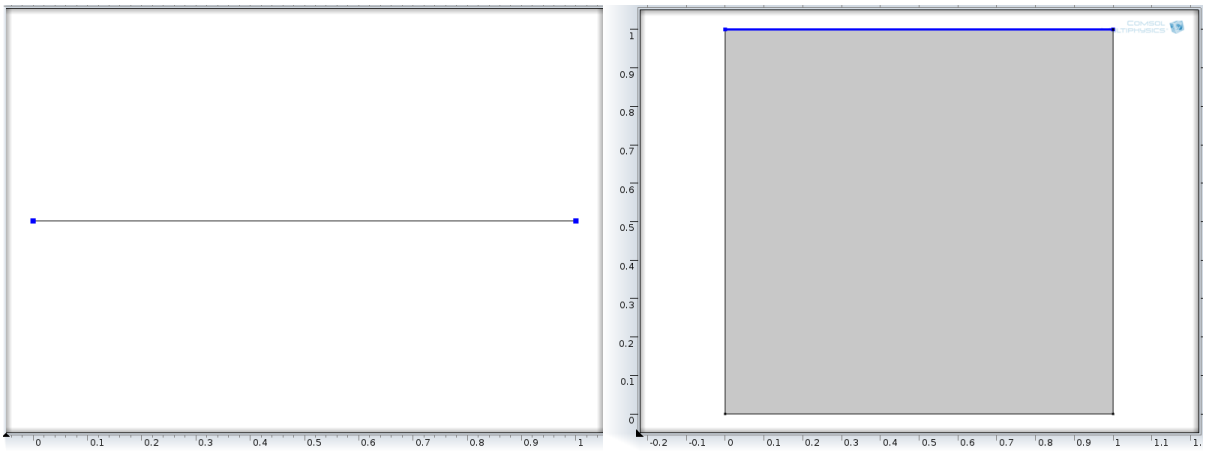

Figure 4-1. Reactor (left) and Catalyst Pellet (right) Geometries

The Transport of Diluted Species and Heat Transfer physics nodes were applied to both the reactor and pellet models to describe the system's mass and energy transfer. At each point along the reactor length a unique solution to the pellet boundary value problem was generated. The boundary condition settings for the reactor included inflow on the left extremity and outflow on the right extremity, and a reaction node to describe the contribution of the catalyst domain and the wall heat supply. The boundary condition settings for the catalyst pellet included flux into the pellet on the top boundary of the model, representing the interface of the catalyst surface with the reactor fluid, insulation on the three other model boundaries not connected to the reactor, and a reaction node to describe the consumption and generation of energy and of each material component. Meanwhile, a Coefficient Form PDE node was added to the reactor domain so that the Ergun equation could be manually entered. Global parameters and variables were added to describe operating conditions, fluid properties, mass and heat transfer correlations, and diffusion coefficients, as seen in Appendices A and B.

The main reaction occurring during the process, leading to the production of hydrogen, is shown in Equation (4-1).

$$C_3H_8O_3 + 3H_2O \rightarrow 3CO_2 + 7H_2 \quad (4\text{-}1)$$

The reaction rate expression was entered as a global variable and the reaction with respect to each component involved was applied to the reactor and catalyst pellet models. The fixed bed reactor and catalyst pellet variables were coupled to connect the two domains. Coupling the two models allowed for integration of the reaction that occurs in the catalyst pellet over the length of the reactor tube. To obtain the boundary condition, $C_{i,bulk}$, for the catalyst pellets at each point along the reactor, the composition of each component in the reactor model was extruded and combined with the transform of the pellet boundary, as illustrated in Figure 4-2.

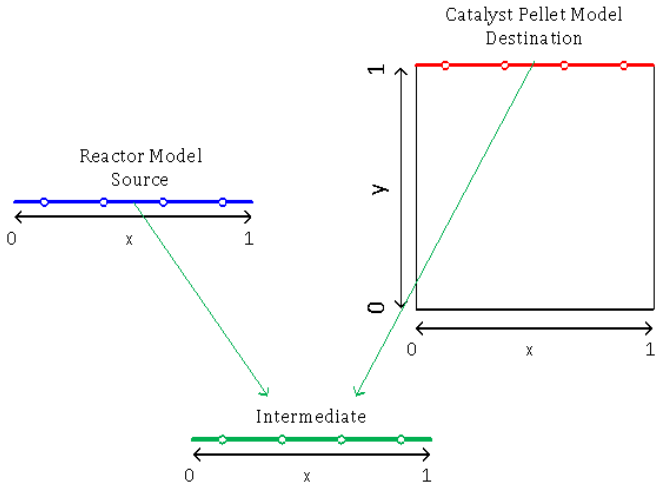

Figure4-2. Variable Coupling - Catalyst Pellet Boundary

Similarly, in order to obtain the flux boundary condition, N_i, for the tube reactor, the composition over the domain of the pellet was extruded and combined with the transform of the reactor boundary, as illustrated in Figure 4-3.

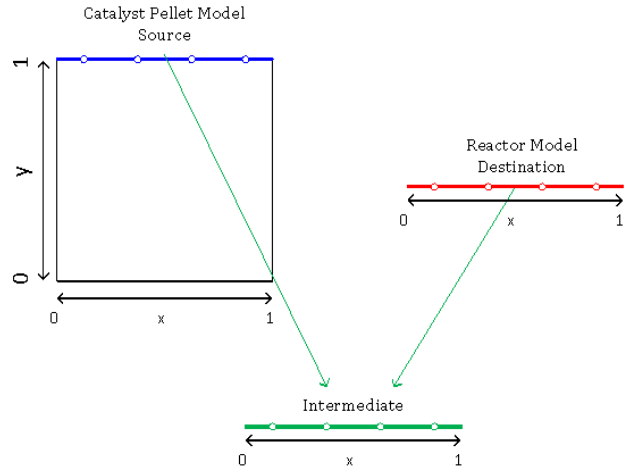

Figure 4-3. Variable Coupling - Reactor Boundary

The same process was used to couple the energy systems of the two domains by extruding the temperature at the surface of the catalyst to the reactor and vice versa, allowing the calculation of heat fluxes across the corresponding boundaries.

Under the Transport of Diluted Species node, COMSOL computed concentration profiles for the four components in the above reaction. The profiles were based on the following material balances accounting for reaction, convection and Fickian diffusion in the spherical catalyst domain, as shown in Equation (4-2).

$$\frac{1}{r^{*2}}\frac{d}{dr^*}\left(D_{ip}r^{*2}\frac{dC_{pi}}{dr^*}\right) = -\sum_{j=1}^{NR}\alpha_{ij}r_j \tag{4-2}$$

where , r^* represents the radial position within the pellet (m), D_{ip} represents the diffusivity of component i in the pellet (m^2/s), C_{pi} represents the concentration of component i in the pellet (mol/m^3), α_{ij} represents the stoichiometric coefficient of component i in reaction j, and r_j represents the rate of reaction j (mol/m^3s). Equation (4-3) describes the concentration profile in the reactor's bulk fluid domain.

$$\frac{1}{A_C}\frac{dF_i}{dz} - a_p(1-\varepsilon_b)k_g\left(c_{pi}^s - c_i\right) = D_{ea}\frac{d^2C_i}{dz^2} \tag{4-3}$$

where A_C represents the cross-sectional area of the reactor tube (m^2), F_i represents the molar flow rate of component i (mol/s), a_p represents the ratio of the pellet's surface area to volume (m^{-1}), $\varepsilon_b$is the bed void fraction, k_g is the particle-to-fluid mass transfer coefficient (m/s), c_{pi}^s is the concentration of component i at the pellet domain's surface (mol/m^3), c_i is the concentration of component i in the reactor domain (mol/m^3), and D_{ea} is the reactor's axial dispersion coefficient (m^2/s).

Coupling Equations (4-2) and (4-3) with the Ergun equation, the pressure drop in a packed column is described as shown in Equation (4-4).

$$\frac{dP}{dz} = -\frac{(1-\varepsilon_b)G}{d_p\varepsilon_b^3\rho_{feed}}\left[150\frac{(1-\varepsilon_b)\mu_f}{d_p} + 1.75G\right]\frac{\rho_{feed}}{\rho} \tag{4-4}$$

where P represents pressure (Pa), z represents the axial coordinate of the reactor (m), ε_b represents the average bed voidage ($\frac{volume\ of\ reactor\ -\ volume\ of\ catalyst\ particles}{volume\ of\ reactor}$), G represents the mass flux (kg/m^2s), d_p represents the catalyst pellet diameter (m), μ_f represents the fluid viscosity (kg/m s), and ρ is the fluid density (kg/m^3). The bed voidage, ε_b, was provided by de Klerk [43], who calculated average bed voidages for various particle-to-column ratios of tubular columns packed with spherical catalysts.

In order to satisfy the ideal gas law, where

$$C_{tot} = \frac{P}{RT} \tag{4-5}$$

in the presence of a net molar increase in the reaction stoichiometry, an average molecular weight approach [44] was applied to the COMSOL simulation by allowing

$$C_i = y_iC_{tot} = y_i\frac{\rho}{\overline{MW}} \tag{4-6}$$

This permitted F_i to be rewritten as $\frac{G}{\overline{MW}}y_i$ rather than C_iuA_c, explicitly adjusting velocity as a result of the composition's effect on average molecular weight.

To satisfy the conservation of mass in the system, where

$$\sum y_i = 1 \tag{4-7}$$

the mass conservation equation was applied to three of the four chemical species in the reactor domain, and the fourth was determined indirectly from the total concentration according to the ideal gas law.

Also, to preserve the units of the material balance equation, a term for the initial concentration of each species before expansion of the gas was defined:

$$C_i^* = y_i C_0 \tag{4-8}$$

which allowed each individual concentration to vary as the total concentration did according to the ideal gas law:

$$C_i = C_i^* \frac{C_{tot}}{C_O} \tag{4-9}$$

Adding these definitions to the material balance on the reactor domain yielded:

$$-\frac{G}{\overline{MW} C_O}\frac{dC_i^*}{dx} + \left[\frac{GC_i^*}{C_O \overline{MW}^2}\frac{d\overline{MW}}{dx} + \alpha_L a_p (1-\varepsilon_B) k_g \left(C_{p,i}^S - C_i^* \frac{C_{tot}}{C_O}\right)\right] = -\frac{D_{ea}}{\alpha_L}\frac{C_{tot}}{C_O}\frac{d^2 C_i^*}{dx^2} \tag{4-10}$$

Where $\overline{MW}$ represents the fluid's average molecular weight (g/mol), C_O represents the total feed concentration (mol/m^3), C_i^* represents the initial concentration of each component i in the reactor before expansion of the gas (mol/m^3), α_L is a unit correction (1m^{-1}), k_g represents the particle-fluid mass transfer coefficient (m/s), $C_{p,i}^S$ represents the concentration of each component i at the surface of the catalyst pellet (mol/m^3), and D_{ea} represents the axial dispersion coefficient (m^2/s). The accompanying boundary conditions are as shown in Equations (4-11) and (4-12).

$$C_i^*(x=0) = y_{i,O} C_O \tag{4-11}$$

$$-\frac{D_{ea}}{\alpha_L}\frac{C_{tot}}{C_O}\frac{d^2 C_i^*}{dx^2}(x=1) = 0 \tag{4-12}$$

Similarly, in the catalyst pellet domain:

$$-\frac{\delta}{\delta y}\left(D_{ip}\frac{\delta C_{ip}}{\delta y}\right) = \left[\alpha^2 \sum_j \alpha_{ij}\rho_s r_j + \frac{2}{y} D_{ip}\frac{\delta C_{ip}}{\delta y}\right] \tag{4-13}$$

The accompanying boundary condition is shown in Equation (4-14).

$$-D_{p,i}\frac{\delta C_{p,i}}{\delta y}(y=1) = \alpha k_g\left(C_{p,i}(y=1) - C_{i,bulk}\right) \tag{4-14}$$

The simulation was run with both isothermal and non-isothermal conditions, as discussed below. When applying non-isothermal conditions to the system, under the Heat Transfer physics node, a temperature profile on the reactor domain gives:

$$\frac{2\alpha_L}{R} q_w + \frac{k_{ea}}{\alpha_L}\frac{d^2 T_f}{dx^2} + \alpha_L a_p (1-\varepsilon) h_g\left(T_s^S - T_f\right) = \rho \hat{C}_{pf} u \frac{dT_f}{dx} \tag{4-15}$$

Where q_w represents the wall heat flux (W/m^2), k_{ea} represents the axial thermal dispersion coefficient (W/m.K), h_g represents the particle-fluid heat transfer coefficient (W/m^{2}K), T_s^S represents the catalyst temperature at its surface (K), T_f represents the fluid temperature (K), $\hat{C}_{pf}$ represents the fluid heat

capacity (J/kg.K), and u represents the linear fluid velocity (m/s). The accompanying boundary conditions are shown in Equations (4-16) and (4-17).

$$T_f(x=0) = T_{in} \tag{4-16}$$

$$-\frac{k_{ea}}{\alpha_L}\frac{dT_f}{dx}(x=1) = 0 \tag{4-17}$$

Similarly, in the catalyst pellet domain:

$$0 = \frac{d}{dy}\left(k_p \frac{dT_s}{dy}\right) + \left[\alpha^2 \sum_i \rho_s\left(-\Delta H_{r,i}\right) r_i + \frac{2}{y} k_p \frac{dT_s}{dy}\right] \tag{4-18}$$

Where k_p represents the thermal conductivity of the catalyst pellet (W/m.K), T_s represents the temperature of the catalyst sphere (K), and $\Delta H_{r,i}$ represents the enthalpy of the reaction (J/mol). The accompanying boundary condition is shown in Equation (4-19).

$$-k_p \frac{dT_s}{dy}(y=1) = \alpha h_g\left(T_s^s - T_f\right) \tag{4-19}$$

Given the extent and depth of the studies done on glycerol steam reforming to date, some assumptions were adopted in order to create a simulation simultaneously studying the kinetics and thermodynamics of the system.

1. The process of glycerol steam reforming is predominantly characterized by the chemical reaction between glycerol and water (Equation 4-1), and therefore additional side reactions were neglected in the process simulation.
2. Given the process's high temperatures and low pressures, the fluid was assumed to behave as an ideal gas.
3. The system could be appropriately represented by a 1D model of the packed bed reactor and a 2D model of the catalyst pellets; i.e. radial variations in the reactor tube could be ignored.

The kinetics model adopted to represent the process was obtained from a study conducted by Cheng, Foo, and Adesina using a bimetallic Co-Ni/Al_2O_3 catalyst [3]. This study was chosen because it reported a kinetics model dependent on both glycerol and steam partial pressures as well as temperature. However, some simplifying assumptions adopted in the study were not extended to this project, including a pseudo-homogeneous chemical phase, constant fluid density, and constant bulk fluid velocity. Instead, the assumptions used in developing this simulation included: constant heat flux into the reactor tube, the refining of glycerol as a preparation step to the actual steam reforming, and the independence of the reaction kinetics from Cheng et al. [3] on catalyst surface area, as explained in greater detail below.

The catalyst's thermal conductivity and density were obtained from a Johnson Matthey model of a methanol plant steam reformer at typical operating conditions that used a similar catalyst [33]. The kinetics model chosen for the simulation was a Langmuir-Hinshelwood model with dual-site associative adsorption of both glycerol and steam with a bimolecular surface reaction that was dependent on the partial pressures of both glycerol and steam, as well as temperature, as shown in Equation (4-20).

$$R = \frac{k_{rxn} P_G P_W}{(1+K_G P_G)(1+K_W P_W)} \tag{4-20}$$

The kinetics parameters were also obtained from Cheng et al., with the following empirically derived parameters for temperature dependence, based on the Arrhenius and Van't Hoff equations [3][45]:

$$k_{rxn} = 0.010471 \cdot e^{\left(\frac{-69360}{RT}\right)} \tag{4-21}$$

$$K_G = 8.2125 \cdot 10^{-3} \cdot e^{\left(\frac{2931.4}{T}\right)} \tag{4-22}$$

$$K_W = 0.379 \cdot e^{\left(\frac{-1904.4}{T}\right)} \tag{4-23}$$

This gave a reaction rate based on catalyst surface area (mol/m^{2}s), so the conservation equations used in this study required conversion of the expression to a volume basis:

$$r = \rho_p \cdot SA_p \cdot R \tag{4-24}$$

where ρ_p is the catalyst pellet's density (kg/m^3) and SA_p is its surface area (m^2/kg), giving the adjusted reaction rate, r, in mol/m^{3}s.

The kinetic study used a high surface area bimetallic 5% Ni – 10% Co/Al_2O_3 catalyst [3]. However, given the diffusion-limited nature of the process, an industrial reactor would perform better with a smaller surface area alumina support. The coarser support would allow for a slower maximum reaction rate, yet would have larger pores and thus would improve internal mass transfer, the limiting factor for the actual reaction rate. Furthermore, such a catalyst support would be ostensibly less costly. Therefore, this project's simulations used the same grade of alumina as Hou and Hughes in their kinetic study of methane steam reforming [46]. Since the kinetics of Cheng et al. were given on a surface area basis, it was assumed that they would not change for a support with a different surface area.

4.1.1 Reversible Reaction

Once the reaction rate expression was incorporated, thermodynamic data and reaction stoichiometry provided a theoretical, temperature-dependent equilibrium constant whose inclusion allowed for reversibility of the model's chemical reaction. Mathematically, this was accomplished by multiplying the reaction expression by the factor shown in Equation (4-25).

$$\left(1 - \frac{P_{CO_2}^3 P_{H_2}^7}{K_a P_G P_W^3}\right) \tag{4-25}$$

where K_a is the temperature-dependent equilibrium constant and is defined in Equation (4-26).

$$K_a = 5.698 \cdot 10^{27} \cdot e^{\left(\frac{-15396}{T}\right)} \tag{4-26}$$

This reversibility was included for accuracy, although it ended up having no significant impact, as the equilibrium position of the reaction lies at completion of the forward reaction at the high temperatures used.

4.2 Isothermal Conditions

Isothermal conditions were employed initially to investigate the relationship between the chemical reaction and the dispersion in a fixed bed reactor. Since glycerol steam reforming was expected to be affected by diffusion limitations, the impact of diffusion on the feasibility of the process was explored in the absence of heat transfer effects on the process. The major reaction involving glycerol and steam to produce hydrogen is presumably favored over other possible reactions, such as the water-gas shift and methanation reactions, under the operating conditions used in this simulation.

4.2.1 Operating Conditions

Chen et al. [26] showed both theoretically and experimentally that hydrogen production is favored by a high molar ratio of steam to glycerol. Others have shown that high steam-to-glycerol ratios also prevent catalyst deactivation via carbon deposition, with a 9:1 ratio universally regarded as optimal [28]. Therefore, this project considered a feed composition of 90% steam and 10% glycerol, assuming that impurities in the crude glycerol either only exist in trace quantities or may be removed prior to the reaction.

Chen et al. [26] also determined that high temperatures and low pressures improve hydrogen production. Yet Chiodo et al. [28] discovered that temperatures above 923K cause catalyst deactivation and at 1023K glycerol decomposes before reaching the catalyst, so a temperature of 823K was chosen for the preliminary isothermal reactor model. Meanwhile, the feed pressure was set to 2atm to allow for pressure drop along the reactor without the need for a vacuum.

4.2.2 Reactor Sizing

The reactor column was initially established as a 1m long tube with a 0.15m diameter packed with spherical catalyst pellets of 0.0254m diameter, values on the same scale as existing steam reformers, but otherwise arbitrary.

4.2.3 Physical Properties - Fluid

The governing differential equations that were solved in this study required values for the viscosity and diffusivity of the gaseous process stream, as well as a mass transfer coefficient for the particle-fluid interface of this heterogeneous system. The Reichenberg correlation [47] was used to estimate the fluid viscosity. Since this method is dependent on fluid temperature and composition, an average viscosity was determined based on the composition occurring at a reaction extent of 30%. Meanwhile, the following correlation from Edwards and Richardson [47] provided the fluid's axial dispersion:

$$\frac{1}{Pe} = \frac{0.73\varepsilon}{Re \cdot Sc} + \frac{0.5}{1+\frac{9.7\varepsilon}{Re \cdot Sc}} \tag{4-27}$$

$$D_{ea} = \frac{u \cdot d_p}{Pe} \tag{4-28}$$

Where ε is the bed void fraction, Re is the Reynolds number, Sc is the Schmidt number, u is the linear fluid velocity (m/s), d_p is the pellet diameter (m) and D_{ea} is the axial dispersion coefficient (m^2/s).

Similarly, the particle-fluid mass transfer coefficient was obtained from the following correlation from Wakao and Funazkri [20]:

$$Sh = 2 + 1.1Re^{0.6}Sc^{1/3} \tag{4-29}$$

$$k_g = \frac{Sh \cdot D_{AB}}{d_p} \tag{4-30}$$

Where D_{AB} is the average binary diffusivity within the particle (m^2/s) and k_g is the particle-fluid mass transfer coefficient (m/s).

4.2.4 Physical Properties - Catalyst

The density of the 5% Co – 10%Ni/Al_2O_3 catalyst pellets was assumed to be the same as a 15%Ni/Al_2O_3 catalyst from a Johnson Matthey methanol plant steam reformer model [33] since nickel and cobalt have nearly identical densities.

4.2.5 Effective Diffusivity

In heterogeneous catalytic reactions, the reactants must adsorb onto the catalyst before the reaction may proceed. With a macroporous solid such as the Ni-Co/Al_2O_3 used in this study, the majority of the catalyst's available surface area is on the walls of the material's pores. Since there is no bulk motion within these catalyst pores, reactant molecules only reach the active sites within the catalyst by diffusion. Thus, the reaction may be limited by the rate of this internal diffusion. Inside the pores, molecular diffusion is complemented by the effect of the reactants colliding with the pore walls, an occurrence known as Knudsen diffusion. The effects of these two types of internal diffusion can be combined into a single effective diffusivity. Since diffusion coefficients represent resistances to mass transfer, the effective diffusivity is related to the sum of the inverses of the molecular and Knudsen diffusivities:

$$\frac{1}{D_{eff}} = \frac{1}{D_{AB}} + \frac{1}{D_K} \tag{4-31}$$

The Fuller-Schettler-Giddings correlation provided binary diffusivities between each pair out of the four reacting species in the model, while an approximate solution to the Stefan-Maxwell diffusion equations converted these to multicomponent molecular diffusion coefficients for each component within the system [21][22]. Like the fluid viscosity, these diffusivities depended on the molar composition of the system, so a molar makeup based on a 30% reaction extent was assumed to represent an average composition.

4.2.6 Summary of Conditions for Isothermal Model

Reactor Operating Conditions			
Temperature (K)	Pressure (kPa)	Steam to Glycerol Ratio	Linear Velocity (m/s)
823	202.65	9:1	10

Effective Diffusivity (m^2/s)			
$C_3H_8O_3$	H_2O	CO_2	H_2

4.63×10^{-7}	1.11×10^{-6}	6.59×10^{-7}	3.06×10^{-6}

Catalyst Pellet Properties
Density (kg/m^3)
1947

Fluid Properties		
Viscosity (kg/m.s)	Particle-Fluid Mass Transfer Coefficient (m/s)	Axial Dispersion Coefficient (m^2/s)
3.93×10^{-5}	0.82266	0.12671

4.3 Non-Isothermal Conditions

4.3.1 Operating Conditions

The same operating conditions and kinetics model described above were used to create a process simulation under non-isothermal conditions. The Heat Transfer in Solids physics node was applied to both the reactor and pellet models. The temperature boundary condition in both the reactor and pellet models was obtained similarly as described above, by extruding and transforming variables from one model and combining them with the domain of the other model. In the reactor model, the inlet temperature was specified as the feed temperature, and an outflow condition was applied to the reactor outlet. In the pellet model, the three sides of the 2D model not touching the reactor were insulated, the top side touching the reactor had an incoming heat flux with external temperature of T_{bulk}, and the initial condition was set to T_{feed}.

4.3.2 Thermal Properties of Fluid and Catalyst

The thermal conductivity of the fluid was estimated with the Wassilweja equation [47], while the heat capacity was determined by a special correlation for high temperature heat capacities [9]. Meanwhile, the conductivity and heat capacity of the solid catalyst came from the Johnson Matthey model of a methanol plant reformer [33].

Heat transfer correlations obtained from Edwards and Richardson [48] then became:

$$\frac{1}{Pe_{ah}} = \frac{k_p/kg}{Re \cdot Pr} + \frac{0.73\varepsilon}{Re \cdot Pr} + 0.5 = \frac{\rho u c_p d_p}{k_{ea}} \tag{4-32}$$

Where ε is the bed void fraction, Re is the Reynolds number, Pr is the Prandtl number, u is the linear fluid velocity (m/s), d_p is the pellet diameter (m) and k_{ea} is the fluid's axial thermal conductivity (W/m.K).

4.3.3 Temperature-Dependent Properties

Expressions were formulated to estimate the temperature dependence of the fluid viscosity, heat capacity and thermal conductivity, as well as the effective diffusivity of each component. While these parameters

each varied with temperature and composition, given the highly endothermic nature of the reaction it seemed wise to incorporate the effect of temperature on these parameters. Viscosity, heat capacity and thermal conductivity of the fluid all varied nearly linearly with T. Effective diffusivity, however, consisted of two different models for diffusion with different relationships to temperature. With the catalyst and operating conditions utilized in this study, however, Knudsen diffusion was the dominant mode of transport in the pellet. Therefore, the variance of Knudsen diffusion with $T^{0.5}$ was applied to the effective diffusivities as a good approximation:

$$\mu = 5.27x10^{-8} \cdot T - 4.1x10^{-6} \tag{4-33}$$

$$C_p = 0.4122 \cdot T + 1{,}915.3 \tag{4-34}$$

$$k_f = 1.355x10^{-4} \cdot T + 0.0119 \tag{4-35}$$

$$D_{ip,i} = M_i \cdot T^{0.5} \tag{4-36}$$

Here μ is the fluid viscosity (kg/m.s), T is the temperature of the fluid (K), C_p is the fluid heat capacity (J/kg.K), k_f is the thermal conductivity of the fluid (W/m.K), $D_{ip,i}$ is the effective diffusivity of component i (m^2/s), and M_i is a calculated constant for each component.

4.3.4 Heat Flux

To model the effect of external heating from a burner, a constant heat flux, q_w, was added to the source term in the heat equation for the reactor domain:

$$Q = \frac{\alpha_L \cdot A_p \cdot h_g \cdot (1 - por_b) \cdot (T_{surf} - T_{feed}) + 2}{R_r \cdot q_w \cdot \alpha_L} \tag{4-37}$$

where Q is the heat source, A_p is the surface area of particles per unit volume (m^{-1}), h_g is the particle-fluid heat transfer coefficient (W/m^2K), por_b is the bed porosity, R_r is the reactor radius (m), q_w is the wall flux into the reactor (W/m^2), and T_{surf} and T_{feed} are the pellet surface and feed temperatures, respectively (K).

4.4 Process Conditions and Reactor Design

The process was simulated under different operating conditions, feed properties, and reactor design specifications. Each parameter was closely studied in order to determine optimal conditions for performing glycerol steam reforming, as well as optimal packed bed reactor dimensions, to allow for maximum hydrogen yield.

While existing research has made recommendations regarding operating temperature and pressure [26], this model was used to analytically examine the effects of these parameters on the process. Likewise, variations in feed velocity and wall heat flux were observed to allow for preliminary process optimization suggestions, while reactor size and dimensions, as well as catalyst pellet size, were also evaluated for reactor design information.

When evaluating reactor design variables, an understanding of the relationship between reactor and catalyst pellet dimensions and bed voidage was needed. Four random packing modes with spherical

catalysts are distinguished [48]. The modes include very loose, loose, poured, and dense random packing, with voidage values of 0.44, 0.40-0.41, 0.375-0.391, and 0.359-0.375 respectively. While this study analyzed the effects of varying column-to-particle diameter ratios, the resulting voidages entered into the equations represented average values calculated by de Klerk [43], and did not acknowledge the potentially significant role of packing mode.

5. Results and Discussion

5.1 Diffusion Limitation and Effectiveness Factor

It is known empirically that in industrial steam reforming the reaction rate is proportional to the outer (geometric) surface area of the catalyst particles, rather than the much larger true surface area that includes the pore walls within the catalyst support [33]. This indicates that the intrinsic reaction rate proceeds much faster than the diffusion of reactants into the pellet's pores, limiting the active region of each catalyst particle mainly to its exterior.

It was suspected that steam reforming of glycerol would display similar behavior [24], and the results of this simulation confirm that. At a suggested set of optimal conditions—T_{in}=823K, P_{in}=2.02kPa, q_w=21000W, u=5m/s, which gives a nearly isothermal system—glycerol concentration and reaction rate within the catalyst domain were both limited to the outside of the pellet. The graphs shown in Figures 5-1 and 5-2 plot glycerol concentration and reaction rate as a function of scaled radial position within a spherical catalyst particle at the reactor inlet and at a point one meter down the length of the tube.

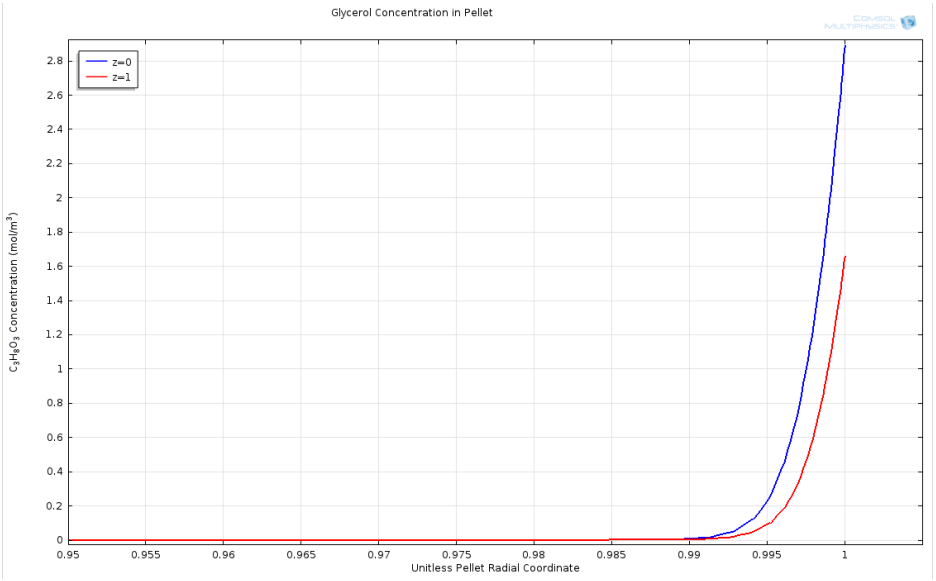

Figure 5-1. Glycerol Concentration as a Function of Radial Position in Catalyst Pellet

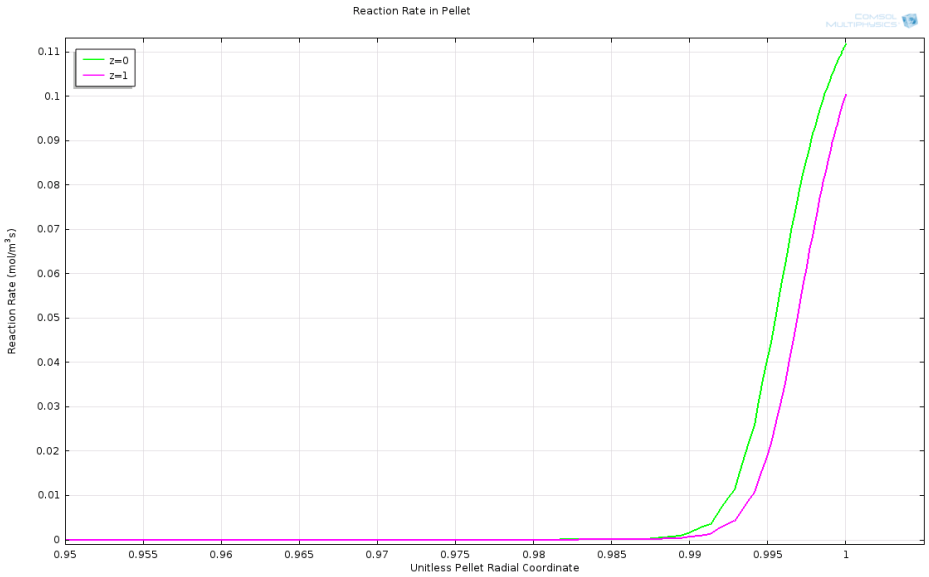

Figure 5-2. Reaction Rate as a Function of Radial Position in Catalyst Pellet

In these plots, the radial coordinate is scaled to run from 0 to 1 to illustrate the fact that all of the glycerol exists almost entirely in the outermost 1% of the sphere volume, regardless of the axial position of the sphere. Therefore, the chemical reaction takes place in the corresponding area of the catalyst pellet where glycerol molecules diffuse to, which explains the close similarity between Figures 5-1 and 5-2.

5.2 Temperature

5.2.1 Temperature and Effectiveness Factor

Significantly low effectiveness factors mean that the majority of the catalyst is wasted, therefore, possible means of improving catalyst use were examined. Here, the relationship between temperature and effectiveness factor is discussed. The plot in Figure 5-3 shows the rate of reaction at inlet conditions as a function of a scaled radial coordinate for three different inlet temperatures, in units of Kelvin.

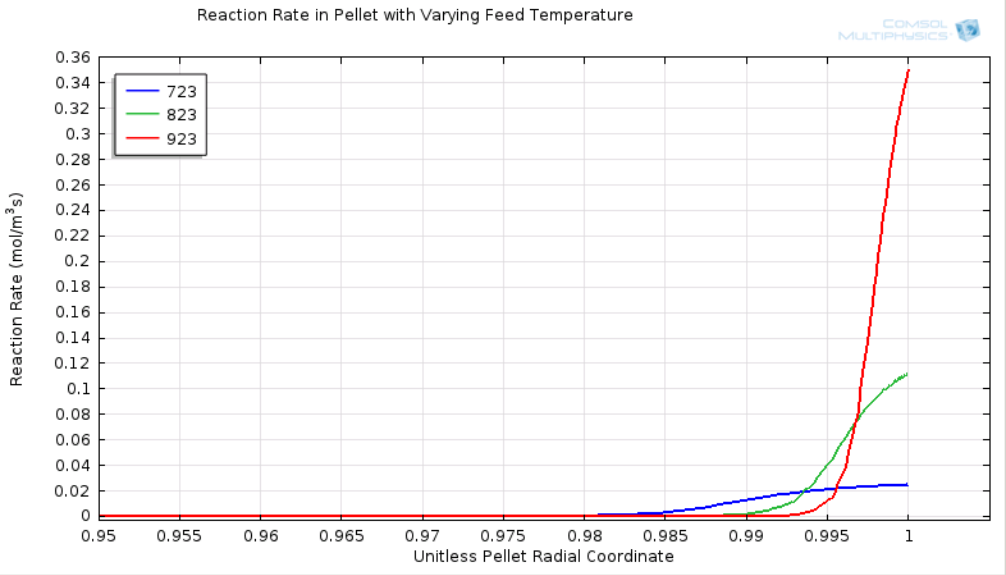

Figure 5-3. Reaction rate as a function of scaled radial coordinate with varying operating temperature

This figure shows the expected behavior of chemical activity becoming increasingly limited to the perimeter of the catalyst with increasing temperature. Furthermore, the trend displayed by this simulation confirms the reason for the low effectiveness factor for glycerol steam reforming being that the rate of reaction dominates the rate of diffusion into the pellet. The maximum reaction rate at the pellet surface shows a strong dependence on temperature, and the increased reaction rate at higher temperature leaves less time for the reactants to diffuse into the pellet's interior before being consumed. This explains why higher rates correspond to smaller zones of nonzero reaction in the interior of the sphere.

The effect of temperature on reaction rate is expected, although it must be noted that diffusion also increases with temperature. Thus, the observed trend in effectiveness factor is not simply the result of the relationship between reaction rate and operating temperature. Rather, the trend shows that the reaction rate increases with temperature to a greater extent than diffusion does. This imbalance is logical, as Knudsen diffusion is the dominant mode of internal mass transfer in this process. Knudsen diffusion varies in proportion to the square root of temperature, whereas the reaction kinetics, with a temperature dependence based on the Arrhenius Equation, dictate that the reaction rate varies with temperature exponentially. Nevertheless, values of the reaction rate and the effective diffusivity as functions of temperature at inlet composition are shown in Table 5-1 for comparison.

Table 5-1. Reaction Rate and Effective Diffusivity at Varying Operating Temperatures

Temperature (K)	Reaction Rate (mol/m^{3}s)	Glycerol Effective Diffusivity (m^2/s)
723	0.02465	4.277 x 10^{-7}
823	0.11194	4.625 x 10^{-7}
923	0.35178	4.949 x 10^{-7}

5.2.2 Temperature and Conversion

While improvements in effectiveness factor are ostensibly desirable in an industrial process, lowering operating temperature does not present an advantage in this process. In fact, the improved reaction rate brought on by higher temperatures vastly outweighs the benefit of having larger active catalyst area when operating at lower temperatures. Figure 5-4 shows the effect of temperature on process efficiency, represented by glycerol conversion [18], shown in Equation (5-1).

$$Conversion = \frac{F_{i,in} - F_i}{F_{i,in}} \tag{5-1}$$

Conversion is an important quantity, because not only does higher conversion equate to increased hydrogen production, but under the assumption that the product stream will undergo a separation procedure to isolate the hydrogen, it also directly impacts the difficulty of the next step in the overall process.

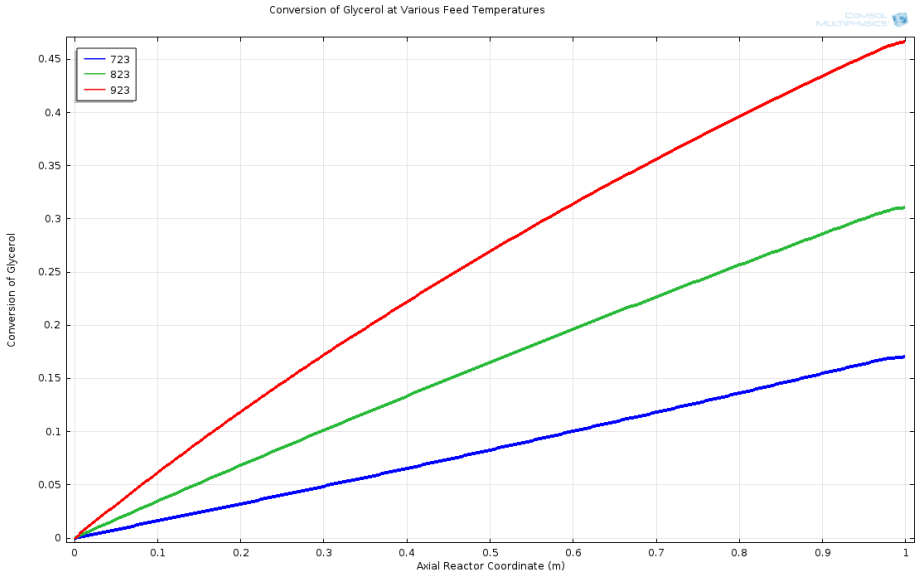

Figure 5-4. Glycerol Conversion along the Reactor with Varying Operating Temperatures

Figure 5-4 shows glycerol conversion as a function of axial position along a one meter long reactor tube at three different feed temperatures. Conversion at the reactor effluent nearly triples when the feed temperature is increased from 723K to 923K, despite the decrease in effectiveness factor, showing that the positive effect of temperature on reaction rate overpowers the negative impact it has on effectiveness factor. It appears that the inherent diffusion-limited nature of this process, as with methane steam reforming, is not a major limiting factor.

5.3 Wall Heat Flux

5.3.1 Heating the Feed vs. Heating the Reactor

Since glycerol reforming is highly endothermic and benefits from high temperature operation, a similar setup to the one typically used for methane steam reforming should be considered. Applying heat to the

reactor as well as the feed in order to balance the energy consumption of the chemical reaction is sensible, so as to maintain thermodynamically favorable conditions throughout the reactor. The distribution of heat application between the feed and the actual reactor, however, is a process variable that is free to be manipulated.

Ideal operation involves adding a significant amount of heat directly to the reactor, so that despite the heat sink created by the reacting catalyst pellets, the fluid and catalysts both increase in temperature down the length of the reactor. The reason for this is that high glycerol conversion is a desirable process quality, so an effective reactor will have a significantly lower concentration of glycerol near the end of the tube. Steam is in excess, so glycerol is the limiting reactant, and therefore a low glycerol partial pressure is crippling to the reaction rate. Thus, a higher temperature is more useful near the effluent side to drive the reaction toward completion when glycerol becomes less abundant.

Two different heating distributions are examined in Figures 5-5 and 5-6. In a one meter long reactor segment, a comparison is made between two cases, one in which the feed stream enters the reactor at 823K and the reactor walls receive a constant 40 kW/m^2 of heat, and the other in which the feed enters at 873K and the walls receive a constant 8 kW/m^2 of heat.

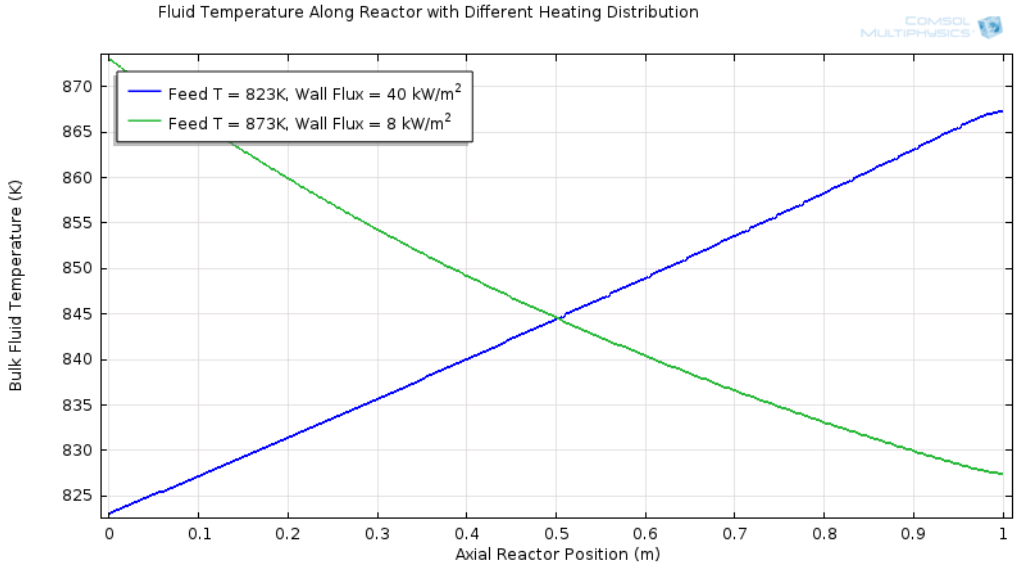

Figure 5-5. Bulk Fluid Temperature along the Length of the Reactor Segment

Figure 5-5 shows the bulk fluid temperature as a function of axial position in the reactor for the two contrasting cases. These conditions were picked because they reach the same temperature in the middle of the tube, and they represent fairly equal average temperatures. Despite these equivalent average temperatures, the first case, in which the fluid is hotter in the second half of the reactor, shows better conversion in Figure 5-6.

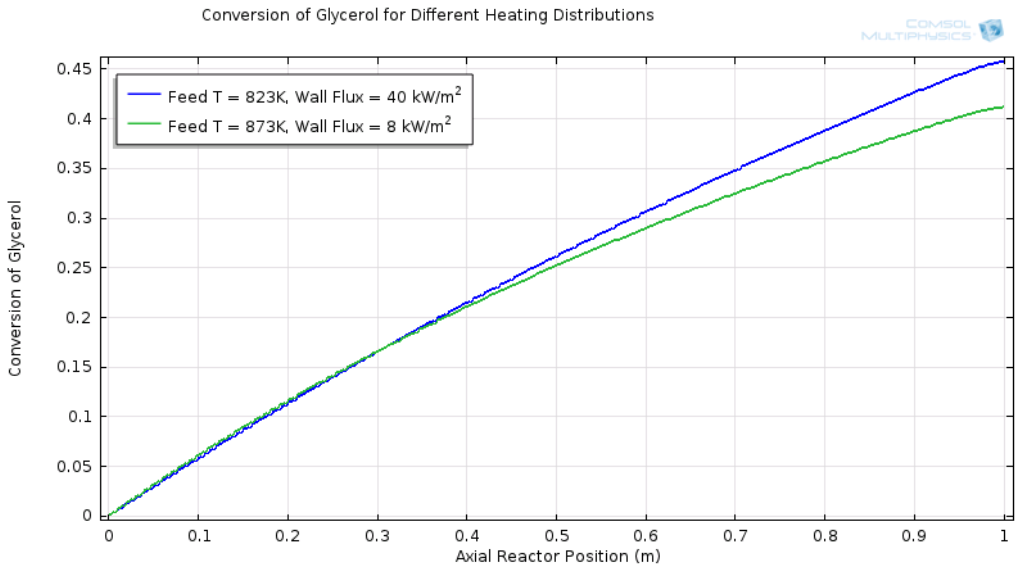

Figure 5-6. Glycerol conversion along the length of the reactor segment

The conversion at the entrance of the tube is slightly higher for the second case (green line), due to the higher feed temperature. However, farther along the reactor segment, where the partial pressure of glycerol depreciates significantly, the effect of the temperature of the bulk fluid becomes more pronounced and a higher conversion is obtained for the first case (blue line).

To confirm that the higher conversion is not due to a higher overall temperature of the system, the average temperature was calculated for each case by integrating the bulk fluid temperature over the reactor's length, as presented in Table 5-2.

Table 5-2. Bulk Fluid Average Temperature in Comparison with Glycerol Conversion for Cases 1 and 2

Case	Feed Temperature (K)	Wall Heat Flux (kW/m^2)	$T_{f,av} = \int T_f(z)dz$	Glycerol Conversion
1	823	40	844.7	45.7%
2	873	8	846.3	41.1%

In the first case, with lower feed temperature and larger heat flux, higher conversion was obtained, despite lower bulk fluid average temperature. If the difference in bulk fluid average temperature is taken to be negligible and it is assumed that a similar amount of energy is supplied to system in each case, then supplying a larger amount of heat to the reactor instead of the feed creates a more efficient process.

This result makes a strong case for using energy resources mostly on the reactor rather than the feed, but other factors beyond the scope of this simulation must be considered. It may be more effective to supply energy to the process stream pre-reaction in a heat exchanger that can be designed solely for the purpose of providing efficient heat transfer than to rely heavily on energy transfer into the reactor.

5.3.2 Wall Flux and Radial Temperature Gradients

Glycerol steam reforming demands operating pressures significantly lower than other reforming processes, making the thermal conductivity of the fluid considerably lower in comparison. As a result, radial temperature gradients, which were not accounted for in this axial reactor model, will be even more impactful for this process, calling for caution in designing a glycerol reformer with very substantial wall heating.

5.4 Operating Pressure

The kinetic model developed by Cheng et al. [3] only accounts for the primary reaction of glycerol with steam to produce hydrogen, so ultimate conclusions cannot be made about optimal operating pressures. Nevertheless, the results obtained in this study can make contributions by examining other effects that operating pressure can have in an industrial packed bed reactor.

Since low pressures are known to be favorable, the outlet pressure will ideally be near but not below atmospheric, as anything below one atmosphere would necessitate the use of a vacuum, creating additional capital and operating costs. Thus, the optimal feed pressure will be just far enough above atmospheric to allow for pressure drop.

5.4.1 Operating Pressure and Reaction Rate

One potential advantage to operating at higher pressure is that more glycerol can be processed at once without using a larger reactor, as a higher pressure gas mixture at a given temperature and volumetric flow rate contains a larger number moles. Since the rate of the glycerol reforming reaction increases with the partial pressures of the reactants [3], an increase in pressure will also increase the reaction rate. This study's model confirmed that relationship, as shown in Figure 5-7.

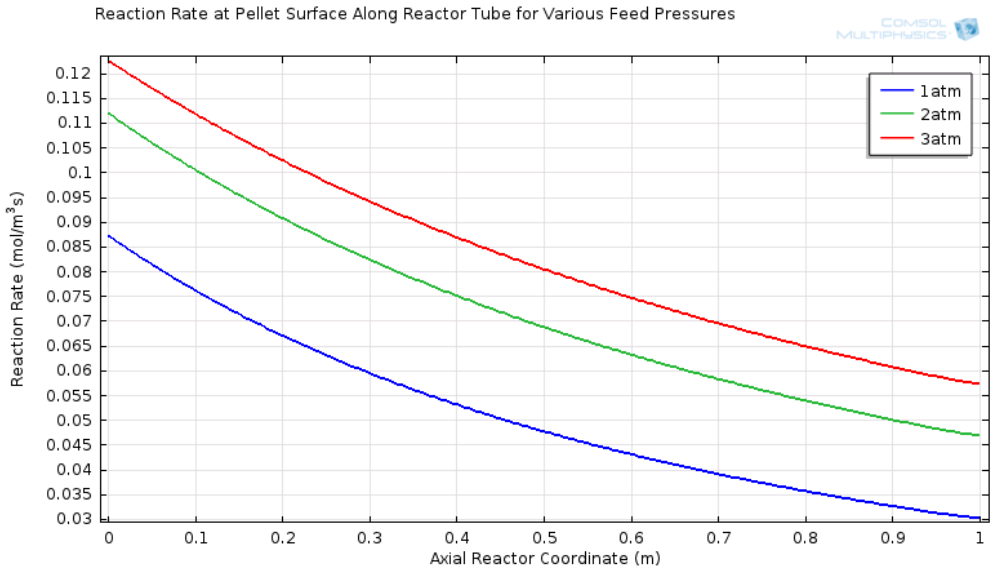

Figure 5-7. Reaction Rate along the Length of the Reactor Segment with Varying Operating Pressures

For this particular parametric solution, the wall heat flux was set to zero because with varying feed pressures, different amounts of feed material enter the reactor. A constant nonzero heat flux would have affected the system's temperature differently in each case, potentially becoming a confounding factor. The feed temperature and velocity were held constant at 823K and 5m/s, respectively.

According to Figure 5-7, the reaction rate did not increase in proportion to the feed pressure. In order to better illustrate this, a relative reaction rate was defined as the molar rate of glycerol consumption per mole of glycerol fed to the system, as shown in Equation (5-2).

$$Relative\ Reaction\ Rate = \frac{r_{gly}}{F_{gly,in}} \tag{5-2}$$

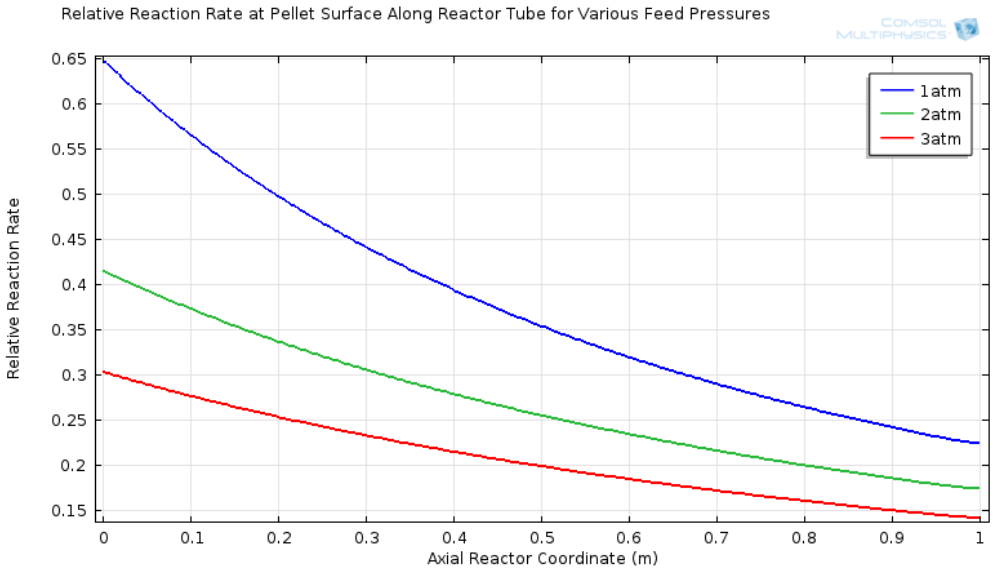

Figure 5-8. Relative Reaction Rate along the Length of the Reactor Segment with Varying Operating Pressure

Figure 5-8 shows that increasing the pressure in the reactor had a negative impact on the rate of glycerol consumption relative to the amount of glycerol present in the system. As a result, better conversion was achieved with lower feed pressure, as seen in Table 5-3.

Table 5-3. Glycerol Conversion with Varying Feed Pressure

Feed Pressure (atm)	Glycerol Conversion
1.00	35.9%
2.00	33.1%
3.00	30.9%

The observed behavior was the result of the heterogeneous reaction kinetics. The dual-site surface reaction proposed by Cheng et al. [3] assumes that the rate-limiting step is the collision and reaction of two molecules adsorbed to the catalyst surface. As a result, the surface concentration of each reactant is at equilibrium with its gas phase, and the equilibrium concentration depends on the gas's partial pressure. So partial pressure directly influences surface concentration, which controls reaction rate. However, as

the partial pressures of the reactants increase, the surface of the catalyst, which has a finite number of adsorption sites, becomes saturated with reactants, and the reaction rate plateaus.

If the temperature and the mole fractions of glycerol and water are held constant, the Langmuir-Hinshelwood model for dual-site adsorption Equation (3-20) rate expression becomes a function of total pressure with an asymptotic limit as the pressure increases, represented in Figure 5-9.

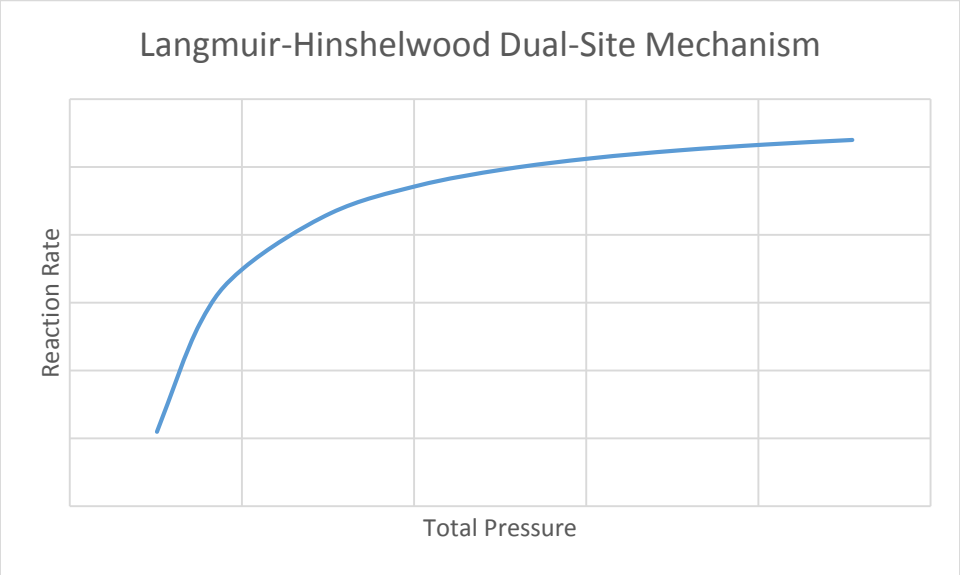

Figure 5-9. Langmuir-Hinshelwood Dual-Site Reaction Rate vs. Total Pressure

This presents another reason for using low operating pressures for the steam reforming of glycerol over the bimetallic Ni-Co/Al_2O_3 catalyst used in this study, as well as any other catalyst that promotes this reaction mechanism.

5.4.2 Pressure and Effectiveness Factor

While low pressures favor diffusion, within the range of pressures observed in this study there was no significant relationship between pressure and effectiveness factor. The Knudsen diffusion mechanism was the limiting resistance in the glycerol process, and it is not affected by pressure.

Table 5-4 shows that with Knudsen diffusivity providing the larger mass transfer resistance, changes to molecular diffusivity resulting from variations in operating pressure have little effect on the effective diffusivity.

Table 5-4. Molecular, Knudsen, and effective diffusivity with varying pressure

Pressure (atm)	Glycerol Molecular Diffusivity (m^2/s)	Glycerol Knudsen Diffusivity (m^2/s)	Glycerol Effective Diffusivity (m^2/s)
1.00	9.628×10^{-5}	4.033×10^{-6}	4.811×10^{-7}
2.00	4.814×10^{-5}	4.033×10^{-6}	4.625×10^{-7}
3.00	3.209×10^{-5}	4.033×10^{-6}	4.453×10^{-7}

4.00	2.407×10^{-5}	4.033×10^{-6}	4.293×10^{-7}
5.00	1.926×10^{-5}	4.033×10^{-6}	4.144×10^{-7}

Note, however, that if a catalyst support with larger pores were used, significantly decreasing the Knudsen diffusion resistance to the point that molecular diffusion became the limiting factor, the pressure would have a non-trivial effect on the effectiveness factor. In that case, lower pressures would increase the effectiveness factors and allow for a larger active surface area on the catalyst.

5.5 Flow Rate and Residence Time

Aside from increasing operating pressure, which was shown to be unfavorable in a number of ways, the only way to boost the amount of glycerol that can be processed without increasing reactor size is to raise the process flow rate. Since the intrinsic reaction rate in glycerol steam reforming is high, the flow rate may be kept fairly high. While it does not have a direct impact on the reaction kinetics, the flow rate impacts the system's transport phenomena.

5.5.1 Boundary Layer

Whereas the large size of the glycerol molecule made internal diffusion the limiting factor in the system's mass transport, the Ni-Co/Al_2O_3 catalyst was a strong thermal conductor, and therefore the external heat transfer resistance produced by the stagnant boundary layer was likely to be the system's limiting factor in terms of energy transport. The low effectiveness factors meant that the heat sink created by the endothermic reaction remained around the outside of the pellet, showing the dominance of the external heat transfer. The boundary layer's thermal resistance is apparent in the steady difference between the solid surface and bulk fluid temperatures along the reactor in the initial simulation in Figure 5-10.

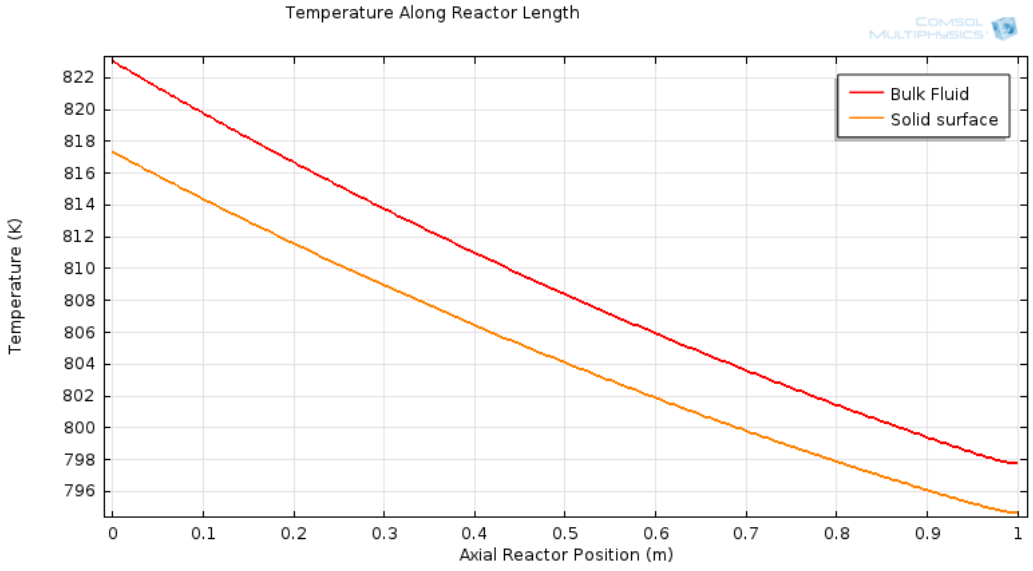

Figure 5-10. Bulk Fluid and Solid Surface Temperatures along Length of Reactor Segment

The model was then rerun at four different flow rates by specifying linear inlet velocities of 3, 6, 9 and 12m/s, with the remaining parameters held constant. Again, the wall heat flux was set to zero, as the varied residence times with a constant heat flux would have led to very different temperature profiles.

The overall thermal resistance due to the boundary layer was represented by finding an average boundary layer temperature difference. The temperature difference was found by integrating the difference between the solid surface temperature and bulk fluid temperature along the length of the reactor, as represented by Equation (5-3) and shown in Table 5-5.

$$\Delta T = \int \left(T_{bulk\ fluid} - T_{solid\ surface}\right) dz \quad \textit{Table} \tag{5-3}$$

5-5. Average Temperature Difference across Boundary Layer with Varying Inlet Velocity

Inlet Velocity (m/s)	Average Boundary Layer Temperature Difference (K)
3.00	7.56
6.00	6.18
9.00	5.17
12.00	4.33

While the effect was not drastic, increasing the velocity had a positive influence on the boundary layer heat transfer.

5.5.2 Turbulence

In laminar flow, mass transport relies on molecular diffusion and mixing is limited, whereas eddies present in turbulent flow greatly aid in chemical dispersion. This model assumed a well-mixed fluid, thus, its applicability relies on the maintenance of turbulent flow conditions. The complex void pattern created by a randomly packed reactor promotes turbulence. Typically, in such reactor, a Reynolds number of 200 is high enough to prevent true laminar flow, and a Reynolds number of 1900 will induce full turbulent flow [50][51]. At a temperature of 823K, pressure of 2atm, particle diameter of 0.0254m, and a molar composition based on a 30% reaction extent, the Reynolds number varies with the fluid's velocity as illustrated in Figure 5-11.

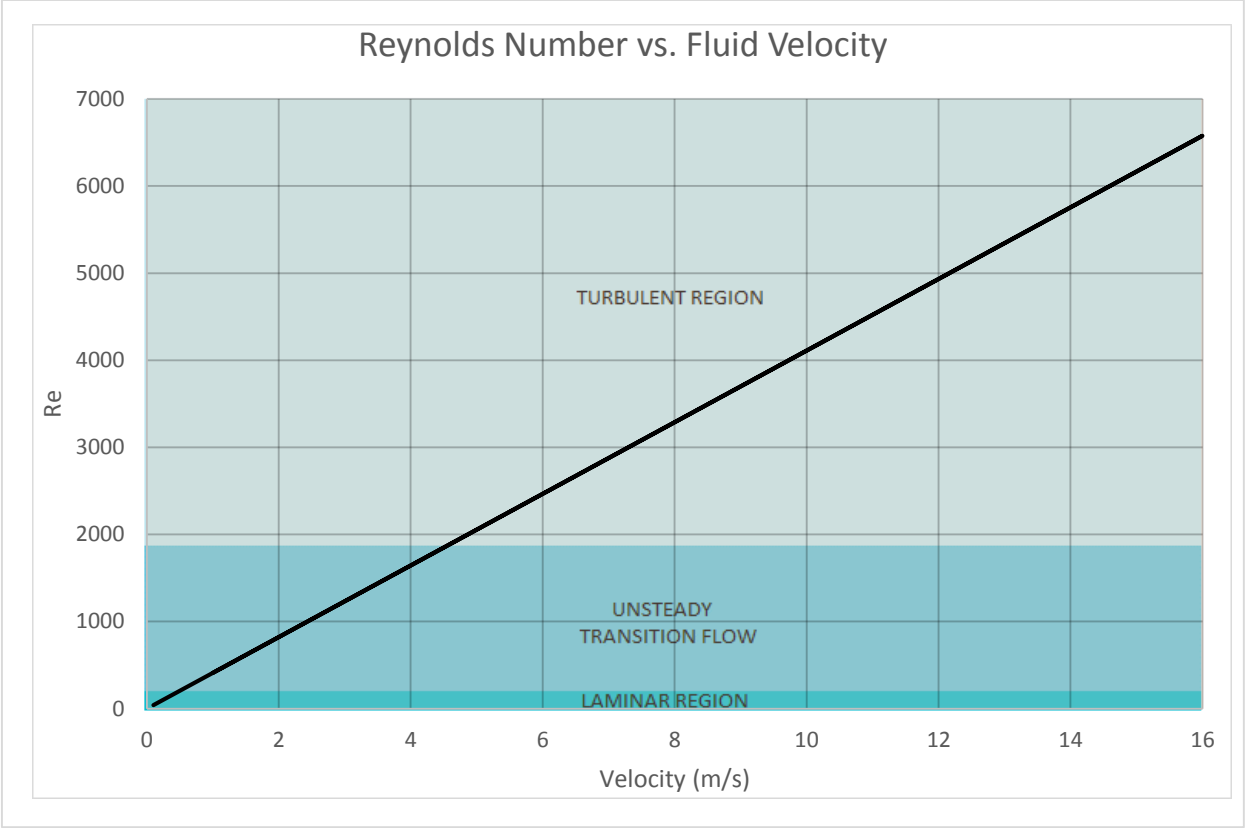

Figure 5-11. Reynolds Number as a Function of Fluid Velocity

Figure 5-11 shows that true laminar flow only exists at fluid velocities below 1m/s, and a velocity of 5m/s is sufficient to create fully turbulent flow. Therefore, while the system should not operate at excessively low flow rates, the fluid flow will not exhibit laminar behavior in the observed range.

5.5.3 Flow Rate vs. Reaction and Conversion

Increasing the flow rate also had a seemingly positive impact on reaction rate, albeit with diminishing returns, as seen in Figure 5-12.

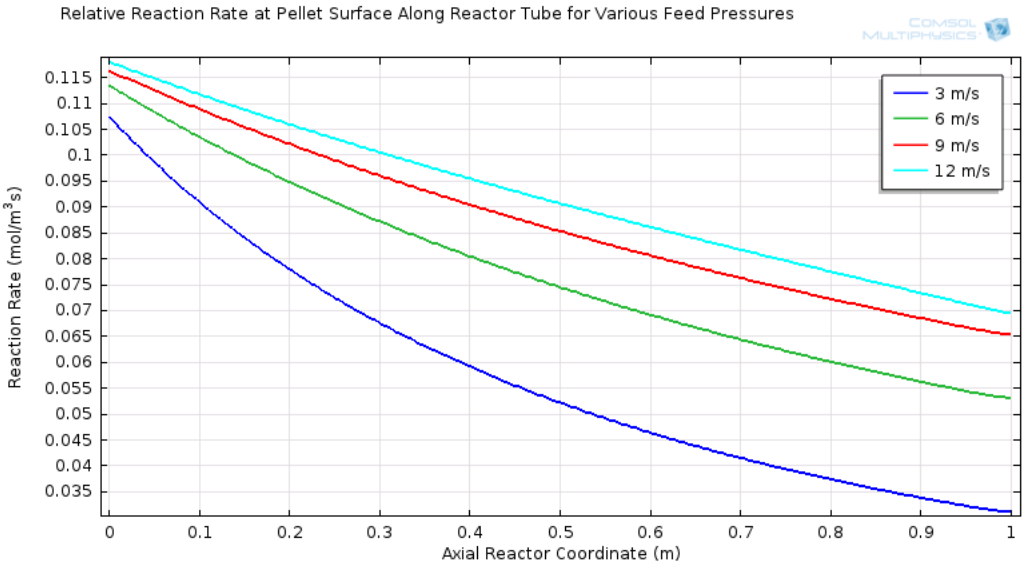

Figure 5-12. Reaction Rate along the Length of the Reactor with Varying Velocities

Higher reaction rates are not necessarily beneficial. With a higher flow rate, the reactants are more rapidly replenished by convective mass transfer as they are consumed by the reaction, maintaining higher partial pressures to drive the reaction. The other consequence of this same effect is poorer conversion due to shorter residence times, as seen in Table 5-6. The residence time's effect on conversion is strong and should be a major consideration in process design.

Table 5-6. Glycerol Conversion with Varying Velocities

Inlet Velocity (m/s)	Glycerol Conversion after 1m
3.00	34.3%
6.00	21.1%
9.00	15.0%
12.00	11.1%

5.5.3 Velocity and Pressure Drop

Perhaps the most significant impact that flow rate had on the steam reforming model was its effect on pressure drop. Velocity and pressure in a flowing fluid have an inverse relationship. The pressure differential, which is the driving force for fluid flow, creates a net force on the fluid toward the direction of lower pressure, causing the fluid to accelerate. In relation to energy conservation, this relationship represents the conversion of internal energy of the fluid pressure to kinetic energy with increasing velocity.

Higher fluid velocities also increase frictional forces within the fluid that contribute to pressure loss. The Ergun equation used in this model accounts for this effect by including the superficial velocity, as mass flux over density, in its main coefficient. As the fluid velocity increases along the length of the reactor segment, it continues to exert a stronger influence on pressure drop. Furthermore, the forward reaction of glycerol with steam has a net molar increase of six. Since this increase in moles does not affect the

temperature or pressure of the system, it results in an expansion of the gas, and thus an increase in volumetric flow rate. The cross-sectional area of the reactor tube is fixed, so the expansion manifests in an increase in axial velocity, further contributing to pressure drop. In contrast, the primary reaction for methane steam reforming has a net increase of just two moles, so pressure drop should be an even more significant consideration in glycerol reforming than it is in current steam reforming operations.

The strong dependence of pressure drop on velocity is shown in Figure 5-13, where fluid pressure along a 1m reactor length is shown for various feed velocities, with feed pressure and temperature held constant.

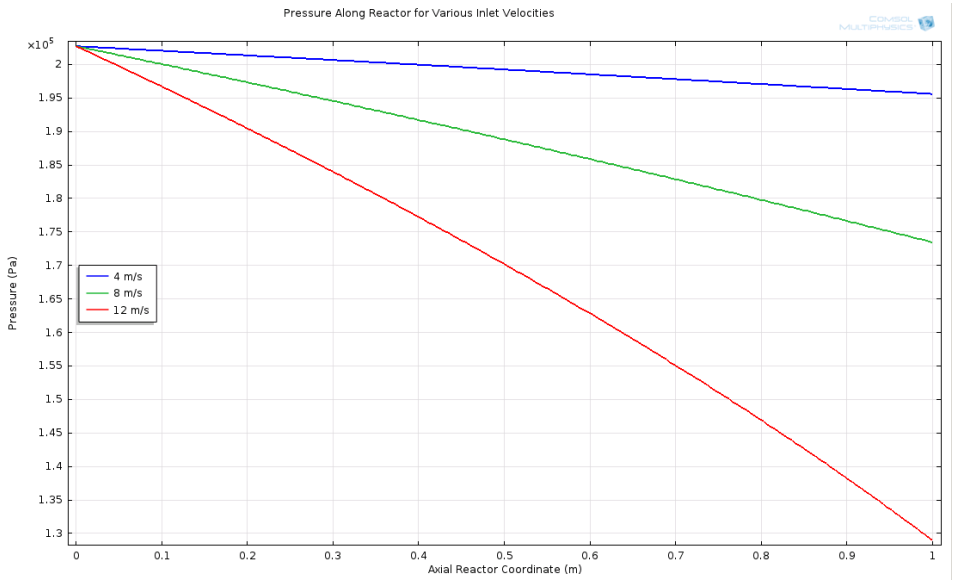

Figure 5-13. Pressure along the Length of the Reactor Segment with Varying Velocities

Figure 5-13 illustrates the high degree to which velocity influences pressure drop. While the drop was almost negligible at an inlet velocity of 4m/s, the pressure dropped by nearly 40% along the reactor segment for the 12m/s case.

Pressure drop is an important parameter economically in any chemical process, as it directly dictates the operating cost of the pump or compressor. However, it has an amplified significance in the case of glycerol steam reforming, where lower pressures favor hydrogen production. As Figure 5-14 elucidates, the smaller pressure drop associated with lower inlet velocity enables the use of a much lower feed pressure, while still maintaining an outlet condition of atmospheric pressure.

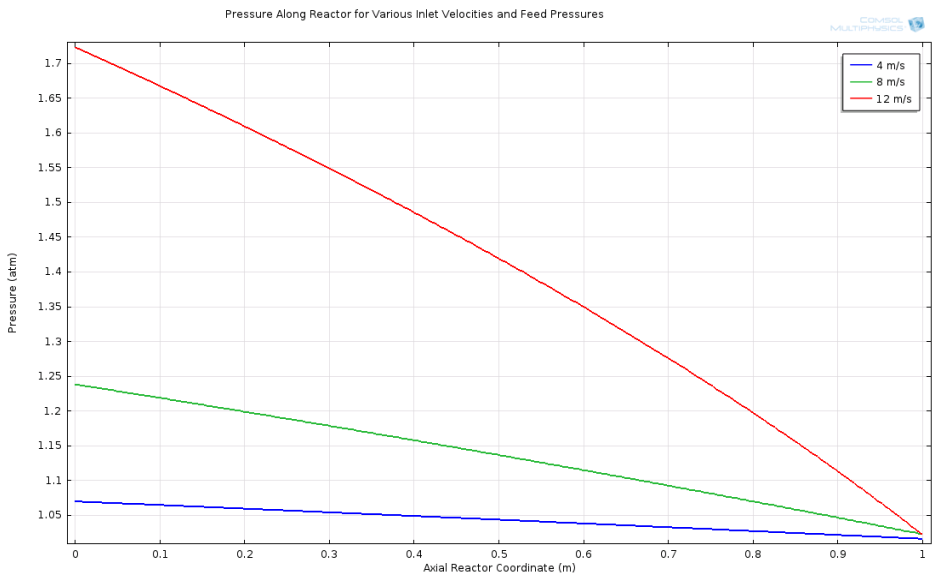

Figure 5-14. Pressure along the Length of the Reactor Segment with Varying Velocities

The need for a higher feed pressure to allow for pressure drop means that the average operating pressure is higher, which will have a negative impact on hydrogen production, as shown in Table 5-7. The use of a lower inlet velocity allows for a lower average pressure across the tube while still maintaining the outlet condition of atmospheric pressure to eliminate the need for a vacuum.

Table 5-7. Operating Pressure with Varying Velocities

Inlet Velocity (m/s)	Average Operating Pressure Along Tube (atm)
4.00	1.04
8.00	1.13
12.00	1.40

5.6 Reactor Design

Given the proposed optimal process design parameters, this study aimed at evaluating reactor design parameters for an industrial glycerol steam reformer. The constraints of the model presented in this study should be taken into consideration, and further analysis is recommended for a model encompassing more extensive reaction modeling. However, the trends observed here provide insightful information into factors influencing the design for an industrial reactor.

5.6.1 Reactor Length

The length of the steam reformer was studied for a process occurring at an operating temperature of 823K, pressure of 2atm, and fluid velocity of 5m/s. Reactor lengths of 1, 2, 3, and 4m were analyzed along with the necessary heat flux needed to allow for efficient process operation.

Conversion and Component Concentration

By operating the process in a longer reactor the conversion of glycerol is directly affected, since the residence time significantly increases in a longer reactor, given the feed velocity is kept at 5m/s. Although the varying heat flux applied to the system with varying reactor lengths does affect conversion, a longer reactor will require lower heat flux when compared to a shorter one, and therefore the trends observed provide valid qualitative reactor design considerations. Figure 5-15 shows the glycerol conversion as a function of scaled axial coordinate for reactors of varying lengths.

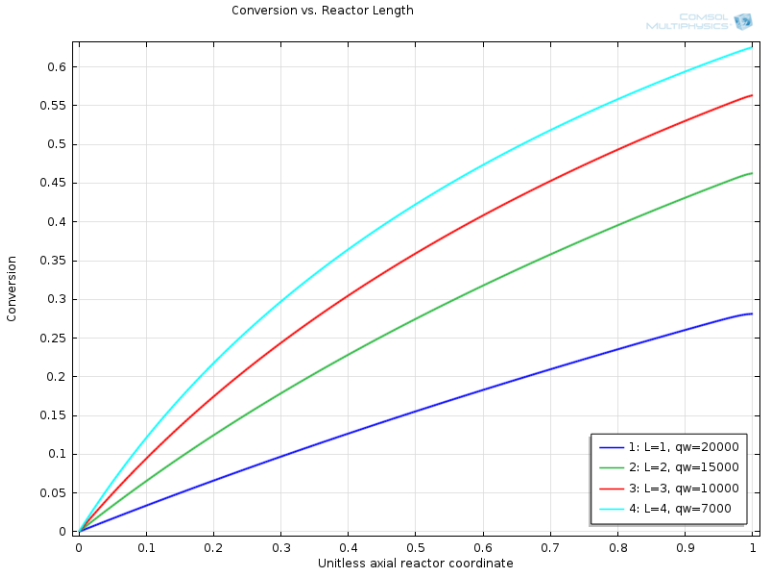

Figure 5-15. Glycerol Conversion as a Function of Scaled Axial Coordinate with Varying Reactor Length

As seen above, glycerol conversion significantly increased as the reactor length increased. Shorter reactors had a more linear conversion profile, while longer ones showed a curved profile. With greater reactor lengths the rate at which glycerol conversion improves slowed down, which further demonstrated the importance of having a high wall heat supply to drive the reaction near the end of the reactor.

Figure 5-16 shows the conversion profile for a 4m long reactor. The dashed lines allow illustration of the progressive increase in conversion at each 1m segment of the reactor. With each 1m long segment increase, the corresponding conversion increase is continuously smaller. It is expected that this trend would continue for even longer reactors until the increase in conversion with increased reactor length becomes insignificant. Such a conversion profile was sought, but none of the solvers used by COMSOL could find convergence when glycerol concentrations became too low.

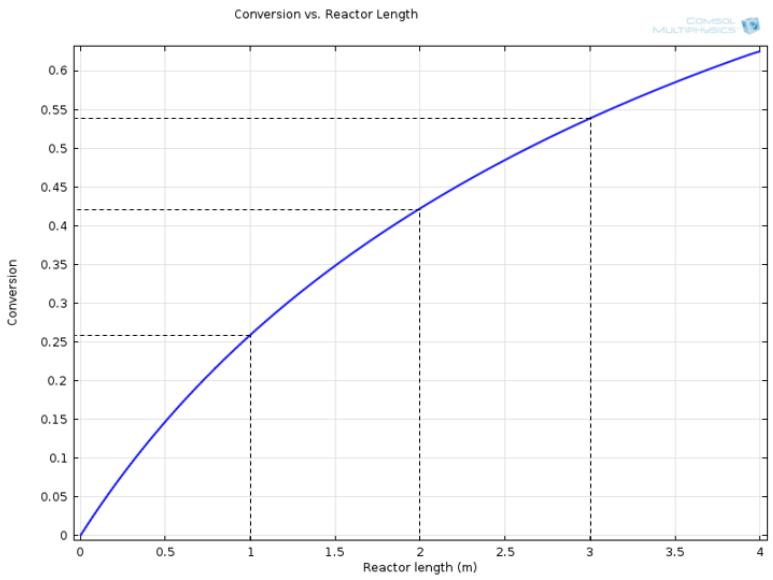

Figure 5-16. Glycerol Conversion in a 4m Long Reactor

Naturally, as glycerol conversion approaches 100%, the decreased partial pressure of this limiting reactant will inhibit the reaction rate. One additional reason for the slowing down of conversion, though, is the increase in velocity due to the stoichiometric gas expansion, which decreases the fluid's residence time. Depending on the application for which glycerol steam reforming is being employed, it may be beneficial to achieve a high conversion on the first pass, making longer reactors desirable. However, if the remaining glycerol in the effluent stream can be recovered for further processing, then shorter reactors which reduced capital cost are suitable.

Given an improvement in glycerol conversion, a change can be seen in the effluent composition. Figures 5-17 and 5-18 show the concentration profiles of the system occurring in 1m and 3m long reactors, respectively.

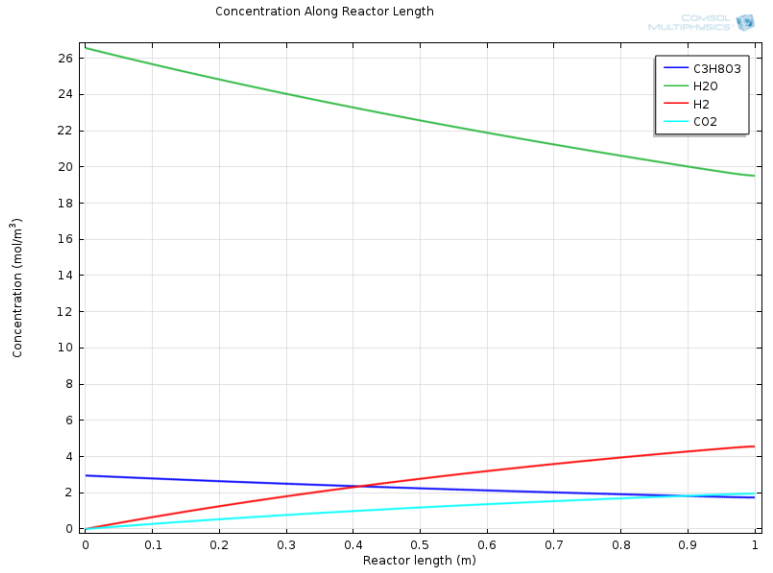

Figure 5-17. Concentration Profile for a 1m Long Reactor

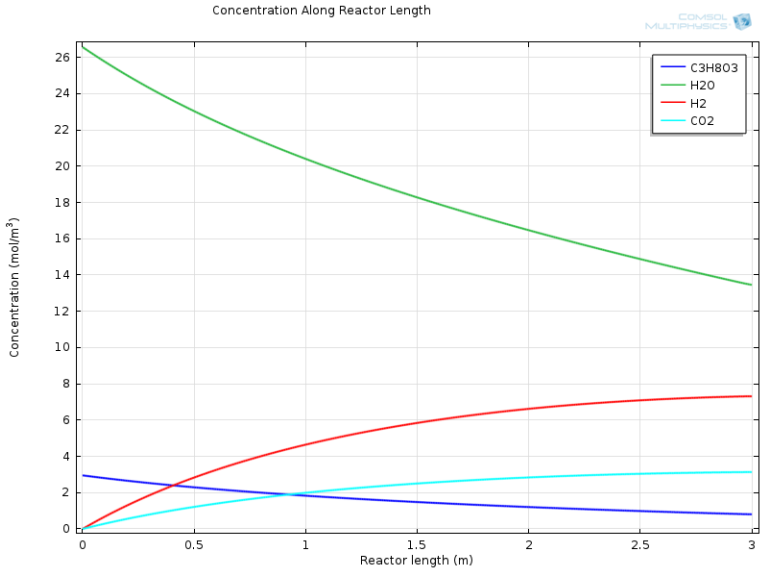

Figure 5-18. Concentration Profile for a 3m Long Reactor

Not only was conversion improved by lengthening the reactor, increasing by approximately 28% in glycerol conversion when increasing the reactor length from 1 to 3m, but the effluent was of significantly higher purity with respect to hydrogen, the desired product. Depending on what application the product is used for, a separation step may be necessary to eliminate the remaining unreacted glycerol and steam in the products, as well as the by-product carbon dioxide. Therefore, it may be economically of interest to design a longer reactor for industrial use, as it would allow for easier separation. Table 5-8 summarizes the findings of glycerol conversion and hydrogen composition in the effluent comparing 1, 2, 3, and 4m long reactor lengths.

Table 5-8. Percent Glycerol Conversion and Hydrogen Mole Fraction in the Effluent for Varying Reactor Lengths

Reactor Length (m)	Glycerol Conversion (%)	Hydrogen in Effluent (%)
1	28.0	17.0
2	46.0	25.5
3	56.0	29.5
4	62.0	32.0

Pressure and Velocity

The pressure drop resulting from operating the process with varying reactor lengths is illustrated in Figure 5-19. The pressure drop observed increased along with the reactor length, as expected.

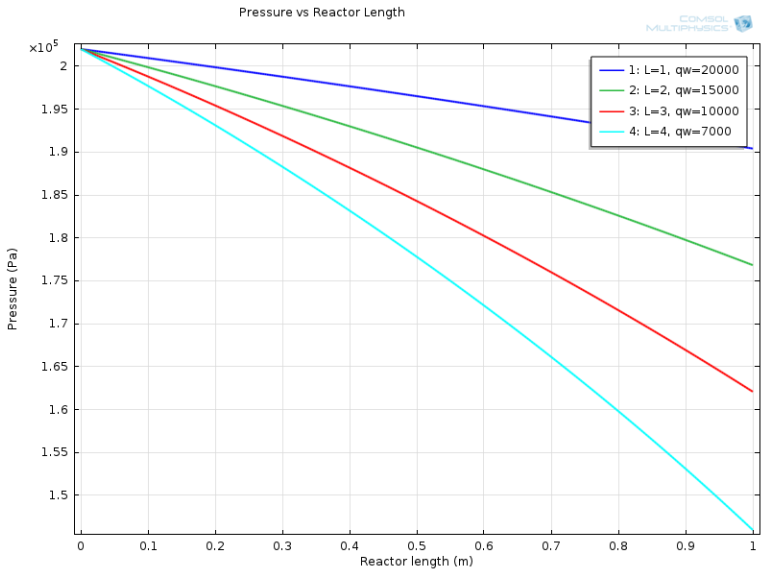

Figure 5-19. Pressure Drop along the Length of the Reactor

Table 5-9 shows the comparison in pressure drop and outlet fluid velocity with varying reactor lengths. As the pressure dropped, the fluid velocity consequently increased, in tandem with the increasing reactor length.

Table 5-9. Pressure Drop and Fluid Velocity Exiting the Reactor for Varying Reactor Lengths

Reactor Length (m)	Pressure Drop (kPa)	Outlet Fluid Velocity (m/s)
1	12.0	6.2
2	25.0	7.2
3	39.0	8.0
4	57.0	8.9

The pressure drop per reactor length, however, was not constant, and the pressure drop through the four meter reactor was more than four times that of the pressure drop through the one meter reactor. The stoichiometry of the reaction is at play here. The further the reaction proceeds, the greater the increase in velocity, which contributes to the pressure drop. This relationship bolsters the earlier claim that lower feed flow rates are ideal. When industrial-length reactors are considered and conversion is high, pressure drop becomes a very significant consideration, and thus a lower flow rate that allows for sufficient residence time in a shorter reactor is quite favorable.

5.6.2 Reactor to Catalyst Pellet Radius Ratio

The reactor-to-catalyst-pellet radius ratio was analyzed for a process occurring at a constant operating temperature, pressure, and fluid velocity in a one meter long reactor. As the ratio of the two radii changes, the packed bed voidage changes as well. The relationship between those two variable was studied by de Klerk [43] and a table with varying ratio values and their corresponding bed voidage values was developed, seen in Appendix F. Varying ratios make different packing types more likely to occur, and it should be noted that this will have a confounding effect on bed voidage [49].

First, the radii ratio was studied by varying the reactor radius and keeping the catalyst pellet radius fixed, with a radius of ½ in. The five ratios taken from de Klerk's study and analyzed with the aid of the process simulation are seen in Table 5-10.

Table 5-10. Reactor-to-Catalyst-Pellet Radius Ratio and Corresponding Bed Voidage [43]

$R_r : r_p$ ratio	Bed Voidage
4.2	0.425
4.9	0.419
7.2	0.397
9.2	0.368
11.2	0.366

It can be seen that as the reactor radius increases, the bed voidage decreases, suggesting increasingly better packing of the bed. Figure 5-20 shows glycerol conversion with varying reactor radius values. As the reactor radius increased, a decrease in conversion was observed, although it only dropped by less than 5%. The increased reactor radius lowered the bed voidage, creating more catalytic surface area for the reaction to occur. Since the heat flux into the system was kept constant though, the smaller reactor would get much hotter than the larger reactor, driving the reaction rate up. These two effects balanced each other, hence the overall similarity in conversion between differing reactor radii.

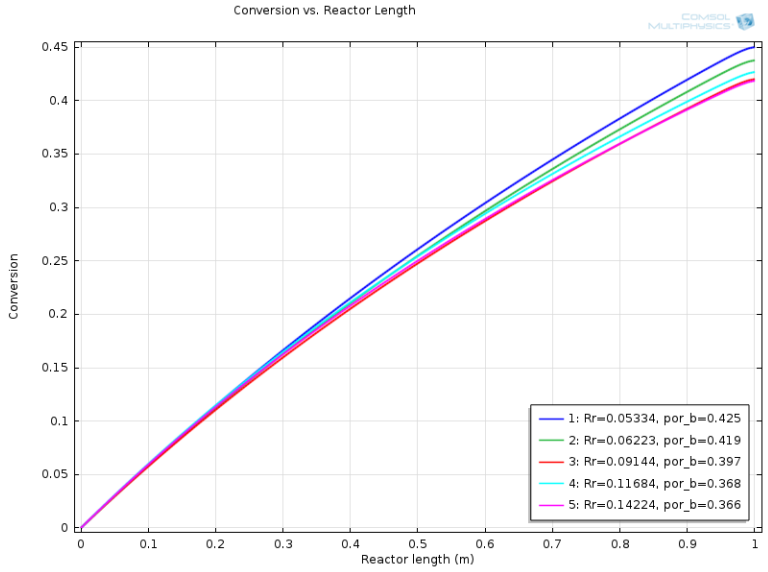

Figure 5-20. Glycerol Conversion with Varying Reactor Radius and Constant Pellet Radius

Figure 5-21 shows the pressure drop along the reactor for reactor radius values corresponding to the R_r:r_p ratios analyzed. As the reactor radius increased the pressure drop across the reactor became more and more prominent. Since the size of the catalyst pellets were kept constant, when increasing the reactor size the effects of the tube walls on packing became less pronounced and the voidage dropped. The decreased voidage meant less space for the fluid to flow through, resulting in a larger pressure drop.

When keeping the catalyst pellet size and wall heat flux constant, a smaller reactor promoted higher glycerol conversion and lower pressure drop across the reactor. It must be remembered, though, that a

larger reactor radius means that significantly more glycerol is being processed at once. Thus, the same heat flux on different reactor volumes would naturally not produce the same conversion. So the more important effect of increasing reactor radius is the resulting decrease in bed voidage, which promotes overall reaction rate but increases pressure drop.

A conclusive result on an optimal reactor size was not achieved, since such a conclusion would require an economic assessment of the interplay between conversion, pressure drop and external heating.

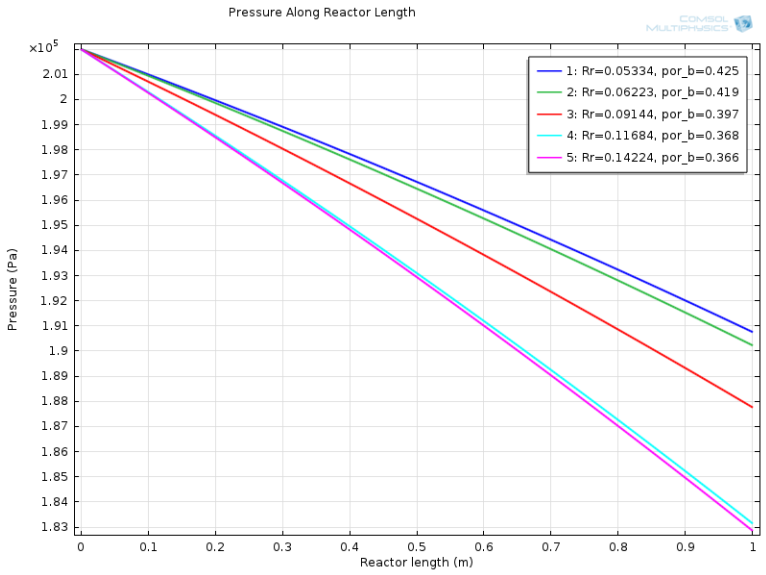

Figure 5-21. Pressure along the Reactor Length with Varying Reactor Radius and Constant Pellet Radius

Similarly, the reactor radii ratio was also tested by keeping the reactor radius constant and changing the radius of the catalyst pellets. Pellets of ½ in and 1in were used in the simulation under the operating conditions described previously. Figure 5-22 shows the glycerol conversion across the reactor length for the two different sizes of catalyst pellets.

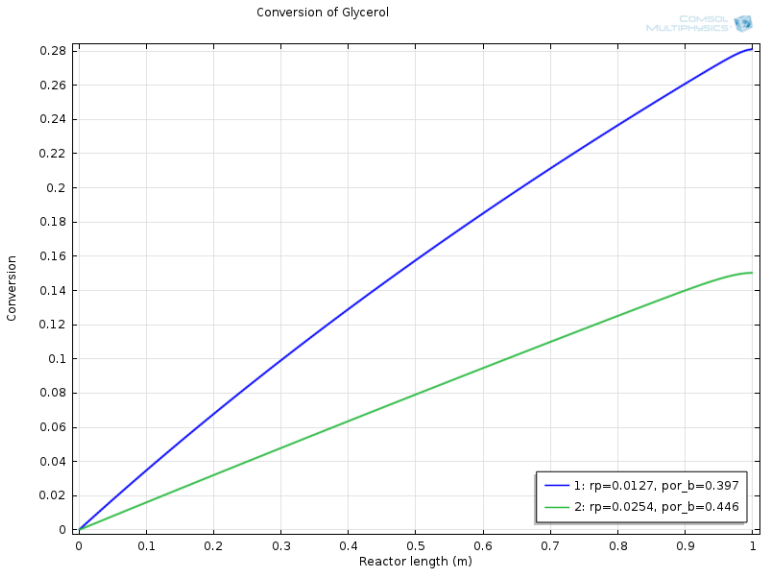

Figure 5-22. Glycerol Conversion along the Reactor Length for Varying Catalyst Pellet Size

As seen in the figure above, a larger catalyst pellet will result in lower glycerol conversion for the steam reforming process. As discussed previously, most of the reaction occurs on the outer surface of the catalyst pellets, and therefore this trend was expected, since with an increase in the pellet size a decrease in overall active surface area occurs.

Figure 5-23 shows the relationship between catalyst pellet size and pressure drop across the reactor. As expected, the smaller catalyst pellet resulted in a significantly larger pressure drop.

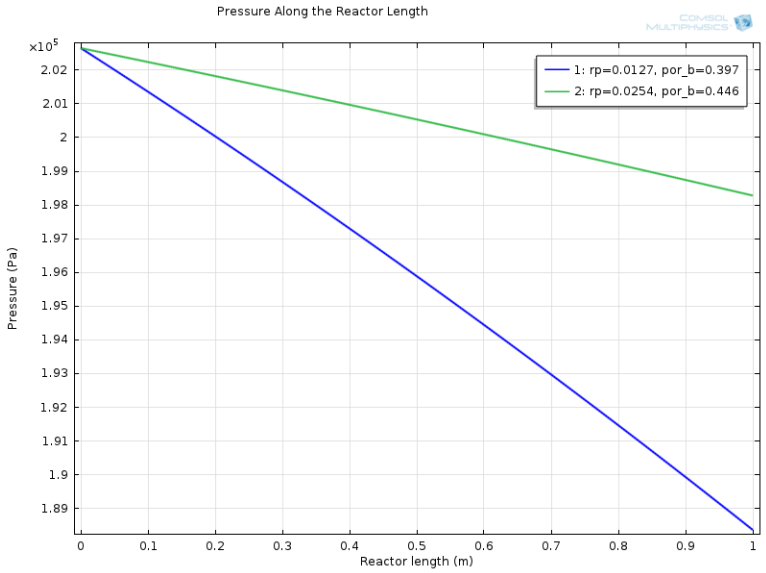

Figure 5-23. Pressure Drop along the Reactor Length with Varying Catalyst Pellet Size

When keeping the reactor radius constant, the impact of external heating is removed from the equation, and the two opposing factors are the desired effect of small catalyst size on conversion and its unwanted effect on pressure drop. Overall, relatively smaller catalyst pellets are preferred, since they promote

higher glycerol conversion. However, as the catalyst pellets become increasingly small, they become difficult to manufacture and pressure drop becomes very significant. A definitive conclusion cannot be drawn, since this model does not assess what an acceptable level of pressure drop would be for glycerol steam reforming.

6. Recommendations

Based on the results of the COMSOL process simulation model, ideal operating conditions for the process design of industrial glycerol steam reforming in a packed bed reactor may be inferred.

6.1 Process Design Recommendations

6.1.1 Operating Temperature

Experiments by Chiodo et al. [28] demonstrated that hydrogen production peaks at around 923K, contrary to thermodynamic predictions, which do not indicate such a limit to the positive effect of temperature on the reaction. They postulated that the reason for this trend was a shift in the type of carbon formation on the catalyst from filamentous to encapsulated. The present study's model did not include the effects of coke formation, so this should be considered in conjunction with the results of the simulation. The model did confirm that the thermodynamic advantage of high temperature had a profound impact on the overall process, greatly outweighing any resulting consequences such as decreased effectiveness factor. Therefore, operating temperature should be maximized, without exceeding 923K.

There still exists an option as to the distribution of the supplied heat between the feed, prior to entering the reactor, and to the reactor itself. The presence of a burner supplying heat directly to the reactor to counterbalance the energy consumption of the endothermic reaction, as is customary in current steam reforming processes, is a critical system component. This study showed that it is beneficial for driving the conversion of glycerol near the reactor outlet, where the lower partial pressure of glycerol due to its consumption weakens the reaction kinetics.

Maintaining a tube temperature near 923K will generate the largest overall reaction rate. However, if the process's end goal is to produce hydrogen as an energy source, then supplying excessive energy to the process is counterproductive. This calls for an investigation into the energetic return on investment before maximum operating temperatures are branded as optimal. While 923K is probably the optimal operating temperature, this study illustrated that high temperatures are more useful near the end of the reactor. The ideal glycerol reformer will therefore have a means of heating the reactor directly so that the fluid temperature reaches approximately 923K at the outlet.

However, rather than maintaining a constant maximum temperature, it may be a more efficient use of energy to supply a large enough portion of the energy needed directly to the reactor so that the fluid temperature rises as it travels through the packed bed. The ideal feed temperature is thus subject to a detailed economic analysis, but based purely on thermodynamic considerations, it should not be lower than 823K, as there is a marked drop in both glycerol conversion and hydrogen selectivity around this temperature [26].

6.1.2 Operating Pressure

Thermodynamic analysis and lab-scale experiments have both demonstrated that the catalytic reaction of glycerol with steam to produce hydrogen is favored by low pressures. The present work contributed to the study of optimal process design by showing that low pressure also improves conversion by preventing crowding on the catalytic surface. The ideal glycerol reforming process will run at the lowest pressures that are operationally feasible. The presence of a vacuum would allow for pressures below atmospheric,

which would undoubtedly improve the efficiency of the reaction alone. Whether the cost of installing and powering a vacuum justifies such an option, however, requires in-depth financial information, and it was assumed in this study that this is not a worthwhile addition. Therefore, the results presented in this work imply that an effective glycerol steam reforming process would run with atmospheric fluid pressure at the reactor outlet.

6.1.3 Flow Rate

The reactor model created in this study showed that the flow rate of the bulk fluid had a positive effect on the transfer of heat from the wall to the bulk fluid to the catalyst by reducing the stagnant boundary layer. However, an increased flow rate had a substantial negative impact on conversion due to the reduction in residence time, as well as a negative effect on the necessary operating pressure by amplifying pressure drop to a very large extent. The results suggest that flow rate, as controlled by manipulating the feed velocity, should be kept rather low. Fluid velocities for methane steam reformers range from 1.62m/s to 15m/s [33][52]. While low flow rates may result in poor mass transport, thus limiting reaction rate, this work showed that laminar flow will only be present in velocities below 1m/s in a packed glycerol reformer with spherical catalyst pellets on the order of 1" in diameter. For that reason, fairly low flow rates may be considered. The major consequence of a slow flowing fluid will most likely be that it limits the amount of glycerol that can be processed over a given time period. A quantitative optimization study will be necessary to find a balance between the physical benefits of low flow rates and the speed of the system, but the qualitative analysis of the contributing factors presented here makes this possible.

6.2 Reactor Design Recommendations

6.2.1 Reactor length

It was observed that in longer reactors, glycerol conversion is improved and the effluent composition is of higher purity in hydrogen. This presents a possible desirable solution for the industrial use of glycerol steam reforming. However, this work did not assess the tradeoff between producing a high purity yield and building larger equipment, along with ancillary considerations such as utility use, pressure drop, and maintenance. It is recommend that an analysis be performed comparing the benefits of using a longer reactor, since higher conversion is obtained, but there are numerous costs associated with building and maintaining larger equipment. Depending on what application the product is produced for, a possibly necessary separation process may be easier to perform after a greater glycerol conversion. However, if hydrogen purity is not of maximum concern and post-reaction separation is not necessary, it may be economically of interest to limit capital costs by using a shorter reactor.

6.2.2 Reactor to Catalyst Pellet Radius Ratio

The ratio of the reactor radius to the catalyst pellet radius was studied by keeping the catalyst pellet size constant and varying the reactor size, and vice versa. An analysis of an optimal reactor radius was inconclusive, therefore it is suggested that the monetary tradeoff between higher energy use and higher pressure drop occurring during the process should be assessed. Similarly, a study on the tradeoff between

higher active catalyst use and higher pressure drop should be made in order to assess an optimal catalyst pellet radius for glycerol steam reforming.

6.3 Research Recommendations

After completing this study, the direction that future research on this topic should take is clear. First and foremost, a model with multidimensional reactor geometry is critical to the scale-up analysis of the process. The present model confirmed the significance of heat transfer effects in the steam reforming of glycerol and postulated that the resistance to heat transfer in the fluid phase may be even more significant than in methane reforming. Radial temperature gradients due to wall heating could therefore pose a major threat to the success of the process, so a two-dimensional axisymmetric reactor model is an important next step.

Another potential pitfall lies in the presence of side reactions, which this model did not account for. Unwanted chemical activity not only possesses the ability to interfere with maximum hydrogen production, but it may also impact the system's heat and mass transport by way of the consumption and generation of energy and various chemical species. Thus, reaction kinetics for possible side reactions should be included in the model, particularly those describing the water-gas shift and methanation reactions.

Moreover, industrial operation of a steam reforming process will inevitably be hindered by some degree of catalyst deactivation. Experimentally derived recommendations regarding the prevention of carbon deposition were taken into account in the process conditions observed in this study. Even at these conditions, some deactivation will occur over time, so further research would ideally include the development of a model which explicitly involves the effects of coking.

7. Conclusions

Hydrogen production via steam reforming provides a promising means of utilizing biodiesel by-product glycerol. Steam reforming is a heterogeneous catalytic reaction process currently performed on hydrocarbons such as methane in packed bed reactors. This study created a true heterogeneous model using the Finite Element Method and an effective continuum approach to distinctly model the gas and solid phases, in order to assess the feasibility of steam reforming with glycerol in a plant-scale packed bed. Advanced catalytic reaction kinetics were combined with momentum, mass and energy balances on the system to analyze the role of transport phenomena in both the fluid and solid phases.

The results confirmed that packed bed reactors are a viable candidate for the steam reforming of glycerol, and that the style of reactor used for methane steam reforming is likely suitable. Potential concerns included strong diffusion limitations and the endothermic nature of the reaction, but the resulting low effectiveness factors and high heat demands did not prevent reasonable conversion. A more sophisticated model with a multidimensional reactor geometry, however, is suggested as the next step before conclusions are drawn, largely because of the probable significance of radial temperature gradients. Additionally, possible side reactions such as water-gas shift and methanation should be modeled, as should the effects of catalyst-deactivating carbon deposition.

Variations in temperature, pressure, flow rate, reactor size and reactor dimensions were all explored to evaluate their effects on the system as a whole, and design recommendations for industrial-scale operation were made. Namely, high operating temperature is necessary, ideally at or near 923K with a rising axial temperature profile created by a large supply of heat applied directly to the reactor walls. Meanwhile, operating pressure near atmospheric is essential for efficient glycerol conversion, while fluid flow rate has a range of effective operation but should probably be kept near the low end of the turbulent region. In terms of reactor design, it was found that a longer reactor with a smaller radius, as well as smaller catalyst pellets result in higher glycerol conversion. However, factors such as energy load, pressure drop, and equipment capital and maintenance costs should be taken into consideration when assessing optimal reactor and catalyst pellet sizes for glycerol steam reforming.

8. References

[1] Leoneti, A.B., V. Aragao-Leoneti, and S.V.W.B. De Oliveira. Glycerol as a by-Product of Biodiesel Production in Brazil: Alternatives for the use of Unrefined Glycerol. *Renewable Energy*, **2012**, 45, 138.

[2] Knothe, G., J. Krahl, and J. Gerpen. Glycerol Technology Options for Biodiesel Industry. *Biodiesel Handbook*, **2010**, 11(1). AOCS Press.

[3] Cheng, C. K., S. Y. Foo, and A.A. Adesina. Glycerol steam reforming over bimetallic Co-Ni/Al2O3. *Industrial and Engineering Chemistry Research,* **2010**, 49, 10804−10817.

[4] National Biodiesel Board. 2014. Accessed on March 1, 2014. < http://www.biodiesel.org/>

[5] U.S. Department of Energy. Alternative Fuels Data Center. <http://www.afdc.energy.gov/laws/law/US/396>

[6] Gupta, M., and N. Kumar. Scope and Opportunities of using Glycerol as an Energy Source. *Renewable and Sustainable Energy Reviews*, 2012, 16.7, 4551-6.

[7] Mario, M. J. "A Comparison Between Raw Material and Technologies for a Sustainable Biodiesel Production Industry." *Economic Effects of Biofuel Production*. N.p.: InTech, 2011. N. pag. Print.

[8] Duque, J. Design and Analysis of Technological Schemes for Glycerol Conversion to Added Value Products. Diss. Universidad Nacional De Colombia, 2011.

[9] Perry, R.H., and D.W. Green. *Perry's Chemical Engineers' Handbook*. McGraw-Hill Professional, New York, 8th edition, 2008.

[10] Pachauri, N., and B. He. Value-Added Utilization of Crude Glycerol from Biodiesel Production: A Survey of Current Research Activities. *American Society of Agricultural and Biological Engineers*. 2006.

[11] Hydrogen Energy. RenewableEnergyWorld.com. March 3, 2014.

[12] Cheng, C.K., S.Y. Foo, and A.A. Adesina. Thermodynamic Analysis of Glycerol-Steam Reforming in the Presence of CO_2 Or H_2 as Carbon Gasifying Agent. *International Journal of Hydrogen Energy*, **2012**, 37.13, 10101.

[13] Ito, T., Y. Nakashimada, K. Senba, T. Matsui, and N. Nishio. Hydrogen and Ethanol Production from Glycerol-Containing Wastes Discharged After Biodiesel Manufacturing Process. *Journal of Bioscience and Bioengineering,* **2005**, 100(3), 260-265.

[14] Wood, A. Novel Reforming Process Converts Biomass Molecules to Hydrogen. *Chemical Week,* **2002**, 164(34): 30.

[15] Huber, G.W., J.W. Shabaker, and J.A. Dumesic. Raney Ni-Sn catalyst for H_2 production from biomass-derived hydrocarbons. *Science,* **2003**, 300(5628): 2075-2077.

[16] Valliyapan, T. Hydrogen or Syn-Gas Production from Glycerol Using Pyrolysis and Steam. M.S Thesis. Saskatoon, Saskatchewan.: University of Saskatchewan, Department of Chemical Engineering. 2004.

[17] Hirai, T., N.O. Ikenaga, T. Miyake, and T. Suzuki. Production of Hydrogen by Steam Reforming of Glycerin on Ruthenium Catalyst. *Energy and Fuels,* **2005***,* 9, 1761-1762.

[18] Fogler, H.S. *Essentials of Chemical Reaction Engineering*. Prentice Hall, NJ. 2011.

[19] Cheng, C. Synthesis Gas Production from Glycerol Steam Reforming over Alumina Supported Bimetallic Co-Ni Catalyst. PhD Thesis. School of Chemical Engineering, The University of New South Wales, Sydney, Australia, 2011.

[20] Wakao, N., and T. Funazkri. Effect of Fluid Dispersion Coefficients on Particle-to-Fluid Mass Transfer Coefficients in Packed Beds. *Chemical Engineering Science*, **1978**, 33.10, 1375-84.

[21] Fuller, E.N., P.D. Schettler, and J.C. Giddings, *Industrial and Engineering Chemistry,* **1966***,* 58(5), 19. Several Other Equations for Predicting Diffusion Coefficients Can Be Found in R. C. Rcid, J. M. Prausnitz and T. K Sherwood, *The Properties of Gases and Liquids* 3rd ed. (New York: McGraw-Hill, 1977), Chap 11.

[22] Taylor, R., and L.W. Smith. On Some Explicit Approximate Solutions of the Maxwell-Stefan Equations for the Multicomponent Film Model. *Chemical Engineering Communications*, **1982**, 14.3-6, 361-70.

[23] Jackson, R. 1977. *Transport in Porous Catalysts*. Elsevier.

[24] Kent, J. Steam Reforming of Biodiesel By-Product Glycerol. A Major Qualifying Project, Worcester Polytechnic Institute, 2013.

[25] Ergun, S., and A. A. Orning. Fluid Flow through Randomly Packed Columns and Fluidized Beds. *Industrial & Engineering Chemistry,* **1949**, 41.6, 1179-84.

[26] Chen, H., Y. Ding, N. Cong, B. Dou, V. Dupont, M. Ghadiri, and P. Williams. A Comparative Study on Hydrogen Production from Steam-Glycerol Reforming: Thermodynamics and Experimental. Elsevier Ltd. 2010.

[27] Adhikari, S., S. Fernando, S. Gwaltney, S. To, R. Bricka, P. Steele, and A. Haryanto. A Thermodynamic Analysis of Hydrogen Production by Steam Reforming of Glycerol. September 2007. *International Journal of Hydrogen Energy,* **2007***,* 32, 2875-2880.

[28] Chiodo, V., S. Freni, A. Galvagno, N. Mondello, and F. Frusteri. Catalytic Features of Rh and Ni Supported Catalysts in the Steam Reforming of Glycerol to Produce Hydrogen. *Applied Catalysis*, **2010**, Volume 381, Issues 1-2, Pages 1-7.

[29] Wang, C., Dou, B., Chen, H., Song, Y., Xu, Y., Du, X., Luo, T., Tan, C. Hydrogen Production from Steam Reforming of Glycerol by Ni-Mg-Al Based Catalysts in a Fixed-Bed Reactor. *Chemical Engineering Journal,* **2013***,* 200, 133-142.

[30] Dieuzeide, M., and N. Amadeo. Thermodynamic Analysis of Glycerol Steam Reforming. *Chemical Engineering and Technology*, **2010**, 33, No. 1, 89-96.

[31] Fishtik, I., A. Alexander., R. Datta, and D. Geana. *International Journal of Hydrogen Energy,* **2000**, 25 (1), 31.

[32] Sundari, V. Reaction Kinetics of Glycerol Steam Reforming Using a Ru/Al_sO_3 Catalyst. *Energy & Fuels*, **2012**, 26, 4195 – 4204.

[33] Dixon, A.G., M. Nijemeisland, and H. Stitt. CFD Simulation of Reaction and Heat Transfer Near the Wall of a Fixed Bed. *International Journal of Chemical Reactor Engineering*, **2003**, 1.1.

[34] Adhikari, S. S. Fernando, and A. Haryanto. Kinetics and Reactor Modeling of Hydrogen Production from Glycerol via Steam Reforming Process over Ni/CeO2 Catalysts. *Chemical Engineering Technology*, **2009**, 32, 541−547.

[35] Cheng, C.K., S.Y. Foo, and A.A. Adesina. Steam Reforming of Glycerol over Ni/Al_2O_3 Catalyst. *Catalysis Today,* **2011**, 128, 25-33.

[36] Deutschmann, O. Computational Fluid Dynamics of Catalytic Reactors. Weinheim, Germany: Wiley-VCH Verlag GmbH & Co. KGaA251-282, 2011.

[37] Jakobsen, H.A. *Chemical Reactor Modeling: Multiphase Reactive Flows*. Berlin: Springer Berlin Heidelberg, 2008.

[38] Dixon, A.G., M. Nijemeisland, and H. Stitt. CFD Simulation of Reaction and Heat Transfer Near the Wall of a Fixed Bed. *International Journal of Chemical Reactor Engineering,* **2003**, 1.1.

[39] Maestri, M., and A. Cuoci. "Coupling CFD with Detailed Microkinetic Modeling in Heterogeneous Catalysis." *Chemical Engineering Science* 96, **2013**, 106.

[40] Liu, G.R., and Safari Books Online. *The Finite Element Method: A Practical Course*. Amsterdam: Elsevier, **2014**.

[41] Waller, C.P. Comparison of Reaction in Catalyst Pellet between Three-Dimensional Computational Fluid Dynamics and One-Dimensional Multiphysics Simulations. Worcester, MA: Worcester Polytechnic Institute, **2011**.

[42] Petera, J., L. Nowicki, and S. Ledakowicz. New Numerical Algorithm for Solving Multidimensional Heterogeneous Model of the Fixed Bed Reactor. *Chemical Engineering Journal* 214, **2013**: 237-46.

[43] de Klerk, A. Voidage Variation in Packed Beds at Small Column to Particle Diameter Ratio. *American Institute of Chemical Engineers Journal*, 49, **2003**, 2022-2029.

[44] Davis, M., and R. Davis. *Fundamentals of Chemical Reaction Engineering*. Boston: McGraw-Hill, **2003**.

[45] Iliuta, I., M. Iliuta, and H. Radfarnia. "Hydrogen Production by Sorption-Enhanced Steam Glycerol Reforming: Sorption Kinetics and Reactor Simulation." *American Institute of Chemical Engineers Journal*, **2013**, 59.6, 2105-18.

[46] Hou, K., and R. Hughes. The Kinetics of Methane Steam Reforming Over a Ni/Alpha-Al_2O Catalyst. Chemical Engineering Unit, University of Salford, UK. *Chemical Engineering Journal*, **2001**, 82, 311-328.

[47] Poling, B.E. et al. *The Properties of Gases and Liquids*. New York: McGraw-Hill Professional, **2001**.

[48] Edwards, M. F., and J. F. Richardson. Gas Dispersion in Packed Beds. *Chemical Engineering Science*, **1968**, 23.2, 109-23.

[49] McWhirter, J. D., M.E. Crawford, and D.E. Klein, 'Wall Region Porosity Distributions for Packed Beds of Uniform Spheres with Modified and Unmodified Walls. *Transport in Porous Media*, **1997**, 27, 99.

[50] Seguin, D., A. Montillet, and J. Comiti. Experimental Characterization of Flow Regimes in Various Porous Media - I: Limit of Laminar Flow Regime. *Chemical Engineering Science,* **1998**, *53*, 3751.

[51] Seguin, D., A. Montillet, J. Comiti, and F. Huet. Experimental Characterization of Flow Regimes in Various Porous Media - II: Transition to Turbulent Regime. *Chemical Engineering Science,* **1998**, *53*, 3897.

[52] Boudreau, J., and A. Rocheleau. Comparison of Catalyst Geometries Using Computational Fluid Dynamics for Methane Steam Reforming. MQP Project, Worcester Polytechnic Institute, MA, **2010**.

[53] Yaws, C.L., Knovel Chemistry &, and Chemical Engineering Library - Academic Collection. *Yaws' Handbook of Properties of the Chemical Elements*. Norwich, N.Y.: Knovel, **2011**.

9. Appendix

Appendix A: Simulation Parameters (Nonisothermal Conditions)

Parameter	Input	Definition
P_feed	2.02e5[Pa]	Feed pressure
T_feed	823[K]	Temperature
C0	P_feed/R_const/T_feed	Total feed concentration
x_C3H8O3_feed	0.1	Molar fraction of C3H8O3 in feed
x_H2_feed	0	Molar fraction of H2 in feed
x_CO2_feed	0	Molar fraction of CO2 in feed
x_H2O_feed	1-x_C3H8O3_feed-x_H2_feed-x_CO2_feed	Molar fraction of H2O in feed
rho_feed	C0*MW_feed	Inlet gas density
u_feed	5.0[m/s]	Linear inflow velocity
G	u_feed*rho_feed	Mass flux
F_feed	u_feed*C0*Ra	Feed molar flow rate
Kp	1[W/(m*K)]	Pellet thermal conductivity
dHr1	-1.28e5[J/mol]	Heat of reaction for R1
por_b	0.397	Porosity of the bed (void/total)
rho_b	1130[kg/m^3]	Density of bed
rho_p	1947[kg/m^3]	Density of pellet
Rr	7.2*rp	Reactor radius
Ra	pi*Rr^2	Reactor area
rp	0.0127[m]	Particle radius
scale	rp/1[m]	Pellet scale factor
dp	2*rp	Pellet diameter
Ap	3/rp	Surface area of particles per unit volume
L	1[m]	Tube length
scale_L	L/1[m]	Tube scale factor
qw	20000[W/m^2]	Wall heat flux
MW_C3H8O3	92.09[kg/kmol]	Mol. wt. methane
MW_H2	2.01594[kg/kmol]	Mol. wt. hydrogen
MW_CO2	44.00995[kg/kmol]	Mol. wt. carbon dioxide
MW_H2O	18.01534[kg/kmol]	Mol. wt. water
MW_feed	MW_C3H8O3*x_C3H8O3_feed+MW_H2*x_H2_feed+MW_CO2*x_CO2_feed+MW_H2O*x_H2O_feed	Mean molar mass of feed
x_C3H8O3_init	0.02508	Initial Guess for C3H8O3 fraction
x_H2_init	0.3311	Initial Guess for H2 fraction
x_CO2_init	0.1419	Initial Guess for CO2 fraction

x_H2O_init	1-x_C3H8O3_init-x_H2_init-x_CO2_init	Initial Guess for H2O fraction
n1	1	Scaling Parameter for bootstrapping procedure
m1	1	Scaling Parameter for bootstrapping procedure
n2	1	Scaling Parameter for bootstrapping procedure
m2	1	Scaling Parameter for bootstrapping procedure
Dab_avg	1.7e-4[m^2/s]	Average Bulk Diffusion Coefficient
eta_feed	(5.27e-8)*T_feed[kg/m/s/K]-4.1e-6	Fluid Viscosity at Feed Conditions
Cp_f_feed	0.4122*T_feed[J/(kg*K*K)]+1915.3	Fluid Heat Capacity at Feed Conditions
kf_feed	(1.355e-4)*T_feed[W/m/K/K]+0.0119	Fluid Thermal Conductivity at Feed Conditions

Appendix B: Simulation Variables (Non-isothermal Conditions)

Parameter	Input	Definition
Ctot	mod1.P/R_const/mod1.Tf	Total concentration
u	G/Ctot/MW_mean	Linear velocity
rho	G/u	Fluid density
Pc3h8o3	mod2.C3H8O3p*R_const*mod2.Ts/(1000[Pa])	partial pressure for CH4 (kPa)
Ph2	mod2.H2p*R_const*mod2.Ts/(1000[Pa])	partial pressure for H2 (kPa)
Pco2	mod2.CO2p*R_const*mod2.Ts/(1000[Pa])	partial pressure for CO2 (kPa)
Ph2o	mod2.H2Op*R_const*mod2.Ts/(1000[Pa])	partial pressure for H2O (kPa)
R1	BET*krxn*Pc3h8o3*Ph2o/((1+KG*Pc3h8o3)*(1+KW*Ph2o))	Rate expression for reaction 1
Conv	(x_C3H8O3_feed*F_feed-x_C3H8O3*F)/(x_C3H8O3_feed*F_feed)	Conversion of Glycerol
F	Ctot*Ra*u	Molar Flow Rate
MW_mean	MW_H2O+(MW_C3H8O3-MW_H2O)*x_C3H8O3+(MW_H2-MW_H2O)*x_H2+(MW_CO2-MW_H2O)*x_CO2	Mean Molecular Weight
MWx	((MW_C3H8O3-MW_H2O)*mod1.C3H8O3x+(MW_H2-MW_H2O)*mod1.H2x+(MW_CO2-MW_H2O)*mod1.CO2x)/C0	Derivative of Molecular Weight with respect to axial position
x_C3H8O3	mod1.C3H8O3/C0	C3H8O3 composition

x_H2	mod1.H2/C0	H2 composition
x_CO2	mod1.CO2/C0	CO2 composition
x_H2O	1-x_C3H8O3-x_H2-x_CO2	H2O composition
BETSA	14300	Surface Area of Catalyst from BET Analysis
krxn	0.010471*exp(-69360/(R_const*mod2.Ts))	Reaction Rate Parameter
KG	0.0082125*exp(2931.4/mod2.Ts)	Glycerol Adsorption Parameter
KW	0.379*exp(-1904.4/mod2.Ts)	Water Adsorption Parameter
eta	(5.27e-8)*mod1.Tf[kg/m/s/K]-4.1e-6	Fluid Viscosity
Cp_f	0.4122*mod1.Tf[J/(kg*K*K)]+1915.3	Fluid Heat Capacity
beta	G*(1-por_b)/(rho_feed*dp*por_b^3)*(150*(1-por_b)*eta/dp+1.75*G)	Ergun Equation Constant
Re	u_feed*rho_feed*dp/eta_feed	Reynolds Number
Sc	eta_feed/(rho_feed*Dab_avg)	Schmidt Number
Sh	2+1.1*(Re^0.6)*(Sc^(1/3))	Sherwood Number
kg	Sh*Dab_avg/dp	Particle-Fluid mass transfer coefficient
Pem	1/((0.73*por_b/(Re*Sc))+(0.5/(1+9.7*por_b/(Re*Sc))))	Peclet Number - Mass transfer
D_ea	u_feed*dp/Pem	Axial dispersion coefficient
kf	(1.355e-4)*mod1.Tf[W/m/K/K]+0.0119	Fluid Thermal Conductivity
Pr	eta_feed*Cp_f_feed/kf_feed	Prandtl Number
Nu	2+1.1*(Re^0.6)*(Pr^(1/3))	Nusselt Number
hg	Nu*kf_feed/dp	Particle-Fluid heat transfer coefficient
Peh	1/((kp/(kf_feed*Re*Pr))+(0.73*por_b/(Re*Pr))+0.5)	Peclet Number - Heat transfer
k_ea	rho_feed*u_feed*Cp_f_feed*dp/Peh	Axial Thermal dispersion coefficient
Dp_C3H8O3	(1.62e-8)*(mod2.Ts^0.5)	C3H8O3 diffusion coefficient in the pellet
Dp_H2O	(3.86e-8)*(mod2.Ts^0.5)	H2O diffusion coefficient in the pellet
Dp_CO2	(2.31e-8)*(mod2.Ts^0.5)	CO2 diffusion coefficient in the pellet
Dp_H2	(1.07e-7)*(mod2.Ts^0.5)	H2 diffusion coefficient in the pellet
Keq	5.698e27*exp(-15396[K]/mod2.Ts)	Reaction Equilibrium Constant

Appendix C: Reactor Model Multiphysics Settings

Parameter	Input	Definition
Transport of diluted species parameters		
Di	D_ea/scale_L*Ctot/C0	Diffusion coefficient
Initial concentration	x_C3H8O3_feed*C0	Initial C3H8O3 concentration
	x_H2_feed*C0	Initial H2 concentration
	x_CO2_feed*C0	Initial CO2 concentration
Reaction rate	n1*(scale_L*Ap*(1-por_b)*kg*(C3H8O3surf-C3H8O3*Ctot/C0)+G*mod1.C3H8O3/C0/MW_mean/MW_mean*MWx)	C3H8O3 reaction rate
	n1*(scale_L*Ap*(1-por_b)*kg*(H2surf-H2*Ctot/C0)+G*mod1.H2/C0/MW_mean/MW_mean*MWx)	H2 reaction rate
	n1*(scale_L*Ap*(1-por_b)*kg*(CO2surf-CO2*Ctot/C0)+G*mod1.CO2/C0/MW_mean/MW_mean*MWx)	CO2 reaction rate
Heat transfer in fluids parameters		
Thermal conductivity	k_ea/scale_L	
Initial temperature	T_feed	
Q	m1*(scale_L*Ap*hg*(1-por_b)*(Tsurf-Tf)+2/Rr*qw*scale_L)	Heat source

Appendix D: Catalyst Pellet Model Multiphysics Settings

Parameter	Input	Definition
Transport of diluted species parameters		
$D_{C3H8O3,\,P}$	Dp_C3H8O3	C3H8O3 diffusion coefficient
$D_{H2,\,P}$	Dp_H2	H2 diffusion coefficient
$D_{H2O,\,P}$	Dp_H2O	H2O diffusion coefficient
$D_{CO2,\,P}$	Dp_CO2	CO2 diffusion coefficient
Initial concentration	x_C3H8O3_init*C0	Initial C3H8O3 concentration

	x_H2_init*C0	Initial H2 concentration
	x_H2O_init*C0	Initial H2O concentration
	x_CO2_init*C0	Initial CO2 concentration
$R_{C3H8O3,\ P}$	n2*((scale^2)*rho_p*(-R1)+2/y*Dp_C3H8O3*C3H8O3py)	C3H8O3 reaction rate
$R_{H2,\ P}$	n2*((scale^2)*rho_p*(7*R1)+2/y*Dp_H2*H2py)	H2 reaction rate
$R_{H2O,\ P}$	n2*((scale^2)*rho_p*(-3*R1)+2/y*Dp_H2O*H2Opy)	H2O reaction rate
$R_{CO2,\ P}$	n2*((scale^2)*rho_p*(3*R1)+2/y*Dp_CO2*CO2py)	CO2 reaction rate
Heat transfer in solids parameters		
k	kp	Thermal conductivity
Initial temperature	T_feed	
Q	m2*((scale^2)*rho_p*(R1*dHr1)+2/y*kp*Tsy)	Heat source
h	scale*hg	Heat transfer coefficient

Appendix E: Property Correlation Calculations

Effective Diffusivity [21][22]

$$C_3H_8O_3 + 3H_2O \Leftrightarrow 3CO_2 + 7H_2$$

Molecular Weights [g/mol]

Mh2 := 1.00794·2

Mco2 := 44.01

Mh2o := 18.0153

Mgsr := 92.09382

Atomic and Structural Diffusion-Volume Increments [cm3/mol]

vh2 := 7.07 vc := 16.5

vco2 := 26.9 vh := 1.98

vh2o := 12.7 vo := 5.48

vgsr := 3·vc + 8·vh + 3·vo = 81.78

tortuosity, τ: τ := 3.54

porosity, ε: ε := 0.44

pellet: ρp := 1.947· g/cm^3

BET surface

Sg := 143000 cm^2/g

T1 := 823 P1 := 2

Equivalent Pore

$$rp := \frac{2\cdot\varepsilon^2}{Sg\cdot\rho p} = 1.391\times10^{-6}$$

Fuller-Schettler-Giddings Correlation

$$Dgsr\_h2o := \frac{10^{-3}\cdot T1^{1.75}\cdot\left(\frac{Mgsr + Mh2o}{Mgsr\cdot Mh2o}\right)^{0.5}}{P1\cdot\left(vgsr^{\frac{1}{3}} + vh2o^{\frac{1}{3}}\right)^2}$$

$$Dgsr\_h2 := \frac{10^{-3}\cdot T1^{1.75}\cdot\left(\frac{Mgsr + Mh2}{Mgsr\cdot Mh2}\right)^{0.5}}{P1\cdot\left(vgsr^{\frac{1}{3}} + vh2^{\frac{1}{3}}\right)^2}$$

$$Dgsr\_co2 := \frac{10^{-3}\cdot T1^{1.75}\cdot\left(\frac{Mgsr + Mco2}{Mgsr\cdot Mco2}\right)^{0.5}}{P1\cdot\left(vgsr^{\frac{1}{3}} + vco2^{\frac{1}{3}}\right)^2}$$

$$Dh2o\_co2 := \frac{10^{-3}\cdot T1^{1.75}\cdot\left(\frac{Mh2o + Mco2}{Mh2o\cdot Mco2}\right)^{0.5}}{P1\cdot\left(vh2o^{\frac{1}{3}} + vco2^{\frac{1}{3}}\right)^2}$$

$$Dh2o\_h2 := \frac{10^{-3}\cdot T1^{1.75}\cdot\left(\frac{Mh2o + Mh2}{Mh2o\cdot Mh2}\right)^{0.5}}{P1\cdot\left(vh2o^{\frac{1}{3}} + vh2^{\frac{1}{3}}\right)^2}$$

$$Dco2\_h2 := \frac{10^{-3}\cdot T1^{1.75}\cdot\left(\frac{Mco2 + Mh2}{Mco2\cdot Mh2}\right)^{0.5}}{P1\cdot\left(vco2^{\frac{1}{3}} + vh2^{\frac{1}{3}}\right)^2}$$

$yco2 := 0.076$

$ygsr := 0.059$

$yh2 := 0.179$

$yh2o := 1 - yco2 - ygsr - yh2$

$ygsr = 0.059$

$yco2 = 0.076$

$yh2 = 0.179$

$yh2o = 0.686$

Knudsen Diffusion

$DK\_gsr := 9700 \cdot rp \cdot \left(\frac{T1}{Mgsr}\right)^{0.5}$ cm2/s $\quad DK\_h2o := 9700 \cdot rp \cdot \left(\frac{T1}{Mh2o}\right)^{0.5}$ cm2/s

$DK\_co2 := 9700 \cdot rp \cdot \left(\frac{T1}{Mco2}\right)^{0.5}$ cm2/s $\quad DK\_h2 := 9700 \cdot rp \cdot \left(\frac{T1}{Mh2}\right)^{0.5}$ cm2/s

$DK\_gsr = 0.04$

gsr $\quad Nh2\_Ngsr := -1 \quad Nh2o\_Ngsr := 10 \quad Nco2\_Ngsr := -1$

h2o $\quad Ngsr\_Nh2o := 0.1 \quad Nco2\_Nh2o := -0.1 \quad Nh2\_Nh2o := -0.1$

co2 $\quad Ngsr\_Nco2 := -1 \quad Nh2o\_Nco2 := -10 \quad Nh2\_Nco2 := 1$

h2 $\quad Ngsr\_Nh2 := -1 \quad Nh2o\_Nh2 := -10 \quad Nco2\_Nh2 := 1$

Glycerol Multicomponent and Effective Diffusivity

$$DEN\_gsr := 1 - ygsr \cdot (Nh2\_Ngsr + Nh2o\_Ngsr + Nco2\_Ngsr)$$

$$NUM\_gsr := \left(\frac{yh2o - ygsr \cdot Nh2o\_Ngsr}{Dgsr\_h2o}\right) + \left(\frac{yco2 - ygsr \cdot Nco2\_Ngsr}{Dgsr\_co2}\right) + \left(\frac{yh2 - ygsr \cdot Nh2\_Ngsr}{Dgsr\_h2}\right)$$

$$Dgsr\_m := \frac{10^{-4}}{\frac{NUM\_gsr}{DEN\_gsr}} \qquad Dgsr\_m = 4.814 \times 10^{-5}\ m2/s$$

$$Dgsr := \frac{1}{\left(\frac{1}{Dgsr\_m}\right) + \left(\frac{1}{DK\_gsr \cdot 10^{-4}}\right)} \qquad Dgsr\_eff := \left(\frac{\varepsilon}{\tau}\right) \cdot Dgsr = 4.625 \times 10^{-7}\ m2/s$$

CO2 Multicomponent and Effective Diffusivity

$$DEN\_co2 := 1 - yco2 \cdot (Nh2\_Nco2 + Nh2o\_Nco2 + Ngsr\_Nco2)$$

$$NUM\_co2 := \left(\frac{yh2o - yco2 \cdot Nh2o\_Nco2}{Dh2o\_co2}\right) + \left(\frac{ygsr - yco2 \cdot Ngsr\_Nco2}{Dgsr\_co2}\right) + \left(\frac{yh2 - yco2 \cdot Nh2\_Nco2}{Dco2\_h2}\right)$$

$$Dco2\_m := \frac{10^{-4}}{\frac{NUM\_co2}{DEN\_co2}} \quad Dco2\_m = 5.859 \times 10^{-5}\ m2/s$$

$$Dco2 := \frac{1}{\left(\frac{1}{Dco2\_m}\right) + \left(\frac{1}{DK\_co2 \cdot 10^{-4}}\right)} \qquad Dco2\_eff := \left(\frac{\varepsilon}{\tau}\right) \cdot Dco2 = 6.594 \times 10^{-7} m2/s$$

H2 Multicomponent and Effective Diffusivity

$$DEN\_h2 := 1 - yh2 \cdot (Ngsr\_Nh2 + Nh2o\_Nh2 + Nco2\_Nh2)$$

$$NUM\_h2 := \left(\frac{yh2o - yh2 \cdot Nh2o\_Nh2}{Dh2o\_h2}\right) + \left(\frac{yco2 - yh2 \cdot Nco2\_Nh2}{Dco2\_h2}\right) + \left(\frac{ygsr - yh2 \cdot Ngsr\_Nh2}{Dgsr\_h2}\right)$$

$$Dh2\_m := \frac{10^{-4}}{\frac{NUM\_h2}{DEN\_h2}} \qquad Dh2\_m = 2.523 \times 10^{-4}\ m2/s$$

$$Dh2 := \frac{1}{\left(\frac{1}{Dh2\_m}\right) + \left(\frac{1}{DK\_h2 \cdot 10^{-4}}\right)} \qquad Dh2\_eff := \left(\frac{\varepsilon}{\tau}\right) \cdot Dh2 = 3.057 \times 10^{-6}\ m2/s$$

H2O Multicomponent and Effective Diffusivity

$$DEN\_h2o := 1 - yh2o \cdot (Nh2\_Nh2o + Ngsr\_Nh2o + Nco2\_Nh2o)$$

$$NUM\_h2o := \left(\frac{ygsr - yh2o \cdot Ngsr\_Nh2o}{Dgsr\_h2o}\right) + \left(\frac{yco2 - yh2o \cdot Nco2\_Nh2o}{Dh2o\_co2}\right) + \left(\frac{yh2 - yh2o \cdot Nh2\_Nh2o}{Dh2o\_h2}\right)$$

$$Dh2o\_m := \frac{10^{-4}}{\frac{NUM\_h2o}{DEN\_h2o}} \qquad Dh2o\_m = 3.5463 \times 10^{-4} m2/s$$

$$Dh2o := \frac{1}{\left(\frac{1}{Dh2o\_m}\right) + \left(\frac{1}{DK\_h2o \cdot 10^{-4}}\right)} \qquad Dh2o\_eff := \left(\frac{\varepsilon}{\tau}\right) \cdot Dh2o = 1.105 \times 10^{-6}\ m2/s$$

Fluid Heat Capacity [9]

$C1\_co2 := 0.2937 \cdot 10^5$ $C3\_co2 := 1.428 \cdot 10^3$ $C5\_co2 := 588$

$C2\_co2 := 0.3454 \cdot 10^5$ $C4\_co2 := 0.264 \cdot 10^5$

$T := 823\ K$ $MW\_co2 := 44.00995$

$$Cp\_co2 := C1\_co2 + C2\_co2 \cdot \left(\frac{\frac{C3\_co2}{T}}{\sinh\left(\frac{C3\_co2}{T}\right)} \right)^2 + C4\_co2 \cdot \left(\frac{\frac{C5\_co2}{T}}{\cosh\left(\frac{C5\_co2}{T}\right)} \right)^2$$

$Cp\_co2 = 5.156 \times 10^4$ J/kmol.K

$Cp\_mass\_co2 := \frac{Cp\_co2}{MW\_co2} = 1172$ J/kg.K

$Cp\_h2 := 14.74 kJ/kg.K$

$Cp\_mass\_h2 := 1000 \cdot Cp\_h2 = 14740$ J/kg.K

$Cp\_gsr := 211.1$ J/mol. $MW\_gsr := 92.09382$

$Cp\_mass\_gsr := \frac{1000 \cdot Cp\_gsr}{MW\_gsr} = 2292$ J/kg.K

weight fractions

$x\_co2 := 0.156$ $x\_h2 := 0.017$ $x\_gsr := 0.253$

$x\_h2o := 1 - (x\_co2 + x\_h2 + x\_gsr) = 0.574$

$Cp\_mix := x\_co2 \cdot Cp\_mass\_co2 + x\_h2 \cdot Cp\_mass\_h2 + x\_gsr \cdot Cp\_mass\_gsr + x\_h2o \cdot Cp\_mass\_h2o$

$Cp\_mix = 2256.07$ J/kg.K

$C1\_h2o := 0.33363 \cdot 10^5$ $C3\_h2o := 2.6105 \cdot 10^3$ $C5\_h2o := 1169$

$C2\_h2o := 0.2679 \cdot 10^5$ $C4\_h2o := 0.08896 \cdot 10^5$

$MW\_h2o := 18.01534$

$$Cp\_h2o := C1\_h2o + C2\_h2o \cdot \left(\frac{\frac{C3\_h2o}{T}}{\sinh\left(\frac{C3\_h2o}{T}\right)} \right)^2 + C4\_h2o \cdot \left(\frac{\frac{C5\_h2o}{T}}{\cosh\left(\frac{C5\_h2o}{T}\right)} \right)^2$$

$$Cp\_h2o = 3.901 \times 10^4 \ \frac{J/kmol.}{K}$$

$$Cp\_mass\_h2o := \frac{Cp\_h2o}{MW\_h2o} = 2165 \quad J/kg.K$$

$mass\_h2o := 0.686 \cdot 18.01534$ $mass\_co2 := 0.076 \cdot 44.00995$

$mass\_gsr := 0.059 \cdot 92.09382$ $mass\_h2 := 0.18 \cdot 2$

$mass\_tot := mass\_gsr + mass\_h2o + mass\_h2 + mass\_co2$

$$\frac{mass\_h2o}{mass\_tot} = 0.575 \qquad \frac{mass\_gsr}{mass\_tot} = 0.253$$

$$\frac{mass\_h2}{mass\_tot} = 0.017 \qquad \frac{mass\_co2}{mass\_tot} = 0.156$$

Fluid Thermal Conductivity [9][47][53]

$T := 823\,K \quad P := 2.0265\,ba$

1 = Glycerol	$M1 := 92.09382$	$Pc1 := 76\,ba$	$Tc1 := 850\,K$	$y1 := 0.059 \quad y3 := 0.076$
2 = H2O	$M2 := 18.01534$	$Pc2 := 220.6$	$Tc2 := 647.1$	
3 = CO2	$M3 := 44.00995$	$Pc3 := 73.75$	$Tc3 := 304.13$	$y2 := 0.686$
4 = H2	$M4 := 2.01594$	$Pc4 := 12.964$	$Tc4 := 33.14$	$y4 := 1 - y1 - y2 - y3 = 0.179$

Perry's Handbook

$C1\_co2 := 3.69 \quad C2\_co2 := -0.3838 \quad C3\_co2 := 964 \quad C4\_co2 := 1860000$

$$\lambda 3 := \frac{C1\_co2 \cdot T^{C2\_co2}}{1 + \left(\frac{C3\_co2}{T}\right) + \left(\frac{C4\_co2}{T^2}\right)} \quad \frac{W/m.}{K}$$

$C1\_h2 := 0.002653 \quad C2\_h2 := 0.7452 \quad C3\_h2 := 12 \quad C1\_h2o := 6.2041 \cdot 10^{-6} \quad C2\_h2o := 1.3973$

$$\lambda 4 := \frac{C1\_h2 \cdot T^{C2\_h2}}{1 + \left(\frac{C3\_h2}{T}\right)} \quad \frac{W/m.}{K} \qquad \lambda 2 := C1\_h2o \cdot T^{C2\_h2o}$$

Yaw's Handbook

$C1\_gsr := -0.010567 \quad C2\_gsr := 0.000063386 \quad C3\_gsr := 0.00000002056$

$$\lambda 1 := C1\_gsr + C2\_gsr \cdot T + C3\_gsr \cdot T^2 \quad W/m.K$$

$$\Gamma 1 := 210 \cdot \left(\frac{Tc1 \cdot M1^{3}}{Pc1^{4}} \right)^{\frac{1}{6}} \quad \Gamma 2 := 210 \cdot \left(\frac{Tc2 \cdot M2^{3}}{Pc2^{4}} \right)^{\frac{1}{6}} \quad \Gamma 3 := 210 \cdot \left(\frac{Tc3 \cdot M3^{3}}{Pc3^{4}} \right)^{\frac{1}{6}} \quad \Gamma 4 := 210 \cdot \left(\frac{Tc4 \cdot M4^{3}}{Pc4^{4}} \right)^{\frac{1}{6}}$$

$$Tr1 := \frac{T}{Tc1} \quad Tr2 := \frac{T}{Tc2} \quad Tr3 := \frac{T}{Tc3} \quad Tr4 := \frac{T}{Tc4}$$

$$\lambda 12 := \frac{\Gamma 2 \cdot (\exp(0.0464 \cdot Tr1) - \exp(-0.2412 \cdot Tr1))}{\Gamma 1 \cdot (\exp(0.0464 \cdot Tr2) - \exp(-0.2412 \cdot Tr2))} \quad \lambda 13 := \frac{\Gamma 3 \cdot (\exp(0.0464 \cdot Tr1) - \exp(-0.2412 \cdot Tr1))}{\Gamma 1 \cdot (\exp(0.0464 \cdot Tr3) - \exp(-0.2412 \cdot Tr3))}$$

$$\lambda 14 := \frac{\Gamma 4 \cdot (\exp(0.0464 \cdot Tr1) - \exp(-0.2412 \cdot Tr1))}{\Gamma 1 \cdot (\exp(0.0464 \cdot Tr4) - \exp(-0.2412 \cdot Tr4))} \quad \lambda 23 := \frac{\Gamma 3 \cdot (\exp(0.0464 \cdot Tr2) - \exp(-0.2412 \cdot Tr2))}{\Gamma 2 \cdot (\exp(0.0464 \cdot Tr3) - \exp(-0.2412 \cdot Tr3))}$$

$$\lambda 24 := \frac{\Gamma 4 \cdot (\exp(0.0464 \cdot Tr2) - \exp(-0.2412 \cdot Tr2))}{\Gamma 2 \cdot (\exp(0.0464 \cdot Tr4) - \exp(-0.2412 \cdot Tr4))} \quad \lambda 34 := \frac{\Gamma 4 \cdot (\exp(0.0464 \cdot Tr3) - \exp(-0.2412 \cdot Tr3))}{\Gamma 3 \cdot (\exp(0.0464 \cdot Tr4) - \exp(-0.2412 \cdot Tr4))}$$

$$\lambda 21 := \lambda 12^{-1} \quad \lambda 31 := \lambda 13^{-1} \quad \lambda 41 := \lambda 14^{-1} \quad \lambda 32 := \lambda 23^{-1} \quad \lambda 42 := \lambda 24^{-1} \quad \lambda 43 := \lambda 34^{-1}$$

$$A12 := \frac{\left[1 + \lambda 12^{0.5} \cdot \left(\frac{M1}{M2} \right)^{0.25} \right]^{2}}{\left[8 \cdot \left[1 + \left(\frac{M1}{M2} \right) \right] \right]^{0.5}} \quad A13 := \frac{\left[1 + \lambda 13^{0.5} \cdot \left(\frac{M1}{M3} \right)^{0.25} \right]^{2}}{\left[8 \cdot \left[1 + \left(\frac{M1}{M3} \right) \right] \right]^{0.5}} \quad A14 := \frac{\left[1 + \lambda 14^{0.5} \cdot \left(\frac{M1}{M4} \right)^{0.25} \right]^{2}}{\left[8 \cdot \left[1 + \left(\frac{M1}{M4} \right) \right] \right]^{0.5}}$$

$$A21 := \frac{\left[1 + \lambda 21^{0.5} \cdot \left(\frac{M2}{M1} \right)^{0.25} \right]^{2}}{\left[8 \cdot \left[1 + \left(\frac{M2}{M1} \right) \right] \right]^{0.5}} \quad A23 := \frac{\left[1 + \lambda 23^{0.5} \cdot \left(\frac{M2}{M3} \right)^{0.25} \right]^{2}}{\left[8 \cdot \left[1 + \left(\frac{M2}{M3} \right) \right] \right]^{0.5}} \quad A24 := \frac{\left[1 + \lambda 24^{0.5} \cdot \left(\frac{M2}{M4} \right)^{0.25} \right]^{2}}{\left[8 \cdot \left[1 + \left(\frac{M2}{M4} \right) \right] \right]^{0.5}}$$

$$A31 := \frac{\left[1 + \lambda31^{0.5} \cdot \left(\frac{M3}{M1}\right)^{0.25}\right]^2}{\left[8 \cdot \left[1 + \left(\frac{M3}{M1}\right)\right]\right]^{0.5}} \quad A32 := \frac{\left[1 + \lambda32^{0.5} \cdot \left(\frac{M3}{M2}\right)^{0.25}\right]^2}{\left[8 \cdot \left[1 + \left(\frac{M3}{M2}\right)\right]\right]^{0.5}} \quad A34 := \frac{\left[1 + \lambda34^{0.5} \cdot \left(\frac{M4}{M1}\right)^{0.25}\right]^2}{\left[8 \cdot \left[1 + \left(\frac{M4}{M1}\right)\right]\right]^{0.5}}$$

$$A41 := \frac{\left[1 + \lambda41^{0.5} \cdot \left(\frac{M4}{M1}\right)^{0.25}\right]^2}{\left[8 \cdot \left[1 + \left(\frac{M4}{M1}\right)\right]\right]^{0.5}} \quad A42 := \frac{\left[1 + \lambda42^{0.5} \cdot \left(\frac{M4}{M2}\right)^{0.25}\right]^2}{\left[8 \cdot \left[1 + \left(\frac{M4}{M2}\right)\right]\right]^{0.5}} \quad A43 := \frac{\left[1 + \lambda43^{0.5} \cdot \left(\frac{M4}{M3}\right)^{0.25}\right]^2}{\left[8 \cdot \left[1 + \left(\frac{M4}{M3}\right)\right]\right]^{0.5}}$$

$$\lambda m := \left(\frac{y1 \cdot \lambda1}{y1 + y2 \cdot A12 + y3 \cdot A13 + y4 \cdot A14}\right) + \left(\frac{y2 \cdot \lambda2}{y1 \cdot A21 + y2 + y3 \cdot A23 + y4 \cdot A24}\right) \ldots + \left(\frac{y3 \cdot \lambda3}{y1 \cdot A31 + y2 \cdot A32 + y3 + y4 \cdot A34}\right) + \left(\frac{y4 \cdot \lambda4}{y1 \cdot A41 + y2 \cdot A42 + y3 \cdot A43 + y4}\right)$$

$\lambda mix := 0.0996$ W/m.K

Fluid Viscosity [9][47][53]

$T := 823\ K \quad P := 2.01325\ bar$

1 = Glycerol	$M1 := 92.09382$	$Pc1 := 76\ ba$	$Tc1 := 850\ K$	$\mu1 := 2.56\ D$	$y1 := 0.059$
2 = H2O	$M2 := 18.01534$	$Pc2 := 220.6$	$Tc2 := 647.1$	$\mu2 := 1.8546$	$y2 := 0.686$
3 = CO2	$M3 := 44.00995$	$Pc3 := 73.75$	$Tc3 := 304.13$	$\mu3 := 0$	$y3 := 0.076$
4 = H2	$M4 := 2.01594$	$Pc4 := 12.964$	$Tc4 := 33.14$	$\mu4 := 0$	$y4 := 0.179$

Dipole

$y1 + y2 + y3 + y4 = 1$

Single Component correlation: Perry's Handbook

$C1\_h2o := 1.7096 \cdot 10^{-8}$ $C2\_h2o := 1.1146$

$\eta2 := 10000000 \cdot C1\_h2o \cdot T^{C2\_h2o}$

$\eta2 = 303.668\ \mu P$

$C1\_co2 := 2.148 \cdot 10^{-6}$ $C2\_co2 := 0.46$ $C3\_co2 := 290$

$$\eta3 := \frac{10000000 \cdot C1\_co2 \cdot T^{C2\_co2}}{1 + \left(\frac{C3\_co2}{T}\right)}$$

$\eta3 = 348.356\ \mu P$

$C1\_h2 := 1.797 \cdot 10^{-7}$ $C2\_h2 := 0.685$ $C3\_h2 := -0.59$ $C4\_h2 := 140$

$$\eta4 := \frac{10000000 \cdot C1\_h2 \cdot T^{C2\_h2}}{1 + \left(\frac{C3\_h2}{T}\right) + \left(\frac{C4\_h2}{T^2}\right)}$$

$\eta4 = 178.574\ \mu P$

Yaw's Handbook

$C1\_gsr := -20.505$

$C2\_gsr := 0.3076$

$C3\_gsr := -0.000053811$

$\eta1 := C1\_gsr + C2\_gsr \cdot T + C3\_gsr \cdot T^2$

$\eta1 = 196.20\ \mu P$

$$Tr12 := \frac{T}{(Tc1 \cdot Tc2)^{0.5}} \quad Tr13 := \frac{T}{(Tc1 \cdot Tc3)^{0.5}} \quad Tr14 := \frac{T}{(Tc1 \cdot Tc4)^{0.5}} \quad Tr23 := \frac{T}{(Tc2 \cdot Tc3)^{0.5}}$$

$$Tr24 := \frac{T}{(Tc2 \cdot Tc4)^{0.5}} \quad Tr34 := \frac{T}{(Tc3 \cdot Tc4)^{0.5}} \quad \mu r1 := \frac{52.46 \cdot \mu1^2 \cdot Pc1}{Tc1^2} \quad \mu r2 := \frac{52.46 \cdot \mu2^2 \cdot Pc2}{Tc2^2}$$

$\mu r3 := 0 \quad \mu r12 := (\mu r1 \cdot \mu r2)^{0.5} \quad \mu r14 := 0 \quad \mu r24 := 0$

$\mu r4 := 0 \quad \mu r13 := 0 \quad \mu r23 := 0 \quad \mu r34 := 0$

$$Tr1 := \frac{T}{Tc1} \quad Tr2 := \frac{T}{Tc2} \quad Tr3 := \frac{T}{Tc3} \quad Tr4 := \frac{T}{Tc4}$$

$$Fr12 := \frac{Tr12^{3.5} + (10 \cdot \mu r12)^7}{Tr12^{3.5} \cdot \left[1 + (10 \cdot \mu r12)^7\right]} \quad Fr13 := \frac{Tr13^{3.5} + (10 \cdot \mu r13)^7}{Tr13^{3.5} \cdot \left[1 + (10 \cdot \mu r13)^7\right]} \quad Fr14 := \frac{Tr14^{3.5} + (10 \cdot \mu r14)^7}{Tr14^{3.5} \cdot \left[1 + (10 \cdot \mu r14)^7\right]}$$

$$Fr23 := \frac{Tr23^{3.5} + (10 \cdot \mu r23)^7}{Tr23^{3.5} \cdot \left[1 + (10 \cdot \mu r23)^7\right]} \quad Fr24 := \frac{Tr24^{3.5} + (10 \cdot \mu r24)^7}{Tr24^{3.5} \cdot \left[1 + (10 \cdot \mu r24)^7\right]} \quad Fr34 := \frac{Tr34^{3.5} + (10 \cdot \mu r34)^7}{Tr34^{3.5} \cdot \left[1 + (10 \cdot \mu r34)^7\right]}$$

$$Fr1 := \frac{Tr1^{3.5} + (10 \cdot \mu r1)^7}{Tr1^{3.5} \cdot \left[1 + (10 \cdot \mu r1)^7\right]} \quad Fr2 := \frac{Tr2^{3.5} + (10 \cdot \mu r2)^7}{Tr2^{3.5} \cdot \left[1 + (10 \cdot \mu r2)^7\right]} \quad Fr3 := \frac{Tr3^{3.5}}{Tr3^{3.5}} \quad Fr4 := 1$$

$$U1 := \frac{Fr1 \cdot \left[1 + 0.36 \cdot Tr1 \cdot (Tr1 - 1)\right]^{\frac{1}{6}}}{(Tr1)^{0.5}} \qquad U2 := \frac{Fr2 \cdot \left[1 + 0.36 \cdot Tr2 \cdot (Tr2 - 1)\right]^{\frac{1}{6}}}{(Tr2)^{0.5}}$$

$$U3 := \frac{Fr3 \cdot \left[1 + 0.36 \cdot Tr3 \cdot (Tr3 - 1)\right]^{\frac{1}{6}}}{(Tr3)^{0.5}} \qquad U4 := \frac{Fr4 \cdot \left[1 + 0.36 \cdot Tr4 \cdot (Tr4 - 1)\right]^{\frac{1}{6}}}{(Tr4)^{0.5}}$$

$$C1 := \frac{M1^{0.25}}{(\eta 1 \cdot U1)^{0.5}} \quad C2 := \frac{M2^{0.25}}{(\eta 2 \cdot U2)^{0.5}} \quad C3 := \frac{M3^{0.25}}{(\eta 3 \cdot U3)^{0.5}} \quad C4 := \frac{M4^{0.25}}{(\eta 4 \cdot U4)^{0.5}}$$

$$H12 := \left[\frac{M1 \cdot M2}{32 \cdot (M1 + M2)^3}\right]^{0.5} (C1 + C2)^2 \cdot \left[\frac{\left[1 + 0.36 \cdot Tr12 \cdot (Tr12 - 1)\right]^{\frac{1}{6}} \cdot Fr12}{(Tr12)^{0.5}}\right]$$

$$H13 := \left[\frac{M1 \cdot M3}{32 \cdot (M1 + M3)^3}\right]^{0.5} (C1 + C3)^2 \cdot \left[\frac{\left[1 + 0.36 \cdot Tr13 \cdot (Tr13 - 1)\right]^{\frac{1}{6}} \cdot Fr13}{(Tr13)^{0.5}}\right]$$

$$H14 := \left[\frac{M1 \cdot M4}{32 \cdot (M1 + M4)^3}\right]^{0.5} (C1 + C4)^2 \cdot \left[\frac{\left[1 + 0.36 \cdot Tr14 \cdot (Tr14 - 1)\right]^{\frac{1}{6}} \cdot Fr14}{(Tr14)^{0.5}}\right]$$

$$H23 := \left[\frac{M2 \cdot M3}{32 \cdot (M2 + M3)^3}\right]^{0.5} (C2 + C3)^2 \cdot \left[\frac{\left[1 + 0.36 \cdot Tr23 \cdot (Tr23 - 1)\right]^{\frac{1}{6}} \cdot Fr23}{(Tr23)^{0.5}}\right]$$

$$H24 := \left[\frac{M2 \cdot M4}{32 \cdot (M2 + M4)^3}\right]^{0.5} (C2 + C4)^2 \cdot \left[\frac{\left[1 + 0.36 \cdot Tr24 \cdot (Tr24 - 1)\right]^{\frac{1}{6}} \cdot Fr24}{(Tr24)^{0.5}}\right]$$

$$H34 := \left[\frac{M3 \cdot M4}{32 \cdot (M3 + M4)^3}\right]^{0.5} (C3 + C4)^2 \cdot \left[\frac{\left[1 + 0.36 \cdot Tr34 \cdot (Tr34 - 1)\right]^{\frac{1}{6}} \cdot Fr34}{(Tr34)^{0.5}}\right]$$

$$K1 := \frac{y1 \cdot \eta1}{y1 + \eta1 \cdot \left[y2 \cdot H12 \cdot \left[3 + \left(\frac{2M2}{M1} \right) \right] + y3 \cdot H13 \cdot \left[3 + \left(\frac{2M3}{M1} \right) \right] + y4 \cdot H14 \cdot \left[3 + \left(\frac{2M4}{M1} \right) \right] \right]}$$

$$K2 := \frac{y2 \cdot \eta2}{y2 + \eta2 \cdot \left[y1 \cdot H12 \cdot \left[3 + \left(\frac{2M1}{M2} \right) \right] + y3 \cdot H23 \cdot \left[3 + \left(\frac{2M3}{M2} \right) \right] + y4 \cdot H24 \cdot \left[3 + \left(\frac{2M4}{M2} \right) \right] \right]}$$

$$K3 := \frac{y3 \cdot \eta3}{y3 + \eta3 \cdot \left[y1 \cdot H13 \cdot \left[3 + \left(\frac{2M1}{M3} \right) \right] + y2 \cdot H23 \cdot \left[3 + \left(\frac{2M2}{M3} \right) \right] + y4 \cdot H34 \cdot \left[3 + \left(\frac{2M4}{M3} \right) \right] \right]}$$

$$K4 := \frac{y4 \cdot \eta4}{y4 + \eta4 \cdot \left[y1 \cdot H14 \cdot \left[3 + \left(\frac{2M1}{M4} \right) \right] + y2 \cdot H24 \cdot \left[3 + \left(\frac{2M2}{M4} \right) \right] + y3 \cdot H34 \cdot \left[3 + \left(\frac{2M3}{M4} \right) \right] \right]}$$

$$\eta m1 := K1 \cdot \left[1 + H12^2 \cdot K2^2 + H13^2 \cdot K3^2 + H14^2 \cdot K4^2 + 2 \cdot (H12 \cdot H13 \cdot K2 \cdot K3) + 2 \cdot (H12 \cdot H14 \cdot K2 \cdot K4) \ldots + 2 \cdot (H13 \cdot H14 \cdot K3 \cdot K4) \right]$$

$$\eta m2 := K2 \cdot \left[1 + 2 \cdot H12 \cdot K1 + H12^2 \cdot K1^2 + H23 \cdot K3^2 + H24^2 \cdot K4^2 + 2 \cdot (H12 \cdot H23 \cdot K1 \cdot K3) \ldots + 2 \cdot (H12 \cdot H24 \cdot K1 \cdot K4) + 2 \cdot (H23 \cdot H24 \cdot K3 \cdot K4) \right]$$

$$\eta m3 := K3 \cdot \left[1 + 2 \cdot (H13 \cdot K1 + H23 \cdot K2) + H13^2 \cdot K1^2 + H23^2 \cdot K2^2 + H34^2 \cdot K4^2 + 2 \cdot (H13 \cdot H23 \cdot K1 \cdot K2) \ldots + 2 \cdot (H13 \cdot H34 \cdot K1 \cdot K4) + 2 \cdot (H23 \cdot H34 \cdot K2 \cdot K4) \right]$$

$$\eta m4 := K4 \cdot \left[1 + 2 \cdot (H14 \cdot K1 + H24 \cdot K2 + H34 \cdot K3) + H14^2 \cdot K1^2 + H24^2 \cdot K2^2 + H34^2 \cdot K3^2 \ldots + 2 \cdot (H14 \cdot H24 \cdot K1 \cdot K2) + 2 \cdot (H14 \cdot H34 \cdot K1 \cdot K3) + 2 \cdot (H24 \cdot H34 \cdot K2 \cdot K3) \right]$$

$$\eta m := \eta m1 + \eta m2 + \eta m3 + \eta m4$$

$$\eta m\_mix := 0.0000001 \cdot \eta m$$

$\eta m = 393.138$ μP $\eta m\_mix = 3.931 \times 10^{-5}$ kg/m.s or Pa.s

Appendix F: Average Bed Voidage for Spherically Packed Column at Various Column-to-Pellet Ratios [43]

Reactor-to-Pellet Radius Ratio	Bed Voidage
1.7	0.657
2.0	0.502
2.4	0.471
2.6	0.483
3.0	0.416
3.3	0.450
3.7	0.445
4.2	0.425
4.4	0.426
4.6	0.406
4.9	0.419
5.4	0.411
7.2	0.397
9.2	0.368
11.2	0.366
13.3	0.362
15.4	0.363
18.0	0.362
19.3	0.363